

# Defects in oscillatory media — towards a classification

Björn Sandstede

Department of Mathematics  
The Ohio State University  
Columbus, OH 43202, USA

Arnd Scheel

Department of Mathematics  
University of Minnesota  
Minneapolis, MN 55455, USA

October 16, 2003

## Abstract

We investigate, in a systematic fashion, coherent structures, or defects, which serve as interfaces between wave trains with possibly different wavenumbers in reaction-diffusion systems. We propose a classification of defects into four different defect classes which have all been observed experimentally. The characteristic distinguishing these classes is the sign of the group velocities of the wave trains to either side of the defect, measured relative to the speed of the defect. Using a spatial-dynamics description in which defects correspond to homoclinic and heteroclinic connections of an ill-posed pseudo-elliptic equation, we then relate robustness properties of defects to their spectral stability properties. Lastly, we illustrate that all four types of defects occur in the one-dimensional cubic-quintic Ginzburg–Landau equation as a perturbation of the phase-slip vortex.

# Contents

<b>1</b>	<b>Introduction</b>	<b>4</b>
1.1	Motivation . . . . .	4
1.2	Main results . . . . .	8
1.3	Examples . . . . .	12
<b>2</b>	<b>Localized travelling waves</b>	<b>15</b>
2.1	Pulses and fronts . . . . .	16
2.2	Modulated waves . . . . .	18
<b>3</b>	<b>Wave trains, group velocities, and spatial dynamics</b>	<b>20</b>
3.1	Existence and stability of wave trains . . . . .	21
3.2	Spectra of wave trains in different frames . . . . .	22
3.3	Spatially homogeneous oscillations . . . . .	23
3.4	Spatial dynamics and relative Morse indices . . . . .	24
<b>4</b>	<b>Spectral properties of defects</b>	<b>26</b>
4.1	Exponential dichotomies . . . . .	27
4.2	Fredholm indices . . . . .	28
4.3	Spectral stability of defects . . . . .	30
<b>5</b>	<b>Robustness of defects in oscillatory media</b>	<b>32</b>
5.1	Invariant manifolds . . . . .	32
5.2	Sinks, sources, and transmission defects . . . . .	34
5.3	Contact defects . . . . .	37
<b>6</b>	<b>Stability, bifurcations, pinning, and truncation</b>	<b>38</b>
6.1	Stability . . . . .	38
6.2	Phase matching . . . . .	41
6.3	Reflection symmetries . . . . .	42
6.4	Bifurcations . . . . .	43
6.5	Pinning at inhomogeneities . . . . .	46
6.6	Frequency locking through periodic forcing . . . . .	49
6.7	Locking of defect speed and phase velocity . . . . .	50
6.8	Large bounded domains . . . . .	50
6.9	Interactions of defects . . . . .	53
6.10	Genericity . . . . .	54
6.11	Higher space dimensions . . . . .	55

<b>7 Example: The cubic-quintic Ginzburg–Landau equation</b>	<b>55</b>
<b>8 Conclusion</b>	<b>64</b>
<b>A Invariant manifolds</b>	<b>64</b>
A.1 Existence of center-stable manifolds . . . . .	64
A.2 Slowly varying coefficients . . . . .	69
<b>B Parameter values for the numerical simulations</b>	<b>70</b>
<b>References</b>	<b>71</b>

### Notation

$u(x, t)$	solution to reaction-diffusion system
$u_{\text{wt}}(kx - \omega t; k)$	wave train ( $2\pi$ -periodic in argument $\phi$ )
$\phi = kx - \omega t$	travelling-wave coordinate (wave train)
$k$	wavenumber
$\omega$	temporal frequency
$\omega_{\text{nl}}(k)$	nonlinear dispersion relation
$c_{\text{p}} = \omega_{\text{nl}}(k)/k$	phase velocity
$c_{\text{g}} = d\omega_{\text{nl}}(k)/dk$	group velocity
$\tilde{\lambda}$	wave-train eigenvalue computed in frame moving with speed $c_{\text{p}}$
$\lambda_{\text{lin}}(\nu)$	linear dispersion relation computed in frame moving with speed $c_{\text{p}}$
$\lambda$	temporal Floquet exponent
$\rho = \exp(2\pi\lambda/\omega_{\text{d}})$	temporal Floquet multiplier
$\nu$	complex spatial Floquet exponent
$\gamma$	spatial Floquet exponent
$c_{\text{d}}$	speed of defect
$\omega_{\text{d}}$	temporal frequency of defect
$\xi = x - c_{\text{d}}t$	travelling-wave coordinate (defect)
$\tau = \omega_{\text{d}}t$	rescaled time ( $2\pi$ -periodic)
$u_{\text{d}}(\xi, \tau)$	defect ( $2\pi$ -periodic in $\tau$ )
$\mathbb{1}$	identity operator
$\text{N}(\mathcal{L}), \text{Rg}(\mathcal{L})$	null space and range of a closed linear operator $\mathcal{L}$
$i(\mathcal{L}) = \dim \text{N}(\mathcal{L}) - \text{codim} \text{Rg}(\mathcal{L})$	index of a Fredholm operator $\mathcal{L}$
$Y = H^{1/2}(S^1, \mathbb{R}^n) \times L^2(S^1, \mathbb{R}^n)$	spaces for spatial dynamical systems
$Y^1 = H^1(S^1, \mathbb{R}^n) \times H^{1/2}(S^1, \mathbb{R}^n)$	

# 1 Introduction

In this paper, we investigate coherent structures in essentially one-dimensional spatially extended systems. Specifically, we are interested in interfaces between stable spatially periodic structures with possibly different spatial wavenumbers as illustrated in Figure 1.1. These interfaces can also be thought of as defects at which the underlying perfectly periodic structure is broken. In many cases, both the periodic structures and the defect will depend on time. We focus on defects where the resulting pattern is time-periodic, possibly after transforming into an appropriate moving frame of reference. Our goal is to investigate the existence and stability properties of such defects. In particular, we are interested in classifying defects according to their codimension and to study their robustness under parameter variations. Throughout this paper, we will use the term *wave trains* to denote spatially periodic travelling waves.

We begin by briefly reviewing some numerical simulations and experiments in which defects have been observed and by introducing, on a heuristic level, the concepts needed for the classification of defects. Afterwards, we recall some facts we need about wave trains before stating the definition of defects and our main results.

## 1.1 Motivation

### Experiments and simulations

To set the scene, we describe numerical simulations of defects and review various experiments in which they have been observed. Consider first the left and center plot in Figure 1.2. Both are space-time contour plots of solutions to the Brusselator (see Appendix B for the equations). Figure 1.2(i), which reproduces simulations from [37], shows a standing defect that emits wave trains alternately to the left and right so that the emitted wave trains travel away from the defect towards the domain boundary. Defects of this type are often referred to as flip-flops or one-dimensional spirals. Note that the defect is time-periodic since the space-time plot is periodic in the vertical time-direction. Figure 1.2(ii) shows a standing defect near the left domain boundary that emits wave trains simultaneously to the left and right: such defects are often referred to as target patterns. In the interior of the domain, a travelling defect is formed between the waves emitted by the target pattern and the spatially homogeneous oscillations that occupy the right half of the domain. The travelling defect is time-periodic when viewed in a co-moving frame. Indeed, shearing the space-time plot appropriately in the horizontal direction renders the figure vertically periodic with the

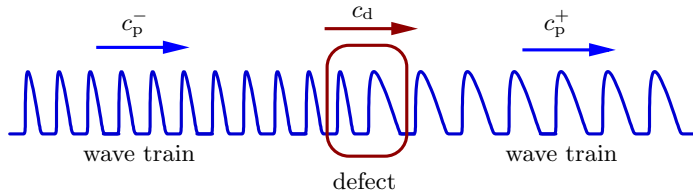


Figure 1.1: A defect travelling with speed  $c_d$  through spatially periodic structures that themselves travel with phase velocities  $c_p^-$  behind and  $c_p^+$  ahead of the defect.

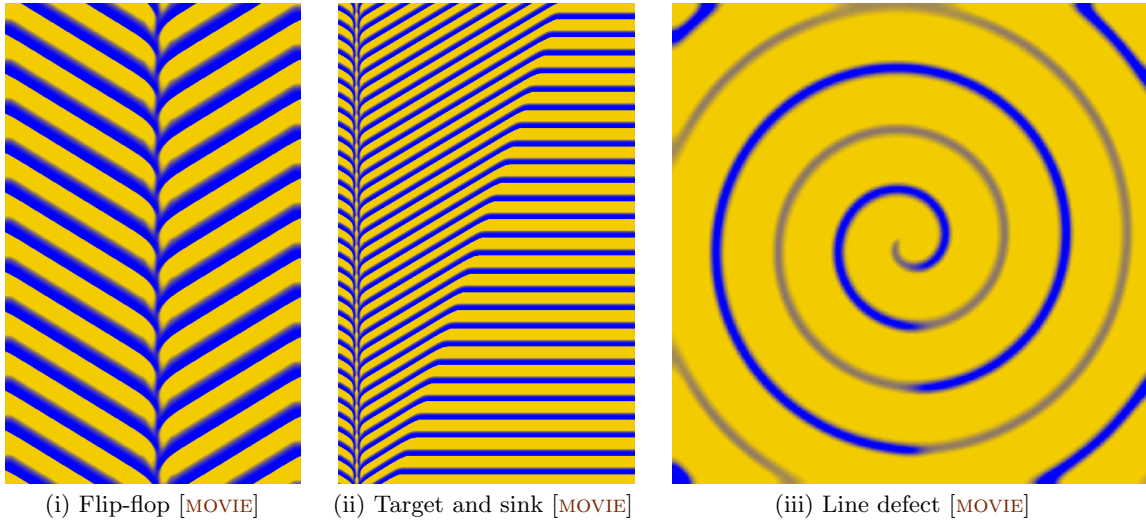


Figure 1.2: *Figure (i) on the left shows a space-time plot (time is plotted upward and space horizontally) of a flip-flop that emits wave trains alternately to the left and right: the emitted wave trains travel away from the defect towards the domain boundary. Figure (ii) in the middle is a space-time plot (time is plotted upward and space horizontally): Near the left boundary, we see a standing target pattern that emits waves simultaneously to the left and right. In the interior of the domain, a traveling defect is formed between the waves emitted by the target pattern and the spatially homogeneous oscillations that occupy the right half of the domain. Figure (iii) is a snap shot of a two-dimensional spiral wave. A one-dimensional line defect emerges from the center of the spiral and connects to the bottom of the domain. Along the line defect, the phase of the oscillations jumps by half a period.*

defect being a vertical line.

Flip-flops of a slightly different nature have been observed in numerical simulations in the excitable regime of the Oregonator [39] where a localized pulse destabilizes and releases pulses in its wake, a mechanism often referred to as backfiring. The emerging pattern resembles Figure 1.2(i) with pulses being released alternately to the left and right. The resulting interfaces can also move with non-zero speed [39].

Chemical oscillations have been generated in various reactions, most of which are related to the original Belousov–Zhabotinsky mechanism. In [37], defect patterns were observed in the chlorite-iodite-malonic-acid (CIMA) reaction in the parameter regime where stable stationary, spatially periodic Turing patterns and time-periodic, spatially homogeneous oscillations coexist. In one space dimension, [37, Figure 2] shows flip-flops of the type plotted in Figure 1.2(i). We emphasize that the waves emerging from the chemical flip-flop in [37] are not generated by an inhomogeneity in the medium. Instead, the defect forms spontaneously. At the defect, the phase of the wave trains jumps by half a period.

Defects with a different type of phase slip were observed in photo-sensitive monolayers on thin Belousov–Zhabotinsky reaction solutions [57]. The two-dimensional spiral waves shown in [57, Figures 2 and 5] exhibit stationary line defects along which the phase of the oscillations jumps by half the period. The spiral waves are presumably generated by a period-doubling bifurcation of spatially homogeneous oscillations that then leads to a Hopf bifurcation of the two-dimensional

spirals [51]. The line defects appear to orient themselves parallel to the propagation direction of the wave trains. We refer to Figure 1.2(iii) for a snap shot of a two-dimensional spiral wave that exhibits such a line defect. The pattern shown there was first found in [17] to which we refer for details on the equation used to generate it.

Hydrothermal waves can also exhibit defects. The recent experiments in [1, 35, 36], in which nonlinear waves and various kinds of defects were triggered by heated wires immersed in thin layers of oil, were motivated by the desire to obtain a quantitative comparison with coupled Ginzburg–Landau equations. Other experiments where defects have been observed are the printer instability [18], laterally heated fluid layers [3], and thermal convection of binary fluids [30].

### Heuristic classification

We are interested in finding characteristic properties of coherent structures of the kind shown in Figure 1.1. It turns out that the group velocities of the asymptotic wave trains are the deciding characteristic. The group velocity  $c_g$  associated with a wave train can be thought of as the speed with which small perturbations are transported along the wave train (we will make this more precise in Section 1.3 below; see also Figure 1.3). Alternatively, the group velocity can be computed as the derivative of the frequency of the wave train with respect to its wavenumber (see Section 1.2 below). We may then distinguish defects according to whether perturbations to the left or right of the defect travel towards, parallel to, or away from the interface. In fact, we propose the following classification:

<i>Sinks:</i>	$c_g^- > c_d > c_g^+$
<i>Contact defects:</i>	$c_g^- = c_d = c_g^+$
<i>Transmission defects:</i>	either $c_g^\pm > c_d$ or $c_g^\pm < c_d$
<i>Sources:</i>	$c_g^- < c_d < c_g^+$

where  $c_d$  is the speed of the defect, and  $c_g^-$  and  $c_g^+$  denote the group velocities of the wave trains to the left and right, respectively, of the interface. We refer to Figure 1.4 for an illustration. We emphasize that the slope of the level sets in the space-time plots of Figure 1.2 reflects the *phase* velocity of the wave trains. In contrast, the characteristic curves sketched in Figure 1.4 indicate the direction of the *group* velocity. In general, the signs of these two velocities are not related. While phase and group velocity of the waves in Figure 1.2(i) and (ii) have the same sign, the group velocity of the waves in Figure 1.2(iii) is directed towards the boundary, while they travel towards the spiral center.

The intuition is that sources generate the wave trains to either side since their group velocity points away from the interface. Sinks are passively created by wave trains who transport from the left and

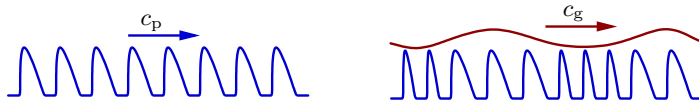


Figure 1.3: *The difference between the phase velocity  $c_p$  and the group velocity  $c_g$  of wave trains. The latter describes the speed with which slowly-varying modulations of the wavenumber propagate.*



Figure 1.4: A sketch of the characteristic curves that enter or leave each defect depending on the speed of the group velocities of the wave trains to the left and right of the defect compared with the speed of the defect. From left to right: sinks, contact defects, transmission defects and sources.

right towards the interface, thus forming it. Contact and transmission defects typically connect identical wave trains: these defects account for phase differences between the wave trains to their left and right.

We remark that there are defects that do not fit into the classification shown above (for instance, those for which  $c_g^- = c_d > c_g^+$ ). Nevertheless, we will argue in Section 6.10 that the only “relevant” defects are those captured by our classification.

Lastly, we briefly revisit the experiments and simulations mentioned above to demonstrate that each of the defect classes indeed arises in physical systems. The flip-flop in Figure 1.2(i), the target pattern in Figure 1.2(ii) and the chemical flip-flops observed by [37] in the CIMA reaction appear to be sources. The interface between travelling and standing waves shown in the center of Figure 1.2(ii) is a sink. We believe that the line defects that are illustrated in Figure 1.2(iii) and that occur in the modified Belousov–Zhabotinsky experiment [57] are contact defects. Transmission defects arise in the ferroin-catalyzed Belousov–Zhabotinsky reaction [19] and in the heated-wire experiments [1, 35]. Sources and sinks have also been observed in the printer instability [18] and in the heated-wire experiments [1, 35].

## Defects in general reaction-diffusion systems

The idea to characterize coherent structures<sup>1</sup> using the group velocity is, of course, not new. Interfaces between wave trains with almost identical wavenumbers were, for instance, studied in great detail in [25]. Defects in the cubic–quintic and in coupled complex Ginzburg–Landau equations were investigated by van Saarloos and co-workers [21, 22, 40] and by Doelman [9].

Our goal is to investigate defects arising in reaction-diffusion equations. The difficulty is that defects cannot be obtained as solutions to an ordinary differential equation (ODE). Instead, they are genuine PDE solutions. In fact, while the formation of periodic structures has been studied comprehensively in one, two and three space dimensions (see [7] and the references therein), defects within these periodic structures are not as well understood, at least from a mathematical viewpoint. There are two reasons for this. Firstly, defects are modulated waves and therefore time-periodic in a co-moving frame. Thus, dynamical-systems methods with respect to the spatial variable, that are so successful when dealing with travelling waves, are not immediately applicable. Secondly, it appears difficult to use period maps to investigate defects as the linearization about a defect has

<sup>1</sup>Throughout this paper, we shall use the terms *defect* and *coherent structure* interchangeably.

essential spectrum up to the imaginary axis. This fact precludes the immediate use of implicit function theorems. Note that the essential spectrum of each defect is generated by the spectrum of the asymptotic wave trains that always touches the imaginary axis. When studying spatially periodic patterns that respect a lattice symmetry group, this issue can be resolved by restricting to functions that respect the same lattice group. Defects, however, inherently break the lattice symmetry.

We focus on essentially one-dimensional media such as the real line  $x \in \mathbb{R}$ , cylindrical domains  $\mathbb{R} \times \Omega \subset \mathbb{R} \times \mathbb{R}^m$  or patterns with a radial symmetry  $x \in \mathbb{R}^+$ . In these cases, we can reverse the role of time and space, and treat the unbounded spatial variable  $x$  as the evolution variable, while time is restricted to the compact interval of periodicity. Dynamical-systems techniques can then be adapted to investigate bifurcations of small-amplitude solutions [26, 29, 54]. It is also possible to study periodic [33] as well as homoclinic and heteroclinic solutions [38, 48] of not necessarily small amplitude. Based on these ideas, we characterize in this paper properties of typical defects of arbitrary amplitude by interpreting them as homoclinic and heteroclinic trajectories that are constructed in a robust, transverse fashion. To classify defects, we count relative dimensions of the infinite-dimensional stable and unstable manifolds.

Lastly, we do not wish to give the impression that all interesting patterns observed in nature are necessarily time-periodic. In fact, there are many fascinating patterns that do not fit at all into the framework described above and that are therefore not captured by the analysis presented here. However, as documented above, many patterns observed in physical systems are time-periodic when viewed in an appropriate frame and therefore fit into our framework.

## 1.2 Main results

### Reaction-diffusion systems

As a prototype for equations that give far-from-equilibrium dynamics, we focus on reaction-diffusion equations

$$u_t = Du_{xx} + f(u), \quad x \in \mathbb{R} \tag{1.1}$$

where  $u \in \mathbb{R}^n$ . We assume that the diffusion matrix is diagonal with strictly positive entries and that the nonlinearity  $f \in C^\infty(\mathbb{R}^n, \mathbb{R}^n)$  is smooth. We think of  $f$  as a generic nonlinearity with no additional symmetries.

### Wave trains

The common feature of the experiments mentioned above is the presence of wave trains which are travelling waves of the form  $u_{\text{wt}}(kx - \omega t; k)$ , where  $u_{\text{wt}}(\phi; k)$  is  $2\pi$ -periodic in  $\phi$ . Typically, the spatial wavenumber  $k$  and the temporal frequency  $\omega$  are related via the nonlinear dispersion relation  $\omega = \omega_{\text{nl}}(k)$ , so that the phase velocity is given by  $c_p = \omega_{\text{nl}}(k)/k$ . A second quantity related

to the nonlinear dispersion relation is the group velocity

$$c_g = \frac{d\omega_{\text{nl}}}{dk} \quad (1.2)$$

of the wave train which will play a central role in our results. The group velocity  $c_g$  gives the speed of propagation of small localized wave-package perturbations of the wave train (see Example II in Section 1.3). Our primary interest is in wave trains that have a non-constant dispersion relation<sup>2</sup> so that  $c_g \neq 0$ .

We shall assume that the wave trains are spectrally stable. If we linearize (1.1) about a wave train in the frame  $\phi = kx - \omega_{\text{nl}}(k)t$ , we obtain the linear operator<sup>3</sup>

$$\mathcal{L}_{\text{wt}} = k^2 D\partial_{\phi\phi} + \omega_{\text{nl}}(k)\partial_{\phi} + f'(u_{\text{wt}}(\phi; k)). \quad (1.3)$$

Spectral stability means that the spectrum of  $\mathcal{L}_{\text{wt}}$  on  $L^2(\mathbb{R}, \mathbb{C}^n)$  is contained strictly in the left half-plane except for a unique curve

$$\lambda_{\text{lin}}(\nu) = a\nu + d\nu^2 + O(\nu^3), \quad \nu \in i\mathbb{R} \quad (1.4)$$

that touches the origin with a quadratic tangency  $d > 0$ . In this case, we actually know that  $a = c_p - c_g$ . We refer to Section 3.1 for details.

## Defects

Next, we consider coherent structures which are waves that are time-periodic in an appropriate frame of reference and asymptotic in space to wave trains with possibly different wavenumbers.

**Definition 1.1** *We say that a solution  $u(x, t) = u_{\text{d}}(x - c_{\text{d}}t, \omega_{\text{d}}t)$  of (1.1) is an elementary defect with speed  $c_{\text{d}}$  and frequency  $\omega_{\text{d}}$  if  $\omega_{\text{d}} \neq 0$  and if there are asymptotic wavenumbers  $k_-$  and  $k_+$ , and smooth phase-correction functions  $\theta_{\pm}(\xi)$  with  $\theta'_{\pm}(\xi) \rightarrow 0$  as  $\xi \rightarrow \pm\infty$  such that*

$$u_{\text{d}}(\xi, \tau) = u_{\text{d}}(\xi, \tau + 2\pi) \quad (1.5)$$

and

$$u_{\text{d}}(\xi, \omega_{\text{d}}t) - u_{\text{wt}}(k_{\pm}\xi + (k_{\pm}c_{\text{d}} - \omega_{\text{nl}}(k_{\pm}))t - \theta_{\pm}(\xi); k_{\pm}) \rightarrow 0 \quad (1.6)$$

uniformly in  $t$  as  $\xi \rightarrow \pm\infty$  for the functions as well as their derivatives with respect to  $(\xi, t)$ . Lastly, we assume that  $\partial_{\xi}u_{\text{d}}(\xi, \tau)$  and  $\partial_{\tau}u_{\text{d}}(\xi, \tau)$  are linearly independent functions.

Formulated in the steady frame, the periodicity (1.5) and convergence (1.6) conditions are

$$u(x, t) = u(x + c_{\text{d}}T_{\text{d}}, t + T_{\text{d}}), \quad T_{\text{d}} = \frac{2\pi}{\omega_{\text{d}}}$$

---

<sup>2</sup>Reversible Turing patterns, for instance, have a degenerate dispersion relation  $\omega_{\text{nl}}(k) \equiv 0$ , so that the group velocity vanishes for all  $k$ . In this case, our proposed classification into four defect types does not make sense.

<sup>3</sup>Some of our expressions below are only valid for  $k \neq 0$ . The results, however, are also true when  $k = 0$ , and we will comment on this in Section 3.3.

and

$$u(x, t) - u_{\text{wt}}(k_{\pm}x - \omega_{\text{nl}}(k_{\pm})t - \theta_{\pm}(x - c_{\text{d}}t); k_{\pm}) \longrightarrow 0$$

uniformly in  $0 \leq t \leq T_{\text{d}}$  as  $x \rightarrow \pm\infty$ .

We will see in Corollary 5.1 that the phase functions  $\theta_{\pm}(\xi)$  can be chosen to be constants  $\theta_{\pm}$  for sinks, sources and transmission defects, whereas contact defects have phase functions  $\theta_{\pm}(\xi) \propto \log \xi + O(1/|\xi|)$  that diverge logarithmically.

Throughout this paper, we denote the phase and group velocities of the asymptotic wave trains by

$$c_{\text{p}}^{\pm} = \frac{\omega_{\text{nl}}(k_{\pm})}{k_{\pm}}, \quad c_{\text{g}}^{\pm} = \frac{d\omega_{\text{nl}}}{dk}(k_{\pm}),$$

respectively. Note that equations (1.5)–(1.6) imply that

$$\omega_{\text{nl}}(k_{+}) - k_{+}c_{\text{d}} = \omega_{\text{d}} = \omega_{\text{nl}}(k_{-}) - k_{-}c_{\text{d}}. \quad (1.7)$$

In particular, the assumption that defects are time-periodic implies the Rankine–Hugoniot condition

$$c_{\text{d}} = \frac{\omega_{\text{nl}}(k_{+}) - \omega_{\text{nl}}(k_{-})}{k_{+} - k_{-}} \quad (1.8)$$

for the defect speed whenever  $k_{+} \neq k_{-}$ . To justify our use of the term Rankine–Hugoniot, we note that the group velocity, which measures transport, is the derivative of the frequency. In conservation laws, transport is the derivative of the flux, so that we may interpret the frequency  $\omega_{\text{nl}}$  as the flux function of a fictitious conservation law. In that sense, (1.8) is the corresponding Rankine–Hugoniot condition. Using these findings, we see that (1.6) is equivalent to

$$u_{\text{d}}(\xi, \tau) - u_{\text{wt}}(k_{\pm}\xi - \tau - \theta_{\pm}(\xi); k_{\pm}) \longrightarrow 0, \quad \xi \rightarrow \pm\infty. \quad (1.9)$$

To illustrate (1.8), consider the sink in the center of Figure 1.2(ii). Since the wave trains to the right of the defect are spatially homogeneous, we have  $k_{+} = 0$ . Inspecting the figure further, we see that  $\omega_{\text{nl}}(k_{-}) > \omega_{\text{nl}}(k_{+})$ , and (1.8) implies that  $c_{\text{d}} > 0$  which is consistent with the simulation.

## Main result

We are now ready to describe the main result of this paper. We begin by introducing four distinct classes of defects. Each type occurs in an open set of reaction-diffusion systems, or, more precisely, for nonempty open subsets  $\mathcal{U}$  of nonlinearities  $f$  in  $C^3(\mathbb{R}^n, \mathbb{R}^n)$  and of diffusion matrices  $D$ . We define the four different defect types as follows:

- (i) *Sinks* are elementary defects with  $c_{\text{g}}^{-} > c_{\text{d}} > c_{\text{g}}^{+}$ .
- (ii) *Contact defects* are elementary defects with  $c_{\text{g}}^{-} = c_{\text{d}} = c_{\text{g}}^{+}$ .
- (iii) *Transmission defects* are elementary defects with either  $c_{\text{g}}^{\pm} > c_{\text{d}}$  or  $c_{\text{g}}^{\pm} < c_{\text{d}}$ .
- (iv) *Sources* are elementary defects with  $c_{\text{g}}^{-} < c_{\text{d}} < c_{\text{g}}^{+}$ .

All contact and transmission defects that we are aware of have  $k_- = k_+$ . In fact, contact defects for which  $k_- \neq k_+$  and  $\omega''(k_-) \neq \omega''(k_+)$  will not persist upon varying  $(k_-, k_+)$ , and we will therefore restrict our analysis to contact defects for which  $k_- = k_+$ . Note also that we include neither sinks that have  $k_- = k_+$  nor degenerate sinks for which  $c_g^- = c_d > c_g^+$  or  $c_g^- > c_d = c_g^+$ , since we do not expect that such defects occur for open sets of wavenumbers  $k_-$  or  $k_+$ , respectively. We refer to Section 6.10 for more details.

Our main result will link robustness properties of defects to spectral properties of the linearization of the period map of (1.1). To describe these properties, we therefore linearize (1.1) in the co-moving frame  $\xi = x - c_d t$  with  $\tau = \omega_d t$  about an elementary defect  $u_d(\xi, \tau)$  and obtain the linear equation

$$\omega_d u_\tau = Du_{\xi\xi} + c_d u_\xi + f'(u_d(\xi, \tau))u. \quad (1.10)$$

We denote the linear period map of this parabolic equation with time-periodic coefficients by

$$\Phi_d : u(\cdot, 0) \longmapsto u(\cdot, 2\pi).$$

For any pair of real numbers  $\eta = (\eta_-, \eta_+)$ , we define  $L_\eta^2(\mathbb{R}, \mathbb{R}^n)$  to be the space of all locally square-integrable functions for which

$$\|u\|_{L_\eta^2}^2 = \int_{\mathbb{R}_-} |u(\xi)e^{\eta-\xi}|^2 d\xi + \int_{\mathbb{R}_+} |u(\xi)e^{\eta+\xi}|^2 d\xi$$

is finite.

**Definition 1.2** Consider  $\Phi_d$  on  $L_\eta^2(\mathbb{R}, \mathbb{R}^n)$  with weights  $\eta_\pm$  that are sufficiently close to zero and satisfy

$$\text{sign } \eta_\pm = \text{sign}(c_d - c_g^\pm). \quad (1.11)$$

We say that an elementary defect is transverse if it has minimal spectrum in the following sense:

- (i) For sinks, we assume that  $\Phi_d - \mathbf{1}$  has a bounded inverse on  $L_\eta^2(\mathbb{R}, \mathbb{R}^n)$ .
- (ii) For contact defects, we assume that  $\Phi_d - \mathbf{1}$  has a bounded inverse  $L_\eta^2(\mathbb{R}, \mathbb{R}^n)$  for all weights  $\eta_- = \eta_+ \neq 0$  that are sufficiently close to zero.
- (iii) For transmission defects, we assume that  $\rho = 1$  has algebraic multiplicity one as an eigenvalue of  $\Phi_d$  on  $L_\eta^2(\mathbb{R}, \mathbb{R}^n)$ .
- (iv) For sources, we assume that  $\rho = 1$  has algebraic multiplicity two as an eigenvalue of  $\Phi_d$  on  $L_\eta^2(\mathbb{R}, \mathbb{R}^n)$ .

It turns out that, in each of the above four cases,  $\Phi_d - \mathbf{1}$  is Fredholm with index zero on  $L_\eta^2(\mathbb{R}, \mathbb{R}^n)$  with weights chosen according to Definition 1.2. The above requirements on the spectra of  $\Phi_d$  can also be formulated in terms of multiplicities of appropriate roots of certain Evans functions (see Section 5). We emphasize, however, that the minimal-spectrum assumption for contact defects does not refer to the usual Evans function that we constructed in [49] since the essential spectrum of contact defects always extends into the right half-plane in the exponentially weighted spaces that we use (see Section 6.1).

We recall the main hypothesis that we require for the wave trains.

**Hypothesis 1.3** *Each of the wave trains that we consider is part of a one-parameter family given locally by solutions  $u_{\text{wt}}(kx - \omega_{\text{nl}}(k)t; k)$  of (1.1), where  $u_{\text{wt}}(\phi; k)$  is  $2\pi$ -periodic in  $\phi$ . We also assume that the dispersion relation  $\omega = \omega_{\text{nl}}(k)$  is well defined and smooth, again locally near each of the wave trains, and that  $\omega''_{\text{nl}}(k) \neq 0$ . Lastly, we assume that each of these wave trains is spectrally stable in the sense sketched in (1.4) and made precise in Hypotheses 3.1 and 3.2 below.*

The following theorem distills the analysis of the present paper into a multiplicity and robustness result.

**Theorem 1** *Assume that Hypothesis 1.3 is met. We then have:*

- (i) *Transverse sinks occur in two-parameter families that are parametrized by the asymptotic wavenumbers  $k_{\pm}$ ,*
- (ii) *Transverse contact defects appear as one-parameter families that are parametrized by the asymptotic wavenumber  $k_- = k_+$ ,*
- (iii) *Transverse transmission defects appear as one-parameter families that are parametrized by the asymptotic wavenumber  $k_+$  if  $c_{\text{g}}^{\pm} < c_{\text{d}}$  [and by  $k_-$  if  $c_{\text{g}}^{\pm} > c_{\text{d}}$ ],*
- (iv) *Transverse sources appear for a discrete set of wavenumbers  $(k_-, k_+)$ ,*

*where we exclude the translation symmetries in time and space from the above multiplicity counting. Each defect depends smoothly on parameters in the nonlinearity and the diffusion matrix (see below).*

Here, we say that a defect depends smoothly on wavenumbers and additional parameters  $\mu$  if there exist smooth functions  $c_{\text{d}}$  and  $\omega_{\text{d}}$  of  $(k_-, k_+, \mu)$  and a family of defects  $u_{\text{d}}(x - c_{\text{d}}t, \omega_{\text{d}}t; k_-, k_+, \mu)$  such that  $u_{\text{d}}$  depends smoothly on  $(k_-, k_+, \mu)$  as a function into  $BC^1(\mathbb{R} \times \mathbb{R}, \mathbb{R}^n)$  after transforming the argument  $\xi = x - c_{\text{d}}t$  according to

$$\xi \longmapsto \xi + \theta(\xi; k_-, k_+, \mu) \tag{1.12}$$

for an appropriate function  $\theta$  for which  $\theta'(\xi; k_-, k_+, \mu) \in BC^0(\mathbb{R})$  is smooth in  $(k_-, k_+, \mu)$ . The coordinate change in  $\xi$  is necessary in order to obtain continuity of the family since the wave trains depend continuously on  $k$  in  $BC^0$  only after a rescaling  $\xi \mapsto \xi/k$  that normalizes the spatial period.

### 1.3 Examples

To illustrate the theorem, we review the complex Ginzburg–Landau equation, whose defect solutions have been studied extensively in the literature, and Burgers equation, which describes the dynamics of modulated wave trains.

#### Example I: The complex Ginzburg–Landau equation

The complex cubic Ginzburg–Landau equation (CGL) is given by

$$A_t = (1 + i\alpha)A_{xx} + A - (1 + i\beta)A|A|^2 \tag{1.13}$$

where the coefficients  $\alpha, \beta \in \mathbb{R}$  are real, and where  $x \in \mathbb{R}$ ,  $t \geq 0$ , and  $A(x, t) \in \mathbb{C}$ . The CGL has a family of wave trains given by

$$A(x, t) = A_{\text{wt}}(kx - \omega t; k) = \sqrt{1 - k^2} e^{i(kx - \omega t)} \quad (1.14)$$

where the spatial wavenumber  $k$  and the temporal frequency  $\omega$  are related via

$$\omega = \omega_{\text{nl}}(k) = \beta + (\alpha - \beta)k^2.$$

Note that these waves exist only for  $|k| < 1$ . Due to the gauge invariance  $A \mapsto e^{i\phi}A$  of the CGL, defects can actually be constructed, in a frame moving with the defect speed  $c_d$ , as heteroclinic and homoclinic orbits of an ODE. Indeed, coherent defects of the CGL are of the form

$$A(x, t) = A_d(x - c_d t, \omega_d t) = a(x - c_d t) e^{i\phi(x - c_d t)} e^{-i\omega_d t} \quad (1.15)$$

so that

$$A_d(\xi, \tau) = a(\xi) e^{i[\phi(\xi) - \tau]}.$$

Substituting this ansatz into (1.13), it follows [21, Appendix B] that  $(a, z)$  satisfies the ODE

$$\begin{aligned} a_\xi &= a \operatorname{Re} z \\ z_\xi &= -z^2 - \frac{1}{1 + i\alpha} [1 + i\omega_d - (1 + i\beta)a^2 + c_d z] \end{aligned} \quad (1.16)$$

where  $z = a_\xi/a + i\phi_\xi$ . Thus, defects of the CGL correspond to heteroclinic orbits of the ODE (1.16), while the equilibria connected by these orbits correspond to wave trains of the CGL. The observation made in [40] is that the dimensions of the unstable and stable manifolds of these equilibria are related to the group velocities of the corresponding wave trains: In a frame moving with the speed of the defect, the dimension of stable manifolds associated with wave trains that transport to the left is larger than that of wave trains that transport to the right. Equivalently, the dimension of unstable manifolds associated with wave trains that transport to the right is larger than that of wave trains that transport to the left. These dimensions, however, are directly related, via counting arguments, to the codimension of connecting orbits between equilibria as these arise as intersections of stable and unstable manifolds. This argument therefore establishes a beautiful connection between the intuition given by the group velocity and rigorous counts of the codimension of defects.

Equation (1.16) has been studied thoroughly in the literature (see, for instance, [2, 9, 20, 21, 40] for references). In particular, the CGL has been shown to admit sources (the so-called Nozaki–Bekki holes), sinks, and transmission defects (commonly referred to as homoclons [20]). We refer to [9] for existence results of these defects and to [27] for the stability of sinks. We will show in Section 7 that the cubic-quintic Ginzburg–Landau equation admits contact defects.

## Example II: The viscous Burgers equation

Arguably, the simplest possible defects are those with “small amplitude” that serve as interfaces between two wave trains with almost the same wavenumber. The term “small amplitude” therefore

refers to the small difference of the asymptotic wavenumbers, not to the actual amplitudes of wave trains and defect which could be large.

One way of finding such defects is to derive an equation that describes slowly varying wavenumber modulations, see Figure 1.3, of the wave trains  $u_{\text{wt}}(kx - \omega_{\text{nl}}(k)t; k)$ . Hence, we fix a wavenumber  $k$  and seek solutions to the reaction-diffusion system (1.1) of the form

$$u(x, t) = u_{\text{wt}}(kx - \omega_{\text{nl}}(k)t + \Phi(X, T); k + \varepsilon \partial_X \Phi(X, T)) + \mathcal{O}(\varepsilon^2) \quad (1.17)$$

where  $0 < \varepsilon \ll 1$ , and where the variables  $(X, T)$  depend on  $(x, t)$  via

$$X = \varepsilon(x - c_g t), \quad T = \frac{1}{2} \varepsilon^2 t. \quad (1.18)$$

Thus, the function  $q(X, T) := \partial_X \Phi(X, T)$  describes the slowly varying modulation of the wavenumber. It can be shown [10, 25] that  $q(X, T)$  satisfies the viscous Burgers equation

$$\partial_T q = \lambda_{\text{lin}}''(0) \partial_X^2 q - \omega_{\text{nl}}''(k) \partial_X (q^2) \quad (1.19)$$

over time scales of order  $\mathcal{O}(1)$  in  $T$  and that any solution to (1.19) yields, in fact, a solution to the reaction-diffusion system (1.1) via (1.17). Using (1.18), this validity result justifies the interpretation of the group velocity as the speed of propagation of small localized wave-package perturbations.

To analyse defects, suppose that the dispersion relation is convex near the wavenumber  $k$  so that  $\omega''(k) > 0$  (the only difference for concave dispersion relations is that some of the signs below may change). Equation (1.19) admits stationary fronts of the form

$$q_{\text{d}}(X) = -\sqrt{\frac{\tilde{\omega}}{\omega_{\text{nl}}''(k)}} \tanh\left(\frac{\sqrt{\tilde{\omega} \omega_{\text{nl}}''(k)}}{\lambda_{\text{lin}}''(0)} X\right) \quad (1.20)$$

that converge to the equilibria  $q_{\pm} = \mp \sqrt{2\tilde{\omega}/\omega_{\text{nl}}''(k)}$  as  $X \rightarrow \pm\infty$  for each  $\tilde{\omega} > 0$ . These fronts of (1.19) correspond to defects of (1.1) that connect the wave train with wavenumber  $k + \varepsilon q_-$  to the wave train with wavenumber  $k + \varepsilon q_+$ . Since the dispersion relation is locally convex, and since  $q_- > 0$  and  $q_+ < 0$ , we see that the group velocity of  $k + \varepsilon q_-$  is larger than  $c_g$ , while the group velocity of  $k + \varepsilon q_+$  is smaller than  $c_g$ . Thus, the defects described by (1.20) are sinks whose characteristics on each side point towards the interface. This is, of course, in agreement with the fact that (1.20) describes the viscous Lax shocks of Burgers equation.

Another consequence of the above discussion is that sources do not exist in the small-amplitude limit. Indeed, for  $\omega''(k) > 0$ , the only waves of the viscous Burgers equation that connect  $q_-$  to  $q_+$  for  $q_- < q_+$  are rarefaction waves<sup>4</sup>.

We remark that it has been proved in [10] that the shocks given in (1.20) persist as transverse defects of the reaction-diffusion equation (1.1); note that this requires a proof as Burgers equation is valid only over finite time intervals.

---

<sup>4</sup>Rarefaction waves appear as stationary fronts of (1.19) if the self-similarity scaling symmetry is exploited that is respected by (1.19) but, in general, not by (1.1).

### Example III: Absolute and essential instability of pulses and fronts

Bifurcations from travelling waves provide another mechanism by means of which defects can be created. Imagine, for instance, a pulse travelling with a non-zero speed through a stable spatially homogeneous background. Now, envision a scenario where the stable background becomes unstable through a Turing or Hopf instability upon varying appropriate external parameters: At a supercritical Turing bifurcation, stationary wave trains with small amplitude and non-zero wavenumber will bifurcate from the homogeneous background state. We proved in [43] that, under certain generic assumptions, modulated pulses arise that travel through these wave trains with non-zero speed. Since the wave trains will have zero group velocity, the modulated pulse is an elementary transverse transmission defect. Linear and nonlinear stability of these defects have been addressed in [44] and [16], respectively. Analogous bifurcations can also occur at fronts when the rest state ahead of the front destabilizes [47]. Lastly, we proved in [50] that both flip-flops and one-dimensional target patterns (see Figure 1.2(i) and (ii)) will bifurcate from standing pulses whose background states undergo a Hopf instability. This appears to be the mechanism that creates the chemical flip-flops observed in [37].

### Plan of the paper

The paper is organized as follows. In Section 2, we review robustness and stability properties of localized pulses and fronts that connect spatially homogeneous equilibria. The purpose of this review is to prepare the spatial-dynamics viewpoint that we shall adopt when we investigate defects. Section 3 is devoted to wave trains and their stability for both the temporal and the spatial dynamical system. In Section 4, we prepare the ground for the proof of Theorem 1 by investigating the spectra of the period maps associated with the linearization about defects. We then prove Theorem 1 in Section 5 by linking robustness properties of defects to geometric transversality conditions of the spatial dynamical system. We also show that the resulting geometric conditions are equivalent to the minimal-spectrum assumption. In Section 6, we address stability, interactions, and bifurcations of defects as well as the influence of boundaries and inhomogeneities on their dynamics. Lastly, in Section 7, we prove that the cubic-quintic Ginzburg–Landau equation has contact defects in appropriate parameter regimes.

## 2 Localized travelling waves

To illustrate the main ideas behind Theorem 1 and its proof, we review travelling waves that approach stable spatially-homogeneous rest states. We describe both rigidly-propagating travelling waves  $u = u_{\text{tw}}(x - c_{\text{tw}}t)$  and oscillatory modulated waves  $u = u_{\text{mtw}}(x - c_{\text{mtw}}t, \omega_{\text{mtw}}t)$  of reaction-diffusion systems

$$u_t = Du_{xx} + f(u), \quad x \in \mathbb{R} \tag{2.1}$$

with  $u \in \mathbb{R}^n$ .

## 2.1 Pulses and fronts

Suppose that  $u_{\text{tw}}(x - ct)$  is a front that satisfies (2.1) and that connects two stable spatially homogeneous equilibria  $u_{\pm}$  of (2.1) so that  $u_{\text{tw}}(\xi) \rightarrow u_{\pm}$  as  $\xi \rightarrow \pm\infty$ . Thus, we use the independent variables  $(\xi, t) = (x - ct, t)$  so that (2.1) becomes

$$u_t = Du_{\xi\xi} + cu_{\xi} + f(u), \quad \xi \in \mathbb{R} \quad (2.2)$$

and  $u_{\text{tw}}(\xi)$  is an equilibrium. The linearization of (2.2) about the front  $u_{\text{tw}}(\xi)$  is given by

$$\mathcal{L}_{\text{tw}}u = Du_{\xi\xi} + cu_{\xi} + f'(u_{\text{tw}}(\xi))u \quad (2.3)$$

which defines a closed, unbounded operator  $\mathcal{L}_{\text{tw}}$  on  $L^2(\mathbb{R}, \mathbb{R}^n)$  and on  $BC^0(\mathbb{R}, \mathbb{R}^n)$ . We shall see below that  $u'_{\text{tw}}(\xi)$  decays exponentially to zero as  $|\xi| \rightarrow \infty$ . As a consequence,  $\lambda = 0$  is always an eigenvalue of  $\mathcal{L}_{\text{tw}}$  with eigenfunction  $u'_{\text{tw}}(\xi)$ . This eigenvalue occurs due to the translation symmetry of (2.2) which implies that  $u_{\text{tw}}(\cdot + \xi_0)$  is a solution for each fixed spatial shift  $\xi_0 \in \mathbb{R}$ . Since  $\mathcal{L}_{\text{tw}}$  is Fredholm with index zero [23], we can apply Lyapunov-Schmidt reduction to the steady-state equation associated with (2.2) near the family of fronts. Exploiting the translation symmetry  $\xi \mapsto \xi + \xi_0$ , it is not difficult to see that fronts and pulses are robust with respect to small perturbations of the nonlinearity provided  $\lambda = 0$  has geometric and algebraic multiplicity one as an eigenvalue of  $\mathcal{L}_{\text{tw}}$  (see [47] and the references therein for details).

An alternative approach to this problem is as follows. We seek travelling-wave solutions  $u_{\text{tw}}(x - ct)$  of (2.1). Substituting this ansatz gives the travelling-wave equation

$$\begin{aligned} u_{\xi} &= v \\ v_{\xi} &= -D^{-1}[cv + f(u)] \end{aligned} \quad (2.4)$$

in the  $2n$ -dimensional phase space, which we also write as

$$\mathbf{u}' = \mathcal{F}(\mathbf{u}; c),$$

where  $\mathbf{u} = (u, v) \in \mathbb{R}^{2n}$ . The front  $u_{\text{tw}}(\xi)$  which connects two stable spatially homogeneous equilibria  $u_{\pm}$  corresponds to a heteroclinic orbit  $\mathbf{u}_{\text{tw}}(\xi)$  of (2.4) which connects the equilibria  $\mathbf{u}_{\pm} = (u_{\pm}, 0)$ . The eigenvalue problem for the operator  $\mathcal{L}_{\text{tw}}$  can now be written as the linear ODE

$$\begin{aligned} u_{\xi} &= v \\ v_{\xi} &= -D^{-1}[cv + f'(u_{\text{tw}}(\xi))u - \lambda u]. \end{aligned} \quad (2.5)$$

For  $\lambda$  close to zero, this equation is close to the ODE linearization of (2.4) about the travelling wave  $\mathbf{u}_{\text{tw}}$ . We can therefore expect that the spectral properties of  $\mathcal{L}_{\text{tw}}$  for  $\lambda$  close to zero are related to properties of the heteroclinic orbit of the travelling-wave ODE (2.4).

First, consider the PDE linearization about a homogeneous equilibrium  $u_{\text{tw}}(\xi) \equiv u_{\pm}$ . Using Fourier transform, it is easy to see that  $\lambda$  belongs to the spectrum if, and only if, (2.5) has a non-trivial bounded solution. For  $\lambda \gg 1$ , equation (2.5) is close to  $u_{\xi\xi} = \lambda D^{-1}u$ , which is a linear hyperbolic

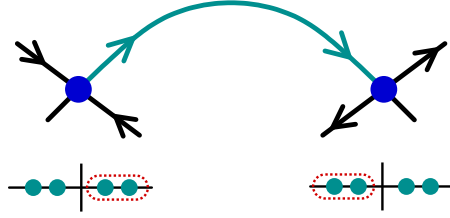


Figure 2.1: A front with stable homogeneous background states corresponds to a heteroclinic orbit that connects saddles whose unstable and stable manifolds have dimension  $n$ . The insets show the eigenvalues of the linearization of (2.4) about the saddles.

equation with  $n$  stable and  $n$  unstable spatial eigenvalues  $\nu = \pm\sqrt{\lambda/d_j}$  where  $D = \text{diag}(d_j)$ . If we therefore assume that the homogeneous equilibria  $u_{\pm}$  are spectrally stable, we can conclude that the corresponding two equilibria  $\mathbf{u}_{\pm} = (u_{\pm}, 0)$  of the travelling-wave ODE (2.4) are saddles whose stable and unstable manifolds have equal dimension  $n$ . In particular, fronts and pulses with stable background states correspond to heteroclinic and homoclinic orbits to saddles with unstable and stable dimension equal to  $n$ .

Next, robustness of fronts corresponds to robustness of the heteroclinic connection  $\mathbf{u}_{\text{tw}} = (u_{\text{tw}}, u'_{\text{tw}})$  as a solution to the ordinary differential equation (2.4). In fact, heteroclinic orbits are robust as solutions in the phase space if, and only if, stable and unstable manifolds intersect transversely upon varying the parameter  $c$  near the wave speed  $c_{\text{tw}}$  of the front or pulse: if we add the equation  $c_{\xi} = 0$  for the parameter  $c$  to (2.4) and denote the center-stable and center-unstable manifolds of the equilibria  $\mathbf{u}_{\pm}$  by  $W_{\text{ext}}^{\text{cu}}(\mathbf{u}_{-})$  and  $W_{\text{ext}}^{\text{cs}}(\mathbf{u}_{+})$ , then robustness is equivalent to requiring

$$T_{(\mathbf{u}_{\text{tw}}, c_{\text{tw}})} W_{\text{ext}}^{\text{cu}}(\mathbf{u}_{-}) + T_{(\mathbf{u}_{\text{tw}}, c_{\text{tw}})} W_{\text{ext}}^{\text{cs}}(\mathbf{u}_{+}) = \mathbb{R}^{2n} \times \mathbb{R}.$$

This, in turn, is equivalent to a minimal intersection in  $\mathbb{R}^{2n}$  for fixed  $c = c_{\text{tw}}$ ,

$$T_{\mathbf{u}_{\text{tw}}} W^{\text{u}}(\mathbf{u}_{-}) \cap T_{\mathbf{u}_{\text{tw}}} W^{\text{s}}(\mathbf{u}_{+}) = \text{span } \mathbf{u}'_{\text{tw}}, \quad (2.6)$$

together with a Melnikov condition

$$M = \int_{-\infty}^{\infty} \langle \boldsymbol{\psi}(\xi), \partial_c \mathcal{F}(\mathbf{u}_{\text{tw}}(\xi); c_{\text{tw}}) \rangle d\xi \neq 0. \quad (2.7)$$

Here,  $\boldsymbol{\psi}$  denotes the unique (up to scalar multiples) non-trivial bounded solution of the adjoint variational equation

$$\begin{aligned} u_{\xi} &= f'(u_{\text{tw}}(\xi))^* D^{-1} v \\ v_{\xi} &= -u + c D^{-1} v. \end{aligned} \quad (2.8)$$

Note that (2.6) holds precisely when  $\lambda = 0$  has geometric multiplicity one as an eigenvalue of  $\mathcal{L}_{\text{tw}}$ , while (2.7) holds exactly when its algebraic multiplicity is one. The relation between the ODE and the functional-analytic robustness argument becomes clearer when we approach the eigenvalue problem from an ODE viewpoint. Eigenfunctions correspond to bounded solutions of

(2.3), while generalized eigenfunctions are found as bounded solutions of the derivative of the variational equation with respect to  $\lambda$ , evaluated in the eigenfunction.

To find bounded solutions of (2.3), we denote by  $E_+^s(\lambda)$  the  $\lambda$ -dependent linear subspace of initial conditions at  $\xi = 0$  that lead to bounded solutions of (2.3) as  $x \rightarrow \infty$ , and by  $E_-^u(\lambda)$  the  $\lambda$ -dependent linear subspace that leads to bounded solutions as  $x \rightarrow -\infty$ . Using exponential dichotomies, we see that both subspaces are  $n$ -dimensional and are given as ranges of analytic families of projections  $P_+^s(\lambda)$  and  $P_-^u(\lambda)$ . We may now choose analytic bases  $\mathbf{e}_j^u$  in  $E_-^u(\lambda)$  and  $\mathbf{e}_j^s$  in  $E_+^s(\lambda)$ , and define the Evans function

$$\mathcal{E}(\lambda) := \det [\mathbf{e}_1^s, \dots, \mathbf{e}_n^s, \mathbf{e}_1^u, \dots, \mathbf{e}_n^u].$$

In particular, we have  $\mathcal{E}(\lambda) = 0$  if, and only if,  $\lambda$  is an eigenvalue of  $\mathcal{L}_{\text{tw}}$ . Furthermore, we have  $\mathcal{E}(0) = 0$  and, upon expanding the determinant, it is also not hard to see that  $\mathcal{E}'(0) \neq 0$  if, and only if, both (2.6) and (2.7) are met.

A related way to solve the eigenvalue problem in a neighborhood of  $\lambda = 0$  consists of finding roots of the injection map

$$\iota(\lambda) : E_-^u(\lambda) \times E_+^s(\lambda) \longrightarrow \mathbb{C}^{2n}, \quad (\mathbf{u}^-, \mathbf{u}^+) \longmapsto \mathbf{u}^- - \mathbf{u}^+. \quad (2.9)$$

Near  $\lambda = 0$ , this map can be pulled back to

$$\iota_0(\lambda) : E_-^u(0) \times E_+^s(0) \longrightarrow \mathbb{C}^{2n}, \quad (\mathbf{u}^-, \mathbf{u}^+) \longmapsto P_-^u(\lambda)\mathbf{u}^- - P_+^s(\lambda)\mathbf{u}^+. \quad (2.10)$$

Note that  $\iota_0(0)$  is Fredholm with index zero and null space  $E_-^u(0) \cap E_+^s(0)$ . If we denote the dimension of this null space by  $\ell$ , which coincides with the geometric multiplicity of  $\lambda = 0$ , then we can compute the roots of  $\iota_0$  near  $\lambda = 0$  via Lyapunov–Schmidt reduction which results in a linear system of  $\ell$  equations in  $\ell$  variables. The  $\lambda$ -dependent determinant of the reduced equation is a reduced Evans function  $\mathcal{E}_0(\lambda)$  whose roots, counted with multiplicity, coincide with those of  $\mathcal{E}(\lambda)$  in a neighborhood of zero. In particular, these two functions differ only by a non-zero analytic factor. In our case, the geometric multiplicity of  $\lambda = 0$  is one so that  $\ell = 1$ . Thus, the reduced Evans function  $\mathcal{E}_0(\lambda)$  is a scalar function, and we have  $\mathcal{E}'_0(0) \neq 0$  if, and only if, the algebraic multiplicity of  $\lambda = 0$  is one.

This latter approach of the construction of a *reduced Evans function* for eigenvalue problems is the one that we shall adopt below.

## 2.2 Modulated waves

Hopf bifurcations from rigidly-propagating travelling waves lead to modulated waves  $u_{\text{mtw}}(x-ct, \omega t)$  for some temporal frequency  $\omega = \omega_{\text{mtw}}$  and an average speed of propagation  $c = c_{\text{mtw}}$ , where the profile  $u_{\text{mtw}}(\xi, \tau)$  is  $2\pi$ -periodic in its second argument. In particular,  $u_{\text{mtw}}(\xi, \tau)$  is a periodic orbit with period  $2\pi$  of the reaction-diffusion system (2.1) in a co-moving frame:

$$\omega u_\tau = Du_{\xi\xi} + cu_\xi + f(u). \quad (2.11)$$

As in the previous section, we assume that  $u_{\text{mtw}}(\xi, \tau)$  converges to two asymptotically stable spatially-homogeneous equilibria  $u_{\pm}$  of (2.1) as  $\xi \rightarrow \pm\infty$ , uniformly in  $\tau$ . In other words, we require  $u_{\text{mtw}}(\xi, \cdot) \rightarrow u_{\pm}$  as  $\xi \rightarrow \pm\infty$ . We shall see later that this convergence is necessarily exponential.

To analyse robustness and stability of modulated waves, we consider the linearized period map  $\Phi_{\text{mtw}}$  that maps initial data  $u(\cdot, 0)$  to the solution  $u(\cdot, 2\pi)$  at time  $\tau = 2\pi$  of

$$\omega u_{\tau} = Du_{\xi\xi} + cu_{\xi} + f'(u_{\text{mtw}}(\xi, \tau))u. \quad (2.12)$$

The operator  $\Phi_{\text{mtw}} - \mathbb{1}$  is Fredholm with index zero when posed on  $L^2(\mathbb{R}, \mathbb{R}^n)$ . Note that  $\rho = 1$  is an eigenvalue of  $\Phi_{\text{mtw}}$  with geometric multiplicity equal to at least two since both  $\partial_{\xi}u_{\text{mtw}}$  and  $\partial_{\tau}u_{\text{mtw}}$  contribute one dimension each to the eigenspace. Using Lyapunov–Schmidt reduction and eliminating the space and time translational symmetries, we see that modulated waves are robust provided  $\rho = 1$  has algebraic multiplicity two.

Alternatively, we may investigate modulated waves by casting (2.12) as the dynamical system

$$\begin{aligned} u_{\xi} &= v \\ v_{\xi} &= D^{-1}[\omega\partial_{\tau}u - cv - f(u)] \end{aligned} \quad (2.13)$$

in the  $\xi$ -variable. Modulated waves satisfy (2.13), which we can view as an abstract differential equation

$$\mathbf{u}' = \mathcal{F}(\mathbf{u}; c, \omega) \quad (2.14)$$

on the phase space  $Y = H^{1/2}(S^1, \mathbb{R}^n) \times L^2(S^1, \mathbb{R}^n)$  of  $2\pi$ -periodic functions. Note that the initial-value problem associated with (2.14) is ill-posed as can be readily seen by solving it using Fourier series for  $f \equiv 0$  and  $c = 0$ . Despite this, we proved in [48] that the stable and unstable manifolds of the equilibria  $(u_+, 0)$  and  $(u_-, 0)$  can be constructed for (2.14) near the modulated-wave solution  $\mathbf{u}_{\text{mtw}} = (u_{\text{mtw}}, \partial_{\xi}u_{\text{mtw}})$ . In this framework, robustness is again equivalent to the transverse crossing of the extended stable and unstable manifolds

$$T_{(\mathbf{u}_{\text{mtw}}, c_{\text{mtw}}, \omega_{\text{mtw}})}W_{\text{ext}}^{\text{cu}}(\mathbf{u}_-) + T_{(\mathbf{u}_{\text{mtw}}, c_{\text{mtw}}, \omega_{\text{mtw}})}W_{\text{ext}}^{\text{cs}}(\mathbf{u}_+) = Y \times \mathbb{R}^2$$

in the two-dimensional parameter  $(c, \omega)$ . As before, this is equivalent [48] to the statement that

$$\dim [T_{\mathbf{u}_{\text{mtw}}}W^{\text{u}}(\mathbf{u}_-) \cap T_{\mathbf{u}_{\text{mtw}}}W^{\text{s}}(\mathbf{u}_+)] = 2, \quad (2.15)$$

where the intersection is spanned by  $\partial_{\xi}\mathbf{u}_{\text{mtw}}$  and  $\partial_{\tau}\mathbf{u}_{\text{mtw}}$ , together with the requirement that

$$\det (M_{ij})_{i=1,2, j=c,\omega} = \det \left( \int_{-\infty}^{\infty} \langle \boldsymbol{\psi}_i(\xi), \partial_j \mathcal{F}(\mathbf{u}_{\text{mtw}}(\xi); c_{\text{mtw}}, \omega_{\text{mtw}}) \rangle_Y d\xi \right)_{i=1,2, j=c,\omega} \neq 0 \quad (2.16)$$

where  $\boldsymbol{\psi}_i$  are the two linearly independent bounded solutions of the adjoint variational equation

$$\begin{aligned} u_{\xi} &= [f'(u_{\text{mtw}}(\xi, \tau))^* + \omega_{\text{mtw}}\partial_{\tau}] D^{-1}v \\ v_{\xi} &= -u + c_{\text{mtw}}D^{-1}v. \end{aligned} \quad (2.17)$$

To elucidate the relation between the analytical and the geometric approaches outlined above, consider the eigenvalue problem  $\Phi_{\text{mtw}}u = \rho u$  for the linear period map  $\Phi_{\text{mtw}}$  which is equivalent to the equation

$$\begin{aligned} u_\xi &= v \\ v_\xi &= D^{-1}[\omega_{\text{mtw}}\partial_\tau u - c_{\text{mtw}}v - f'(u_{\text{mtw}}(\xi, \tau))u + \lambda u] \end{aligned} \tag{2.18}$$

on  $Y$ . Here, we have used the Floquet ansatz  $(u, v) \mapsto e^{\lambda t}(u, v)$  where  $\lambda$  is the Floquet exponent and  $\rho = \exp(2\pi\lambda/\omega_{\text{mtw}})$  the associated Floquet multiplier which corresponds to an eigenvalue of  $\Phi_{\text{mtw}}$ . We can now construct stable and unstable subspaces for (2.18) that depend analytically on  $\lambda$  for  $\lambda$  close to zero [48]. Both subspaces are infinite-dimensional, whence it is not obvious how to construct an Evans function using determinants as in the case of travelling waves.

One way is to employ Galerkin approximations and to replace  $f'(u_{\text{mtw}})$  by  $P_m f'(u_{\text{mtw}})$  where  $P_m$  is the orthogonal projection in  $L^2$  onto the first  $m$  temporal Fourier modes. Following [48], it is not difficult to see that roots of the approximate Evans functions that are defined for the  $2mn$ -dimensional Fourier approximation converge with multiplicity as  $m \rightarrow \infty$ . In particular, for  $m \gg 1$ , winding-number calculations for the complex-analytic approximate Evans function give the correct number of eigenvalues for the full problem (2.18) on open bounded regions of the complex plane that do not intersect the absolute spectrum [46].

If we are only interested in computing roots locally, we can proceed as in the previous section and use the injection maps  $\iota(\lambda)$  and  $\iota_0(\lambda)$  that we defined in (2.9) and (2.10). The results in [48] imply in particular that the injection maps are again Fredholm with index zero. Using Lyapunov–Schmidt reduction, we see that eigenvalues can be computed locally as roots of a reduced determinant  $\mathcal{E}_0(\lambda)$  which we may refer to as the reduced Evans function. For modulated waves, we then have  $\mathcal{E}_0(0) = \mathcal{E}'_0(0) = 0$  and  $\mathcal{E}''_0(0) \neq 0$  provided both (2.15) and (2.16) are satisfied.

### 3 Wave trains, group velocities, and spatial dynamics

We are interested in defects that are spatially asymptotic to wave trains instead of to homogeneous steady states. In contrast to the exponentially stable homogeneous equilibria, wave trains always have a neutral mode, associated with their phase, and a resulting group velocity.

When interpreted in terms of spatial dynamical systems, defects correspond to heteroclinic orbits of the modulated-wave equation (2.13) that connect two periodic orbits instead of two hyperbolic equilibria. The asymptotic periodic orbits have again a neutral direction. We will prove in this section that, after eliminating the neutral eigenvalue, the unstable dimension, and therefore the Fredholm index of the injection maps  $\iota$  and  $\iota_0$  that we defined in the previous section, depends only on whether the group velocity of the wave train is larger or smaller than the speed of the defect. This result therefore allows us to relate group velocities of wave trains and Morse indices of the spatial dynamical system.

We refer to [10, 44, 52] for more details and references concerning the material in this section.

### 3.1 Existence and stability of wave trains

We assume that, for some non-zero temporal frequency  $\omega_0$  and a certain spatial wavenumber  $k_0$ , there exists a non-constant wave-train solution  $u(x, t) = u_{\text{wt}}(k_0x - \omega_0t)$  of (1.1) where  $u_{\text{wt}}(\phi)$  is  $2\pi$ -periodic in its argument. Throughout this section, we focus on the case  $k_0 \neq 0$  and discuss the somewhat simpler case  $k_0 = 0$  in Section 3.3 below.

Substituting the ansatz for  $u(x, t)$  into (1.1), we see that  $u_{\text{wt}}(\phi)$  must be a  $2\pi$ -periodic solution of the ODE

$$k_0^2 D \partial_{\phi\phi} u + \omega_0 \partial_{\phi} u + f(u) = 0. \quad (3.1)$$

Linearizing this equation about  $u_{\text{wt}}$ , we obtain the linear operator  $\mathcal{L}_{\text{wt}}$

$$\mathcal{L}_{\text{wt}} := k_0^2 D \partial_{\phi\phi} + \omega_0 \partial_{\phi} + f'(u_{\text{wt}}(\phi)), \quad (3.2)$$

which defines a closed operator on  $L^2(0, 2\pi)$  with domain  $H_{\text{per}}^2(0, 2\pi)$ .

**Hypothesis 3.1** *The origin  $\lambda = 0$  is algebraically simple as an eigenvalue of  $\mathcal{L}_{\text{wt}}$  on  $L^2(0, 2\pi)$  with eigenfunction  $\partial_{\phi} u_{\text{wt}}$ .*

Spectral stability of the wave train  $u_{\text{wt}}$  on  $\mathbb{R}$  is determined as follows. A complex number  $\check{\lambda}$  is in the spectrum of  $\mathcal{L}_{\text{wt}}$  considered as a closed operator on  $L^2(\mathbb{R}, \mathbb{C}^n)$  with domain  $H^2(\mathbb{R}, \mathbb{C}^n)$  if, and only if, there is a  $\nu \in i\mathbb{R}$  and a  $2\pi$ -periodic function  $w(\phi)$  such that  $\mathcal{L}_{\text{wt}} u = \check{\lambda} u$  for  $x \in \mathbb{R}$  where

$$u(\phi) = e^{\nu\phi/k_0} w(\phi). \quad (3.3)$$

Note that the resulting equation for  $w$  is

$$\check{\lambda} w = D [k_0 \partial_{\phi} + \nu]^2 w + c_p [k_0 \partial_{\phi} + \nu] w + f'(u_{\text{wt}}(\phi)) w \quad (3.4)$$

where  $c_p = \omega_0/k_0$  is the phase speed of the wave trains. Hypothesis 3.1 implies that there is an analytic function  $\lambda_{\text{lin}}(\nu)$  with  $\lambda_{\text{lin}}(0) = 0$  such that  $\check{\lambda}$  close to zero is in the spectrum if, and only if,  $\check{\lambda} = \lambda_{\text{lin}}(\nu)$  for some  $\nu \in i\mathbb{R}$  close to zero.

**Hypothesis 3.2** *The linear dispersion relation is dissipative so that  $d_{\parallel} := \lambda_{\text{lin}}''(0) > 0$ . Furthermore, the spectrum of  $\mathcal{L}_{\text{wt}}$  on  $L^2(\mathbb{R}, \mathbb{C}^n)$  lies in the open left half-plane except for the spectrum near  $\check{\lambda} = 0$  which is captured by the linear dispersion relation  $\check{\lambda} = \lambda_{\text{lin}}(\nu)$  with  $\nu \in i\mathbb{R}$  close to zero.*

The coefficient  $d_{\parallel}$  measures the effective diffusion rate of perturbations in the direction of propagation of the wave train (see (1.19)). Planar wave trains in  $x \in \mathbb{R}^2$  have an additional diffusion coefficient  $d_{\perp}$  that measures diffusive decay of perturbations transverse to the direction of propagation.

Hypothesis 3.1 implies that there exists a family  $u_{\text{wt}}(kx - \omega t; k)$  of wave trains, defined for  $k$  close to  $k_0$ , which are stable and whose frequency is given by a smooth nonlinear dispersion relation  $\omega = \omega_{\text{nl}}(k)$  with  $\omega_{\text{nl}}(k_0) = \omega_0$ .

**Hypothesis 3.3** *We assume that the nonlinear dispersion relation is genuinely nonlinear which means that  $\omega_{\text{nl}}''(k_0) \neq 0$ .*

We denote the phase and group velocities by

$$c_{\text{p}} = \frac{\omega_{\text{nl}}(k)}{k}, \quad c_{\text{g}} = \frac{d\omega_{\text{nl}}(k)}{dk}. \quad (3.5)$$

Using these definitions, it turns out [10, 52] that the Taylor series of the linear dispersion relation  $\lambda_{\text{lin}}(\nu)$  at  $\nu = 0$  is given by

$$\lambda_{\text{lin}}(\nu) = [c_{\text{p}} - c_{\text{g}}]\nu + d_{\parallel}\nu^2 + \mathcal{O}(\nu^3). \quad (3.6)$$

### 3.2 Spectra of wave trains in different frames

We discuss the dependence of the linear dispersion relation on the frame in which it is computed. This issue will play a crucial role below. Consider the reaction-diffusion equation (1.1) in a frame moving with an arbitrary, but fixed, speed  $c_{\text{d}}$ . In the variable  $\xi = x - c_{\text{d}}t$ , we get

$$\phi = k_0x - \omega_0t = k_0\xi - (\omega_0 - k_0c_{\text{d}})t.$$

Thus, we set  $\omega_{\text{d}} = \omega_0 - k_0c_{\text{d}}$  and define  $\tau = \omega_{\text{d}}t$ . In the  $(\xi, \tau)$  coordinates, (1.1) becomes

$$\omega_{\text{d}}u_{\tau} = Du_{\xi\xi} + c_{\text{d}}u_{\xi} + f(u), \quad (3.7)$$

and the wave trains are time-periodic solutions  $u(\xi, \tau) = u_{\text{wt}}(k_0\xi - \tau)$  with period  $2\pi$  in  $\tau$ .

Following Section 2.2, we linearize the period map of (3.7) about the wave train, so that

$$\Phi_{\text{wt}} : u(\xi, 0) \mapsto u(\xi, 2\pi)$$

is the solution map of the linear equation

$$\omega_{\text{d}}u_{\tau} = Du_{\xi\xi} + c_{\text{d}}u_{\xi} + f'(u_{\text{wt}}(k_0\xi - \tau))u.$$

Note that the operator  $\Phi_{\text{wt}}$  is not Fredholm on  $L^2(\mathbb{R}, \mathbb{C}^n)$ . Its spectrum can be computed as follows [44]. A non-zero number  $\rho \in \mathbb{C}$  is in the spectrum of  $\Phi_{\text{wt}}$  if, and only if, the linearized eigenvalue problem

$$\lambda u = Du_{\xi\xi} + c_{\text{d}}u_{\xi} - \omega_{\text{d}}u_{\tau} + f'(u_{\text{wt}}(k_0\xi - \tau))u \quad (3.8)$$

has a bounded non-zero solution  $u(\xi, \tau)$  that is  $2\pi$ -periodic in  $\tau$ , where the Floquet multiplier  $\rho$  and the Floquet exponent  $\lambda$  are related via  $\rho = \exp(2\pi\lambda/\omega_{\text{d}})$ . These solutions can be calculated using the Floquet ansatz

$$u(\xi, \tau) = e^{\nu\xi} w(k_0\xi - \tau) \quad (3.9)$$

where  $w(\phi)$  is  $2\pi$ -periodic and  $\nu \in i\mathbb{R}$ . Upon substituting this ansatz into (3.8), we see after some calculations that  $w$  needs to satisfy the equation

$$[\lambda + (c_{\text{p}} - c_{\text{d}})\nu]w = D[k_0\partial_{\phi} + \nu]^2 w + c_{\text{p}}[k_0\partial_{\phi} + \nu]w + f'(u_{\text{wt}}(\phi))w \quad (3.10)$$

where  $c_p = \omega_0/k_0$  is the phase speed of the wave trains.

Comparing (3.10) with (3.4), we see that  $\check{\lambda}$  is in the spectrum of the wave trains, computed in the frame moving with the phase speed  $c_p$ , if, and only if,

$$\lambda = \check{\lambda} + (c_d - c_p)\nu \quad (3.11)$$

is a Floquet exponent of  $\Phi_{\text{wt}}$ , computed in a frame moving with speed  $c_d$ , where  $\nu \in i\mathbb{R}$  is the associated spatial Floquet exponent. We denote by  $\Sigma_{\text{wt}}$  the set of all Floquet exponents  $\lambda$  of  $\Phi_{\text{wt}}$ .

In particular, it follows from (3.6) that  $\lambda$  close to zero is in the Floquet spectrum of  $\Phi_{\text{wt}}$  on  $L^2(\mathbb{R}, \mathbb{C}^n)$ , computed in the frame moving with speed  $c_d$ , if, and only if,

$$\lambda = \lambda_{\text{lin}}(\nu) + (c_d - c_p)\nu = [c_d - c_g]\nu + d_{\parallel}\nu^2 + O(\nu^3) \quad (3.12)$$

for some  $\nu \in i\mathbb{R}$  close to zero. Note that  $c_g - c_d$  represents the relative group velocity, i.e., the group velocity of the wave trains measured in the frame that moves with speed  $c_d$ .

### 3.3 Spatially homogeneous oscillations

In this section, we account for the differences that occur when the wavenumber of the wave trains vanish. In other words, we consider spatially homogeneous oscillations  $u(x, t) = u_{\text{wt}}(-\omega_0 t)$  where  $\omega_0 \neq 0$  and  $u'_{\text{wt}}(\phi)$  is not the zero function.

The spectrum of the period map  $\Phi_{\text{wt}}$  associated with the spatially homogeneous oscillations can be computed easily. Indeed, Fourier transform in space reduces the time-periodic linearized parabolic equation

$$\omega_d u_\tau = Du_{\xi\xi} + c_d u_\xi + f'(u_{\text{wt}}(-\tau))u \quad (3.13)$$

to the collection

$$\omega_d \hat{u}_\tau = \nu^2 D\hat{u} + c_d \nu \hat{u} + f'(u_{\text{wt}}(-\tau))\hat{u} \quad (3.14)$$

of ODEs for purely imaginary Fourier exponents  $\nu = i\gamma$  with  $\gamma \in \mathbb{R}$ . Note that  $\omega_d = \omega_0$  since  $k_0 = 0$ . We denote by  $\rho = \exp(2\pi\lambda/\omega_d)$  the complex temporal Floquet multipliers of the parabolic equation (3.13).

First, we need to replace Hypothesis 3.1 by the assumption that  $\rho = 0$  is an algebraically simple multiplier for  $\nu = 0$  and  $c_d = 0$ . This allows us to continue the Floquet multiplier  $\rho$  as smooth function  $\rho = \rho(\nu)$  for any  $\nu$  close to zero. The resulting dispersion relation for the temporal Floquet exponents is denoted by  $\lambda(\nu)$  where  $\lambda(0) = 0$ . When  $c_d = 0$ ,  $\nu$  enters only at quadratic order so that

$$\lambda = d_{\parallel}\nu^2 + O(\nu^4).$$

Applying Fenichel's singular perturbation theory [15] to (3.1), it is straightforward to see that the spatially homogeneous oscillations are accompanied by a family of wave trains for wavenumbers

$k$  close to zero<sup>5</sup>, where wavenumber and frequency are related via a smooth nonlinear dispersion relation  $\omega_{\text{nl}}(k)$ .

Next, we replace Hypothesis 3.2 by the assumption that  $d_{\parallel} > 0$  and that the curve  $\lambda(\nu)$ , with  $\nu$  close to the origin, captures all temporal Floquet exponents of the collection of ODEs (3.14) in the closed right half-plane  $\text{Re } \lambda \geq 0$ . Lastly, we assume that Hypothesis 3.3 is met also when  $k_0 = 0$ . Inspecting the boundary-value problem

$$\lambda \hat{u} = D\nu^2 \hat{u} + c_d \nu \hat{u} + f'(u_{\text{wt}}(-\tau)) \hat{u}, \quad \hat{u}(0) = \hat{u}(2\pi) \quad (3.15)$$

for the temporal Floquet exponents  $\lambda$ , we see immediately that the dispersion relation for  $c_d \neq 0$  is related to the dispersion relation for  $c_d = 0$  via

$$\lambda = \lambda_{\text{lin}}(\nu) + c_d \nu = c_d \nu + d_{\parallel} \nu^2 + \text{O}(\nu^3),$$

which is the equivalent to (3.12) after formally setting  $c_g = 0$ .

### 3.4 Spatial dynamics and relative Morse indices

We explore the implications of the results reviewed in the previous sections for the spatial dynamical system associated with (3.7). Thus, we write (3.7) as

$$\begin{aligned} u_{\xi} &= v \\ v_{\xi} &= D^{-1}[\omega_d \partial_{\tau} u - c_d v - f(u)] \end{aligned} \quad (3.16)$$

where  $\mathbf{u} = (u, v) \in Y = H^{1/2}(S^1, \mathbb{R}^n) \times L^2(S^1, \mathbb{R}^n)$ . One of the key features of (3.16) that we shall exploit over and over again is its equivariance with respect to the  $S^1$ -symmetry

$$\Gamma_{\theta} : Y \longrightarrow Y, \quad (u, v)(\tau) \longmapsto (u, v)(\tau - \theta), \quad \theta \in S^1 \quad (3.17)$$

that is induced by the temporal time shift. Note that the wave trains  $u_{\text{wt}}(k\xi - \tau; k)$  of (1.1) correspond to periodic orbits

$$\mathbf{u}_{\text{wt}}(\xi) = (u_{\text{wt}}(k\xi - \cdot; k), k \partial_{\phi} u_{\text{wt}}(k\xi - \cdot; k))$$

of (3.16) with period  $2\pi/k$  which are, in fact, relative equilibria with respect to the temporal time-shift symmetry. The eigenvalue problem (3.8) becomes

$$\begin{aligned} u_{\xi} &= v \\ v_{\xi} &= D^{-1}[\omega_d \partial_{\tau} u - c_d v - f'(u_{\text{wt}}(k\xi - \tau; k))u + \lambda u]. \end{aligned} \quad (3.18)$$

For each fixed value of  $\lambda$ , we say that  $\nu$  is a spatial Floquet exponent of (3.18) if there is a  $2\pi$ -periodic function  $\mathbf{w}(\phi)$  with values in  $Y$  so that  $\mathbf{u}(\xi) = e^{\nu \xi} \mathbf{w}(k\xi)$  is a solution of (3.18). In fact,

---

<sup>5</sup>In passing, we remark that we are not aware of a short direct proof of this fact that does not use Fenichel's theorem. Ginzburg–Landau approximations of the dynamics near homogeneous oscillations [55] capture waves with long wavelength but are, unfortunately, only valid over finite time intervals.

$\mathbf{w}(k\xi)$  will be of the form  $[\mathbf{w}(k\xi)](\tau) = \check{\mathbf{w}}(k\xi - \tau)$  where the first component of  $\check{\mathbf{w}}$  satisfies (3.10). Note that the spatial Floquet exponents  $\nu$  are not unique, so that we should restrict their imaginary parts to  $0 \leq \text{Im } \nu < k$ .

Spatial Floquet theory [33, 48] implies the following facts. For each fixed  $\lambda$ , there are projections  $P_{\text{wt}}^j(\xi; \lambda) \in L(Y)$ , labelled by  $j = c, s, u$ , with the following properties. The projections are  $2\pi/k$ -periodic and strongly continuous in  $\xi$ , and their sum is the identity. The ranges of the stable and unstable projections  $P_{\text{wt}}^s(\xi_0; \lambda)$  and  $P_{\text{wt}}^u(\xi_0; \lambda)$  are infinite-dimensional and consist of all initial data at  $\xi = \xi_0$  of solutions to (3.18) that decay exponentially for  $\xi \rightarrow \infty$  and  $\xi \rightarrow -\infty$ , respectively. The range of the center projection  $P_{\text{wt}}^c(\xi_0; \lambda)$  is finite-dimensional, and, for each initial value in  $\text{Rg}(P_{\text{wt}}^c(\xi_0; \lambda))$ , the corresponding solution to (3.18) exists for  $\xi \in \mathbb{R}$  and grows at most algebraically in  $\xi$  as  $\xi \rightarrow \pm\infty$ . The ranges of the projections  $P_{\text{wt}}^j(\xi; \lambda)$  can be obtained by taking the closure of the eigenfunctions  $\mathbf{w}(k\xi) \in Y$ , together with the associated generalized eigenfunctions if these exist, of all spatial Floquet exponents  $\nu$  with  $\text{Re } \nu = 0$  for  $j = c$ ,  $\text{Re } \nu > 0$  for  $j = u$ , and  $\text{Re } \nu < 0$  for  $j = s$ .

The center projection  $P_{\text{wt}}^c(\xi; \lambda)$  is non-zero if, and only if,  $\lambda$  is a temporal Floquet exponent of  $\Phi_{\text{wt}}$ . In particular,  $P_{\text{wt}}^c(\xi; \lambda) = 0$  for all  $\lambda$  with  $\text{Re } \lambda > 0$  since  $|\rho| > 1$  belongs to the resolvent set of  $\Phi_{\text{wt}}$ . In this case, the remaining projections  $P_{\text{wt}}^s(\xi; \lambda)$  and  $P_{\text{wt}}^u(\xi; \lambda)$  are analytic in  $\lambda$ . We are interested in counting the dimension of  $\text{Rg}(P_{\text{wt}}^u(\xi; \lambda))$  by comparing it to  $\text{Rg}(P_{\text{wt}}^u(0; \lambda_*))$ , where  $\lambda_*$  is fixed so that  $\text{Re } \lambda_* \gg 1$  is positive.

**Definition 3.4** *The relative Morse index  $i_{\text{wt}}(\lambda)$  is defined to be the Fredholm index of*

$$P_{\text{wt}}^u(\xi; \lambda) : \text{Rg}(P_{\text{wt}}^u(0; \lambda_*)) \longrightarrow \text{Rg}(P_{\text{wt}}^u(\xi; \lambda)). \quad (3.19)$$

We proved in [48] that the relative Morse index is well defined for all  $\lambda$  that are not temporal Floquet exponents of  $\Phi_{\text{wt}}$ . Furthermore, it does not depend on  $\xi$  and on the choice of  $\lambda_*$  (as long as  $\text{Re } \lambda_* > 0$ ).

Hence, the relative Morse index  $i_{\text{wt}}(\lambda)$  is constant on each connected component of  $\mathbb{C} \setminus \Sigma_{\text{wt}}$ , which corresponds to the resolvent set of  $\Phi_{\text{wt}}$ . Note that we have  $i_{\text{wt}}(\lambda) = 0$  for all  $\lambda$  in the connected component of  $\mathbb{C} \setminus \Sigma_{\text{wt}}$  that contains the open right half-plane in  $\mathbb{C}$ . To compute Morse indices, we will use the following straightforward bordering lemma whose proof we shall omit.

**Lemma 3.5** *Suppose that  $\mathcal{X}$  and  $\mathcal{Y}$  are Banach spaces and that  $\mathcal{A} : \mathcal{X} \rightarrow \mathcal{Y}$  is a Fredholm operator with index  $i(\mathcal{A})$ . The operator*

$$\mathcal{S} = \begin{pmatrix} \mathcal{A} & \mathcal{B} \\ \mathcal{C} & \mathcal{D} \end{pmatrix} : \mathcal{X} \times \mathbb{R}^p \longrightarrow \mathcal{Y} \times \mathbb{R}^q$$

*is then Fredholm with index  $i(\mathcal{S}) = i(\mathcal{A}) + p - q$  provided  $\mathcal{B}$ ,  $\mathcal{C}$ , and  $\mathcal{D}$  are bounded and linear.*

The following lemma predicts how the relative Morse index  $i_{\text{wt}}(\lambda)$  changes if we vary  $\lambda$  near  $\lambda = 0$ .

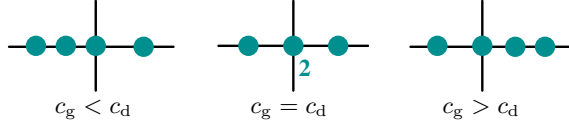


Figure 3.1: The spatial Floquet spectrum of wave trains at  $\lambda = 0$ .

**Lemma 3.6** *Assume that the hypotheses stated in Section 3.1 are met. The spatial dynamical system (3.18) has a geometrically simple spatial Floquet exponent  $\nu = 0$  for  $\lambda = 0$ . The Floquet exponent  $\nu = 0$  is simple if  $c_d \neq c_g$ , while it has algebraic multiplicity two if  $c_d = c_g$ . If  $c_d \neq c_g$ , then (3.18) has a simple spatial Floquet exponent  $\nu = \nu(\lambda)$  for all  $\lambda$  close to zero and*

$$\left. \frac{d\nu}{d\lambda} \right|_{\lambda=0} = \frac{1}{c_d - c_g}. \quad (3.20)$$

For  $\lambda < 0$  close to zero, the relative Morse index  $i_{\text{wt}}(\lambda)$  is therefore  $+1$  if  $c_g > c_d$ , and  $-1$  if  $c_g < c_d$ .

**Proof.** The statement follows immediately from (3.12), the Cauchy–Riemann equations, and the bordering lemma 3.5.  $\blacksquare$

## 4 Spectral properties of defects

We now turn to elementary defects  $u_d(\xi, \tau)$  that satisfy

$$\omega_d u_\tau = Du_{\xi\xi} + c_d u_\xi + f(u). \quad (4.1)$$

We are interested in the spectrum of the linear period map

$$\Phi_d : u(\xi, 0) \longmapsto u(\xi, 2\pi)$$

associated with the linearization

$$\omega_d u_\tau = Du_{\xi\xi} + c_d u_\xi + f'(u_d(\xi, \tau))u$$

of (4.1) about the defect  $u_d(\xi, \tau)$ . We denote by  $\lambda$  the Floquet exponents of  $\Phi_d$  and by  $\rho = \exp(2\pi\lambda/\omega_d)$  its Floquet multipliers, i.e. elements in its spectrum.

We adopt a dynamical-systems point-of-view and write (4.1) as the modulated-wave equation

$$\begin{aligned} u_\xi &= v \\ v_\xi &= D^{-1}[\omega_d \partial_\tau u - c_d v - f(u)]. \end{aligned} \quad (4.2)$$

We write  $\mathbf{u} = (u, v)$  and consider (4.2) on the space  $Y = H^{1/2}(S^1, \mathbb{R}^n) \times L^2(S^1, \mathbb{R}^n)$ . We shall also use the space  $Y^1 = H^1(S^1, \mathbb{R}^n) \times H^{1/2}(S^1, \mathbb{R}^n)$ . We say that  $\mathbf{u}(\xi)$  is a *solution* of (4.2) on an interval  $J \subset \mathbb{R}$  if  $\mathbf{u}$  is contained in  $L^2(J, Y^1) \cap H^1(J, Y)$  and it satisfies (4.2) in  $Y$  for all  $\xi \in J$ .

Definition 1.1 implies that

$$\mathbf{u}_d(\xi) = (u_d(\xi, \cdot), \partial_\xi u_d(\xi, \cdot))$$

satisfies (4.2) and that  $\mathbf{u}_d(\xi, \cdot) - \mathbf{u}_{wt}(k_\pm \xi + \theta_\pm(\xi) - \cdot; k_\pm)$  converges to zero in  $Y^1$  as  $\xi \rightarrow \pm\infty$ .

Throughout this section, we denote by  $\Sigma_{wt}^\pm$  the set of all temporal Floquet exponents  $\lambda$  of the asymptotic wave trains with wavenumber  $k_\pm$ , computed in the frame moving with speed  $c_d$ .

## 4.1 Exponential dichotomies

We begin by analysing the linear system

$$\begin{aligned} u_\xi &= v \\ v_\xi &= D^{-1}[\omega_d \partial_\tau u - c_d v - f'(u_d(\xi, \cdot))u + \lambda u] \end{aligned} \quad (4.3)$$

where the parameter  $\lambda$  represents potential temporal Floquet exponents of  $\Phi_d$ .

Given one of the sets  $J = \mathbb{R}^+$ ,  $J = \mathbb{R}^-$  or  $J = \mathbb{R}$ , we say that (4.3) has an exponential dichotomy on  $J$  if there exist strongly continuous families  $\{\Phi^s(\xi, \zeta)\}_{\xi \geq \zeta, \xi, \zeta \in J}$  and  $\{\Phi^u(\xi, \zeta)\}_{\xi \leq \zeta, \xi, \zeta \in J}$  of operators in  $L(Y)$  as well as positive constants  $C$  and  $\kappa$  such that

- $\Phi^j(\xi, \sigma)\Phi^j(\sigma, \zeta) = \Phi^j(\xi, \zeta)$  for  $j = s, u$  and  $\Phi^s(\xi, \xi) + \Phi^u(\xi, \xi) = \mathbb{1}$ ,
- $\|\Phi^s(\xi, \zeta)\| + \|\Phi^u(\zeta, \xi)\| \leq Ce^{-\kappa|\xi - \zeta|}$ ,
- $\Phi^s(\xi, \zeta)\mathbf{u}_0$  and  $\Phi^u(\xi, \zeta)\mathbf{u}_0$  satisfy (4.3) for  $\xi > \zeta$  and for  $\xi < \zeta$ , respectively, for each  $\mathbf{u}_0 \in Y$  provided  $\xi, \zeta \in J$ .

Thus, if a dichotomy<sup>6</sup> exists, then the operators  $P^j(\xi) := \Phi^j(\xi, \xi)$  with  $j = s, u$  are complementary projections in  $Y$ . We denote their ranges at  $\xi = 0$  by  $E^s(\lambda)$  and  $E^u(\lambda)$  where  $E^s(\lambda) \oplus E^u(\lambda) = Y$ .

Corollary A.2 in Appendix A.1 states that (4.3) has an exponential dichotomy on  $J = \mathbb{R}^\pm$  if, and only if, the asymptotic equation

$$\begin{aligned} u_\xi &= v \\ v_\xi &= D^{-1}[\omega_d \partial_\tau u - c_d v - f'(u_{wt}(k_\pm \xi - \cdot; k_\pm))u + \lambda u] \end{aligned} \quad (4.4)$$

has an exponential dichotomy on  $\mathbb{R}$ . Furthermore, the projections  $P_{wt, \pm}^j(\xi)$  of the asymptotic equation (4.4) and those of the linearization (4.3) about the defect differ only by a compact operator.

Thus, it remains to find out when the asymptotic equation has an exponential dichotomy on  $\mathbb{R}$ . The criterion in [33] for the existence of dichotomies to (4.4) is simply that it does not have purely imaginary Floquet exponents  $\nu \in i\mathbb{R}$ , i.e. solutions of the form  $\mathbf{u}(\xi) = \exp(\nu\xi)\mathbf{w}(k\xi)$  for some  $2\pi$ -periodic function  $\mathbf{w}$ . Using the results reviewed in Section 3, we can therefore conclude that (4.4) has an exponential dichotomy on  $\mathbb{R}$  precisely when  $\lambda \notin \Sigma_{wt}^\pm$ .

Lastly, we discuss what happens if the asymptotic equation does not have an exponential dichotomy. Since the Floquet multipliers of the asymptotic equation form a discrete set and accumulate at the

<sup>6</sup>The dichotomies and projections will depend on  $\lambda$ . We will suppress this dependence in our notation.

origin [33], there are at most a finite number of them on the unit circle for any given  $\lambda$ . The idea is then to seek solutions to (4.3) of the form

$$\mathbf{u}(\xi) = e^{\eta\xi} \check{\mathbf{u}}(\xi) \quad (4.5)$$

for a small non-zero weight  $\eta$ , so that  $\check{\mathbf{u}}(\xi)$  satisfies the equation

$$\begin{aligned} \check{u}_\xi &= -\eta\check{u} + \check{v} \\ \check{v}_\xi &= -\eta\check{v} + D^{-1}[\omega_d \partial_\tau \check{u} - c_d \check{v} - f'(u_d(\xi, \tau))\check{u} + \lambda\check{u}]. \end{aligned} \quad (4.6)$$

Suppose now that at least one spatial Floquet exponent  $\nu = i\gamma$  of (4.3) lies on the imaginary axis. A small exponential weight  $\eta \neq 0$  will move this Floquet multiplier off the imaginary axis. Exploiting the conjugacy (4.5) between solutions to (4.6) and (4.3), we can construct center-stable dichotomies  $\Phi^{\text{cs}}(\xi, \zeta)$  and complementary strong-unstable dichotomies  $\Phi^{\text{uu}}(\xi, \zeta)$  for (4.3) by using the stable and unstable dichotomies of (4.6) for sufficiently small, but non-zero, weights  $\eta > 0$ . Analogously, upon using  $\eta < 0$  close to zero, we find center-unstable and strong-stable dichotomies,  $\Phi^{\text{cu}}(\xi, \zeta)$  and  $\Phi^{\text{ss}}(\xi, \zeta)$ , respectively, for (4.3). We can use these dichotomies to define a center projection

$$\text{Rg}(\Phi^c(\xi, \xi)) := \text{Rg}(\Phi^{\text{cs}}(\xi, \xi)) \cap \text{Rg}(\Phi^{\text{cu}}(\xi, \xi)), \quad \text{N}(\Phi^c(\xi, \xi)) := \text{N}(\Phi^{\text{cs}}(\xi, \xi)) + \text{N}(\Phi^{\text{cu}}(\xi, \xi))$$

and a corresponding center evolution  $\Phi^c(\xi, \zeta)$  for all  $\xi, \eta \in J$ . Since the unstable subspaces for  $J = \mathbb{R}^+$  are arbitrary at  $\xi = 0$  [38], we may also arrange that

$$\Phi^{\text{cu}}(\xi, \zeta) = \Phi^c(\xi, \zeta) + \Phi^{\text{uu}}(\xi, \zeta), \quad \Phi^{\text{cs}}(\xi, \zeta) = \Phi^c(\xi, \zeta) + \Phi^{\text{ss}}(\xi, \zeta).$$

We use subscripts  $\pm$  to distinguish the exponential dichotomies on  $\mathbb{R}^+$  and on  $\mathbb{R}^-$ .

## 4.2 Fredholm indices

Suppose that  $\lambda$  is not a temporal Floquet exponent of either one of the asymptotic wave trains, i.e.  $\lambda \notin \Sigma_{\text{wt}}^- \cup \Sigma_{\text{wt}}^+$ . The discussion in the preceding section shows that (4.3) has exponential dichotomies on both  $\mathbb{R}^+$  and  $\mathbb{R}^-$ . We denote by  $E_+^s(\lambda)$  the stable subspace at  $\xi = 0$  of the dichotomy on  $\mathbb{R}^+$  and by  $E_-^u(\lambda)$  the unstable subspace at  $\xi = 0$  of the dichotomy on  $\mathbb{R}^-$ . Thus, we conclude that there exists a bounded solution to the linear equation (4.3) if, and only if,  $E_-^u(\lambda)$  and  $E_+^s(\lambda)$  intersect non-trivially.

For each  $\lambda \notin \Sigma_{\text{wt}}^- \cup \Sigma_{\text{wt}}^+$ , we therefore define the injection map

$$\iota(\lambda) : E_-^u(\lambda) \times E_+^s(\lambda) \longrightarrow Y, \quad (\mathbf{u}^-, \mathbf{u}^+) \longmapsto \mathbf{u}^- - \mathbf{u}^+.$$

Since the evolutions  $\Phi_\pm^j$  with  $j = s, u$  can be chosen to depend analytically on  $\lambda$  [48], the injection map  $\iota$  is analytic in  $\lambda$ . Whenever  $\iota(\lambda_*)$  is Fredholm of index zero with a non-trivial null space, we can use Lyapunov–Schmidt-reduction to reduce the equation  $\iota(\lambda) = 0$  in a neighborhood of  $\lambda_*$  to an equation  $\iota_{\text{red}}(\lambda) = 0$  where

$$\iota_{\text{red}}(\lambda) : \text{N}(\iota(\lambda_*)) \longrightarrow \text{Rg}(\iota(\lambda_*))^\perp$$

for  $\lambda$  close to  $\lambda_*$ . Non-trivial intersections are then given by zeros of the reduced Evans function

$$\mathcal{E}(\lambda) = \det(\iota_{\text{red}}(\lambda)).$$

Recall that Floquet exponents  $\lambda$  and Floquet multipliers  $\rho$  of the linear period map  $\Phi_{\text{d}}$  are related via  $\rho = \exp(2\pi\lambda/\omega_{\text{d}})$ . We also denote by  $i(\mathcal{A})$  the index of a Fredholm operator  $\mathcal{A}$ .

**Lemma 4.1** *The linear operator  $\Phi_{\text{d}} - \rho$  on  $L^2(\mathbb{R}, \mathbb{C}^n)$  is Fredholm if, and only if,  $\lambda \notin \Sigma_{\text{wt}}^- \cup \Sigma_{\text{wt}}^+$ . Furthermore, if  $\lambda \notin \Sigma_{\text{wt}}^- \cup \Sigma_{\text{wt}}^+$ , then the Fredholm index of  $\Phi_{\text{d}} - \rho$  on  $L^2(\mathbb{R}, \mathbb{C}^n)$  is given by*

$$i(\Phi_{\text{d}} - \rho) = i(\iota(\lambda)) = i_{\text{wt}}^-(\lambda) - i_{\text{wt}}^+(\lambda)$$

where  $i_{\text{wt}}^\pm(\lambda)$  are the relative Morse indices of the asymptotic wave trains defined in Section 3.4. Lastly, if the Fredholm index is zero, then roots  $\lambda$  of the reduced Evans function  $\mathcal{E}(\lambda)$  correspond to isolated eigenvalues  $\rho$  of  $\Phi_{\text{d}}$ , and the order of a root  $\lambda$  is equal to the algebraic multiplicity of the corresponding Floquet multiplier  $\rho$  of  $\Phi_{\text{d}}$ .

**Proof.** The relation between properties of the linearized period map  $\Phi_{\text{d}}$  and the bundles  $E_+^s(\lambda)$  and  $E_-^u(\lambda)$  was shown in [48, Remark 2.5 and Theorem 2.6]. The fact that the order of roots of the reduced Evans function coincides with the algebraic multiplicity of the associated Floquet multiplier is a straightforward adaptation of the corresponding facts for eigenvalue problems of travelling waves.  $\blacksquare$

Since we assumed that the wave trains are spectrally stable, we know that  $\text{Re } \lambda > 0$  lies in the resolvent set of  $\Phi_{\text{d}}$  (in the Floquet-exponent space). This fact allows us to compute the Fredholm indices of the map

$$\iota_{\text{d}}(\lambda) : E_-^{\text{cu}}(\lambda) \times E_+^{\text{cs}}(\lambda) \longrightarrow Y, \quad (\mathbf{u}^-, \mathbf{u}^+) \longmapsto \mathbf{u}^- - \mathbf{u}^+$$

for each of the four defect classes for  $\lambda$  close to zero, where we set  $E_-^{\text{cu}}(\lambda) := \text{Rg}(\Phi_-^{\text{cu}}(0, 0))$  and  $E_+^{\text{cs}}(\lambda) := \text{Rg}(\Phi_+^{\text{cs}}(0, 0))$ . Note that, by using small exponential weights as outlined in the preceding section, we can choose the dichotomies  $\Phi_-^{\text{cu}}$  and  $\Phi_+^{\text{cs}}$  so that they depend analytically on  $\lambda$  for  $\lambda$  close to zero [48]. We then have the following result.

**Lemma 4.2** *The Fredholm index  $i$  of  $\iota_{\text{d}}(0)$  is equal to*

$$\begin{aligned} i = 2 & && \text{for sinks and contact defects} \\ i = 1 & && \text{for transmission defects} \\ i = 0 & && \text{for sources.} \end{aligned}$$

**Proof.** First, the Fredholm index of  $\iota_{\text{d}}(0)$  is given by the difference of the Morse indices of the projections  $P_{\text{wt},-}^{\text{cu}}(0)$  and  $P_{\text{wt},+}^{\text{cs}}(0)$  associated with the asymptotic wave trains. Indeed, we can apply Lemma 4.1 to the equation

$$\begin{aligned} \check{u}_\xi &= -\check{\eta}(\xi)\check{u} + \check{v} \\ \check{v}_\xi &= -\check{\eta}(\xi)\check{v} + D^{-1}[\omega_{\text{d}}\partial_\tau\check{u} - c_{\text{d}}\check{v} - f'(u_{\text{d}}(\xi, \tau))\check{u} + \lambda\check{u}] \end{aligned}$$

where  $\check{\eta}(\xi) = -\eta \operatorname{sign} \xi$  for some small  $\eta > 0$ . It therefore remains to compute the Morse indices.

For contact defects, the center subspace is two-dimensional, and the two spatial Floquet exponents  $\nu_{1,2}$  are determined by (3.12) with  $c_d = c_g$  so that  $\nu_j^2 = \lambda/d_{\parallel} + O(|\lambda|^{3/2})$  where  $d_{\parallel} > 0$  by Hypothesis 3.2. In particular,  $\nu_1$  and  $\nu_2$  have opposite real parts for  $\lambda > 0$ . At  $\lambda = 0$ , the center-stable subspace  $E_{\text{wt},+}^{\text{cs}}$  and the center-unstable subspace  $E_{\text{wt},-}^{\text{cu}}$  are therefore both augmented by one-dimensional subspaces compared with the subspaces in the Fredholm index zero regime. Invoking the bordering lemma 3.5 shows that the index of  $\iota_d$  is two.

For the other defects, the center subspace is one-dimensional. To illustrate the idea, we consider the center-stable subspace  $E_{\text{wt},+}^{\text{cs}}$  when  $c_g^+ < c_d$ , i.e., when transport occurs towards the defect. Lemma 3.6 shows that the real part of the critical Floquet exponent  $\nu$  is positive for  $\lambda > 0$ , and the center subspace continues therefore as part of the center-stable subspace so that  $E_{\text{wt},+}^{\text{cs}}(\lambda) = E_{\text{wt},+}^{\text{c}}(\lambda) \oplus E_{\text{wt},+}^{\text{s}}(\lambda)$ . The same argument proves that  $E_{\text{wt},+}^{\text{cs}}(\lambda) = E_{\text{wt},+}^{\text{s}}(\lambda)$  whenever  $c_g^+ > c_d$  so that transport occurs away from the defect. The analogous statements for  $E_{\text{wt},-}^{\text{cu}}$  show that the subspace  $E_{\text{wt},-}^{\text{u}}$  is again augmented by a one-dimensional subspace when the transport is towards the defect so that  $c_g^- > c_d$ . Invoking the bordering lemma 3.5, it is now straightforward to compute the Fredholm indices of  $\iota_d$  for sources, sinks, and transmission defects.  $\blacksquare$

### 4.3 Spectral stability of defects

We conclude this exposition of the linear theory by commenting on the effects of exponential weights on the spectra of defects. The discussion of weights in Section 4.1 together with Lemma 4.1 can be used to infer useful properties of the spectra of the linearized period map in the exponentially weighted spaces

$$L_{\eta_-, \eta_+}^2 = \left\{ u \in L_{\text{loc}}^2; \|u\|_{L_{\eta_-, \eta_+}^2} < \infty \right\}, \quad \|u\|_{L_{\eta_-, \eta_+}^2}^2 = \int_{\mathbb{R}^-} |u(\xi)e^{\eta_-\xi}|^2 d\xi + \int_{\mathbb{R}^+} |u(\xi)e^{\eta_+\xi}|^2 d\xi.$$

Indeed, the linearized period map  $\Phi_d - \rho$  is Fredholm on  $L_{\eta_-, \eta_+}^2$  precisely if there are no spatial Floquet exponents  $\nu_{\pm}$  of the asymptotic wave trains  $\mathbf{u}_{\text{wt},\pm}$  for which  $\operatorname{Re} \nu_{\pm} = -\eta_{\pm}$ . Invoking (3.12),

$$\lambda = [c_d - c_g^{\pm}] \nu + d_{\parallel} \nu^2 + O(\nu^3)$$

with  $d_{\parallel} > 0$ , we see that the critical dispersion curve  $\lambda(\nu)$  moves into the left half-plane provided the weights  $\eta_{\pm}$  satisfy  $\pm\eta_{\pm} > 0$  (thus enforcing localization of  $u(\xi)$ ) when transport occurs towards the defect, whereas the weights  $\eta_{\pm}$  have to satisfy  $\pm\eta_{\pm} < 0$  (thus allowing exponential growth) when transport is away from the defect. In formulas, we need

$$\operatorname{sign}[c_d - c_g^{\pm}] = \operatorname{sign} \operatorname{Re} \nu \neq \operatorname{sign}[-\eta_{\pm}]$$

to ensure that the Floquet spectrum lies in  $\operatorname{Re} \lambda < 0$ , which is equivalent to choosing  $\eta_{\pm}$  such that

$$\operatorname{sign} \eta_{\pm} = \operatorname{sign}[c_d - c_g^{\pm}].$$

In summary, we have proved the following result.

**Lemma 4.3** *The essential Floquet spectrum of the period map, linearized about sinks, sources and transmission defects, is contained in the open left half-plane when considered on  $L^2_{\eta_-, \eta_+}$  for any choice of weights  $\eta_{\pm}$  close to zero so that*

$$\begin{aligned} \eta_- < 0 < \eta_+ & \quad \text{for sinks with } c_g^- > c_d > c_g^+ \\ \eta_-, \eta_+ > 0 & \quad \text{for transmission defects with } c_g^\pm < c_d \\ \eta_- > 0 > \eta_+ & \quad \text{for sources with } c_g^- < c_d < c_g^+. \end{aligned}$$

*The essential Floquet spectrum of contact defects intersects the right half-plane in any  $L^2_{\eta_-, \eta_+}$  space with exponential weights  $\eta_- \neq 0$  or  $\eta_+ \neq 0$ .*

The next lemma gives lower bounds for the multiplicity of  $\lambda = 0$  as an isolated eigenvalue of the linearization  $\Phi_d$  about each defect when considered on  $L^2_{\eta_-, \eta_+}$  with  $\eta_{\pm}$  chosen as in Lemma 4.3. We also refer to Figure 6.1.

**Lemma 4.4** *Assume that there is a  $\delta > 0$  such that*

$$\partial_\tau \mathbf{u}_d(\xi, \cdot) = -\mathbf{u}'_{\text{wt}}(k_{\pm}\xi - \cdot) + O(e^{-\delta|\xi|}), \quad \partial_\xi \mathbf{u}_d(\xi, \cdot) = k_{\pm} \mathbf{u}'_{\text{wt}}(k_{\pm}\xi - \cdot) + O(e^{-\delta|\xi|}) \quad (4.7)$$

*for  $|\xi| \rightarrow \infty$ . The geometric multiplicity of  $\lambda = 0$  as an eigenvalue in the point spectrum of the linearized period map  $\Phi_d$  posed on  $L^2_{\eta_-, \eta_+}$  with  $\eta_{\pm}$  chosen as in Lemma 4.3 is then at least equal to*

$$\begin{aligned} 0 & \quad \text{for sinks} \\ 1 & \quad \text{for transmission defects} \\ 2 & \quad \text{for sources.} \end{aligned}$$

**Proof.** Any linear combination of  $\partial_\tau u_d$  and  $\partial_\xi u_d$  satisfies the linearized equation and is time-periodic with the correct period. We have to check which of these linear combinations belongs to the space  $L^2_{\eta_-, \eta_+}$  with  $\eta_{\pm}$  chosen as in Lemma 4.3. For sinks, there is nothing to prove. For transmission defects with  $c_d > c_g^\pm$ , eigenfunctions need to be exponentially localized as  $\xi \rightarrow \infty$ . By assumption,  $(k_+ \partial_\tau + \partial_\xi) \mathbf{u}_d(\xi, \cdot)$  generates a one-dimensional subspace of solutions that decay exponentially with rate  $\delta$  at  $\xi = \infty$ . For sources, the exponential weights allow for exponential growth. Thus, any linear combination of  $\partial_\tau u_d$  and  $\partial_\xi u_d$  contributes to the null space of  $\Phi_d$ . ■

The following result for contact defects has been proved in [49]. It will not be relevant for the robustness results in Theorem 1, although it is crucial for various dynamical stability considerations.

**Theorem 2 ([49])** *Let  $\Omega = \{\lambda \in \mathbb{C}; |\lambda| < \delta\}$ , where  $\delta > 0$  is sufficiently small. We consider a contact defect and assume that the null space of the map  $\iota_d(0)$  is two-dimensional. There exists then an analytic Evans function  $\mathcal{E}(\lambda)$ , defined for  $\lambda \in \Omega \setminus \mathbb{R}^-$ , whose roots, counted with their order, are in 1-1 correspondence with Floquet multipliers  $\exp(2\pi\lambda/\omega_d)$ , counted with algebraic multiplicity, of the linearization  $\Phi_d$  of the period map about a contact defect. Moreover,  $\mathcal{E}$  can be extended into  $\lambda = 0$  as a  $C^2$ -function of  $\sqrt{\lambda}$ , and we have  $\mathcal{E}(0) = 0$  and  $\mathcal{E}'(0) \neq 0$  so that  $\lambda = 0$  is a Floquet exponent with algebraic multiplicity one.*

Lastly, we state the following corollary which we shall exploit later. Note that the adjoint equation associated with (1.10) is given by

$$\omega_d u_\tau = Du_\xi \xi - c_d u_\xi + f'(u_d(\xi, \tau))^* u. \quad (4.8)$$

We denote its period map by  $\Phi_d^{\text{ad}}$ .

**Corollary 4.5** *Assume that  $u_d(\xi, \tau)$  is a transverse source. The null space of the adjoint operator  $\Phi_d^{\text{ad}} - \mathbf{1}$  on  $L^2(\mathbb{R}, \mathbb{C}^n)$  is at least two-dimensional and contains two linearly independent functions  $\psi_d^c(\xi, 0)$  and  $\psi_d^\omega(\xi, 0)$  that satisfy*

$$\int_{\mathbb{R}} \begin{pmatrix} \langle \psi_d^c(\xi, 0), \partial_\xi u_d(\xi, 0) \rangle & \langle \psi_d^c(\xi, 0), \partial_\tau u_d(\xi, 0) \rangle \\ \langle \psi_d^\omega(\xi, 0), \partial_\xi u_d(\xi, 0) \rangle & \langle \psi_d^\omega(\xi, 0), \partial_\tau u_d(\xi, 0) \rangle \end{pmatrix} d\xi = \begin{pmatrix} 1 & 0 \\ 0 & 1 \end{pmatrix}.$$

Furthermore, the corresponding solutions  $\psi_d^c(\xi, \tau)$  and  $\psi_d^\omega(\xi, \tau)$  of (4.8) decay exponentially with a uniform rate as  $\xi \rightarrow \pm\infty$  for all  $\tau$ .

**Proof.** The corollary is a consequence of [48, Lemma 5.1 and Section 6] and Lemma 4.3 and 4.4. Note that these results imply that  $\Phi_d^{\text{ad}} - \mathbf{1}$  is bounded and Fredholm with index zero on  $L^2_{-\eta}(\mathbb{R}, \mathbb{C}^n)$  where  $\eta = (\eta_-, \eta_+)$  is chosen as in Lemma 4.3. ■

## 5 Robustness of defects in oscillatory media

### 5.1 Invariant manifolds

We begin by investigating the existence of stable and unstable manifolds for the ill-posed equation (4.2)

$$\begin{aligned} u_\xi &= v \\ v_\xi &= D^{-1}[\omega_d \partial_\tau u - c_d v - f(u)]. \end{aligned}$$

Throughout this section, we fix an integer  $1 \leq \ell < \infty$  and use the term *smooth* to refer to functions of class  $C^\ell$ .

We define the *stable manifold* of the wave train  $\mathbf{u}_{\text{wt}}$  to be the set of initial conditions  $\mathbf{u}_0$  for which there exists a solution  $\mathbf{u}(\xi)$  of (4.2) with  $\mathbf{u}(0) = \mathbf{u}_0$  and a continuous phase function  $\theta(\xi)$  such that

$$\|\mathbf{u}(\xi) - \mathbf{u}_{\text{wt}}(k\xi + \theta(\xi); k)\|_Y \rightarrow 0$$

as  $\xi \rightarrow \infty$ . The *unstable manifold* is defined in the same way with the limit considered as  $\xi \rightarrow -\infty$ . A *center manifold*  $\mathcal{W}^c$  is a locally invariant manifold that contains all solutions which stay in a sufficiently small neighborhood of the orbit  $\mathbf{u}_{\text{wt}}(k\xi - \cdot)$  for all  $\xi \in \mathbb{R}$ . Local invariance means that, for each  $\mathbf{u}_0 \in \mathcal{W}^c$ , there exists a constant  $\delta > 0$  and a solution  $\mathbf{u}(\xi) \in \mathcal{W}^c$ , defined for  $|\xi| < \delta$ , with  $\mathbf{u}(0) = \mathbf{u}_0$ . Similarly, *center-stable* and *center-unstable manifolds* are locally invariant in forward

and backward  $\xi$ -direction, respectively, and contain all solutions that stay in a sufficiently small neighborhood of the wave-train orbit for all  $\xi \in \mathbb{R}^+$  and  $\mathbb{R}^-$ , respectively. The *strong-stable manifold* of a point  $\mathbf{u}_{\text{wt}}(\theta)$  consists of all  $\mathbf{u}_0$  for which there is a solution  $\mathbf{u}(\xi)$  with  $\|\mathbf{u}(\xi) - \mathbf{u}_{\text{wt}}(k\xi + \theta - \cdot)\|_Y \rightarrow 0$  as  $\xi \rightarrow \infty$ . The *strong-unstable manifold* is defined analogously using the limit  $\xi \rightarrow -\infty$ .

We say that the above manifolds are *smooth* if they are smooth as manifolds *and* if the solutions  $\mathbf{u}(\xi; \mathbf{u}_0)$  define smooth local semiflows for  $\xi \geq 0$  and/or  $\xi \leq 0$  for initial data  $\mathbf{u}_0$  in these manifolds. We say that the center-stable manifold is smoothly fibered over the center manifold if it is the union of disjoint smooth fibers that intersect the center manifold transversely, depend continuously on the base point in the center manifold, and are mapped into each other by the local semiflow. We say that the above manifolds are *local* if they contain all solutions with the prescribed behavior whose initial data are close to the defect  $\mathbf{u}_d(0)$  and its  $\tau$ -translates. The following result will be proved in Appendix A.1.

**Theorem 3** *Each wave train has smooth local strong-stable, center-stable, center-unstable and strong-unstable manifolds that depend smoothly on the parameters  $c$  and  $\omega$ . If  $c_d \neq c_g$ , the center-stable and center-unstable manifolds are smoothly fibered by the union of the strong-stable and strong-unstable manifolds. The latter manifolds are parametrized by the asymptotic phase  $\theta$  of the periodic wave train that the solutions approach. The center-stable (center-unstable) manifolds can be chosen so large that the given orbit  $\{\mathbf{u}_d(\xi); \xi \geq 0\}$  ( $\{\mathbf{u}_d(\xi); \xi \leq 0\}$ ) and its  $\tau$ -translates are contained in their interior. The tangent space of the invariant manifolds evaluated at the defect  $\mathbf{u}_d(0)$  coincide with the corresponding ranges  $E_{\pm}^j(0)$ , with  $j = \text{ss, cs, s, c, u, cu, uu}$ , of the exponential dichotomies for the linearized equation (4.3) with  $\lambda = 0$  that we constructed in Section 4.1.*

**Corollary 5.1** *Sinks, sources, and transmission defects have an asymptotic phase. More precisely, there are constants  $\delta > 0$  and  $\theta_{\pm} \in \mathbb{R}$  such that*

$$\mathbf{u}_d(\xi) = \mathbf{u}_{\text{wt}}(k_{\pm}\xi - \cdot + \theta_{\pm}; k_{\pm}) + O(e^{-\delta|\xi|})$$

in  $Y$  as  $|\xi| \rightarrow \infty$ . The same estimate is true for the derivatives with respect to  $\xi$  and  $\tau$ . In particular, Hypothesis (4.7) in Lemma 4.4 is automatically satisfied for sinks, sources, and transmission defects.

The following proposition is a reformulation of Lemma 4.2 using Theorem 3.

**Proposition 5.2** *Denote by  $E_-^{\text{cu}}$  and  $E_+^{\text{cs}}$  the tangent spaces of the center-unstable and the center-stable manifold at  $\mathbf{u}_d(0)$ . The injection map*

$$\iota : W_-^{\text{cu}} \times W_+^{\text{cs}} \longrightarrow Y, \quad (\mathbf{u}^-, \mathbf{u}^+) \longmapsto \mathbf{u}^- - \mathbf{u}^+ \quad (5.1)$$

is Fredholm, i.e., it has continuous derivatives near  $\mathbf{u}^- = \mathbf{u}^+ = \mathbf{u}_d(0)$  which are Fredholm. Furthermore, the Fredholm index of the derivative  $\iota'$  is given by

$$\begin{aligned} i = 2 & & \text{if } c_g^- \geq c_d \geq c_g^+ & & (\text{sinks and contact defects}) \\ i = 1 & & \text{if } c_g^{\pm} < c_d \text{ or } c_g^{\pm} > c_d & & (\text{transmission defects}) \\ i = 0 & & \text{if } c_g^- < c_d < c_g^+ & & (\text{sources}). \end{aligned}$$

Lastly,  $\partial_\tau \mathbf{u}_d(0)$  and  $\partial_\xi \mathbf{u}_d(0)$  belong to  $E_-^{\text{cu}} \cap E_+^{\text{cs}}$ , and the null space of  $l'$  is therefore at least two-dimensional.

The map  $\iota$  can be constructed for all  $(\omega, c)$  close to  $(\omega_d, c_d)$ . If we view  $W_+^{\text{cs}}(\omega, c)$  as the graph of a smooth function  $G_+^{\text{cs}}$  that maps  $W_+^{\text{cs}}(\omega_d, c_d)$  into  $E_+^{\text{uu}}$  and that depends smoothly on  $(\omega, c)$ , and if we define in an analogous fashion a function  $G_-^{\text{cu}}$ , then we can define a parameter-dependent injection map  $\iota_p$

$$\begin{aligned} \iota_p : \quad W_-^{\text{cu}}(\omega_d, c_d) \times W_+^{\text{cs}}(\omega_d, c_d) \times \mathbb{R} \times \mathbb{R} &\longrightarrow Y \\ (\mathbf{u}^-, \mathbf{u}^+, \omega, c) &\longmapsto \mathbf{u}^- + G_-^{\text{cu}}(\mathbf{u}^-, \omega, c) - \mathbf{u}^+ - G_+^{\text{cs}}(\mathbf{u}^+, \omega, c). \end{aligned}$$

Our goal is to show the persistence of defects upon varying the asymptotic wavenumbers and, possibly, external parameters. The geometric intuition that leads to our results is illustrated in Figure 5.1.

## 5.2 Sinks, sources, and transmission defects

For sinks, we set

$$\iota_{\text{si}} = \iota_p(\cdot, \cdot, \omega_d, c_d) : \quad W_-^{\text{cu}} \times W_+^{\text{cs}} \longrightarrow Y. \quad (5.2)$$

For transmission defects with  $c_g^\pm < c_d$ , we fix  $k_+$  which, on account of (1.7), implies  $\omega = \omega_{\text{nl}}(k_+) - ck_+$ . We then define

$$\iota_{\text{tr}} : \quad W_-^{\text{cu}} \times W_+^{\text{cs}} \times \mathbb{R} \longrightarrow Y, \quad \iota_{\text{tr}}(\mathbf{u}^-, \mathbf{u}^+, c) := \iota_p(\mathbf{u}^-, \mathbf{u}^+, \omega_{\text{nl}}(k_+) - ck_+, c). \quad (5.3)$$

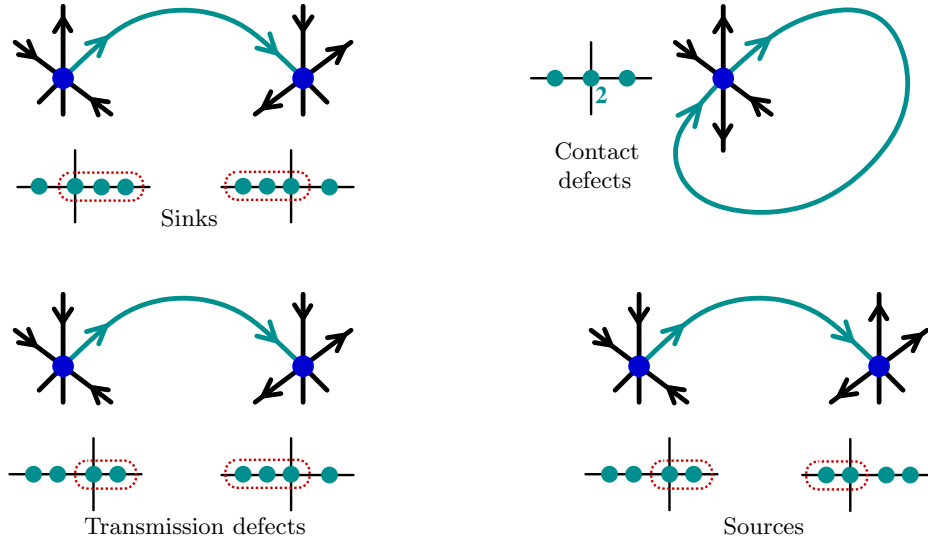


Figure 5.1: *Sinks, contact defects, transmission defects (with  $c_g^\pm < c_d$ ), and sources correspond to homoclinic and heteroclinic orbits of the spatial dynamical system (4.2). The asymptotic equilibria symbolize periodic orbits, which in turn correspond to wave trains, after factoring the time-shift symmetry (3.17). The insets show the spatial spectra of the linearization of (4.2) about the wave trains.*

Lastly, for sources, we set

$$\iota_{\text{so}} = \iota_{\text{p}} : W_-^{\text{cu}} \times W_+^{\text{cs}} \times \mathbb{R} \times \mathbb{R} \longrightarrow Y. \quad (5.4)$$

**Lemma 5.3** *The maps  $\iota_j$  with  $j = \text{si}, \text{tr}, \text{so}$  are Fredholm maps with index  $i(\iota'_j) = 2$ . If  $\iota'_j$  is onto, then each defect is robust. In particular, sinks occur then as two-parameter families (parametrized by  $(k_-, k_+)$ ), transmission defects as one-parameter families (parametrized by  $k_+$  if  $c_{\text{g}}^{\pm} < c_{\text{d}}$ ), and sources are isolated.*

**Proof.** The index formula follows from the bordering lemma 3.5. Thus, suppose that  $\iota'_j$  is onto. For sources, there is then a locally unique root of  $\iota_{\text{so}}$ . For sinks, we can solve the equation  $\iota_{\text{si}} = 0$  for  $(\mathbf{u}^-, \mathbf{u}^+)$ , which lives in a complement of the two-dimensional null space of  $\iota'_{\text{si}}$ , as a function of  $(\omega_{\text{d}}, c_{\text{d}})$  using the implicit function theorem. The result is a two-parameter family of sinks parametrized by  $(\omega_{\text{d}}, c_{\text{d}})$ . Note that  $(\omega_{\text{d}}, c_{\text{d}})$  depend on the asymptotic wavenumbers  $(k_-, k_+)$  through (1.7) and (1.8):

$$(k_+, k_-) \longmapsto (\omega_{\text{d}}, c_{\text{d}}) = \left( \frac{\omega_{\text{nl}}(k_-)k_+ - \omega_{\text{nl}}(k_+)k_-}{k_+ - k_-}, \frac{\omega_{\text{nl}}(k_+) - \omega_{\text{nl}}(k_-)}{k_+ - k_-} \right).$$

Since the determinant of the derivative of this map is given by

$$\frac{(c_{\text{g}}^+ - c_{\text{d}})(c_{\text{g}}^- - c_{\text{d}})}{k_+ - k_-} \neq 0,$$

we can alternatively parametrize sinks by the asymptotic wavenumbers  $(k_-, k_+)$ . Recall here that we assumed that sinks have  $k_- \neq k_+$ . Lastly, for transmission defects, the same arguments show that they persist as one-parameter families which are parametrized by the wavenumber  $k_+$ .

Note that the smooth dependence of  $\mathbf{u}_{\text{d}}(0)$  on parameters implies the smooth dependence of  $\mathbf{u}_{\text{d}}(\xi)$  on parameters on any finite interval  $\xi \in [-L, L]$ . For large values of  $\xi$ , the defects select a strong-stable fiber that itself depends smoothly on parameters and on its base point in a uniform topology, possibly after reparametrizing  $\xi$ . We refer to Appendix A.1 for the existence of these fibers. ■

We remark that we may also include external parameters, for instance, parameters in the nonlinearity  $f$  or the diffusion matrix  $D$ , in the definition of our maps  $\iota_j$ . As a result, the defects considered in Lemma 5.3 depend smoothly on external parameters provided the maps  $\iota'_j$  are onto.

The following proposition links spectral properties of transverse defects to the codimension of the range of  $\iota'_j$ .

**Proposition 5.4** *For sinks, sources, and transmission defects, the linear operator  $\iota'_j$  with  $j = \text{si}, \text{tr}, \text{so}$  is onto if, and only if, the defect is transverse, i.e., if, and only if, the spectrum of the defect at the origin is minimal.*

**Proof.** We have to show that, under the spectral assumptions for elementary transverse defects, the map  $\iota_j$  is onto if, and only if, the critical spectrum is minimal. This then proves the robustness theorem for sinks, transmission defects, and sources, invoking Lemma 5.3.

**Sinks:** Suppose that  $\iota'_{\text{si}}$  is onto. Proposition 5.2 and Lemma 5.3 imply that each bounded solution to equation (4.3) with  $\lambda = 0$ ,

$$\begin{aligned} u_\xi &= v \\ v_\xi &= D^{-1}[\omega_d \partial_\tau u - c_d v - f'(u_d(\xi, \cdot))u], \end{aligned} \tag{5.5}$$

is a linear combination of  $\partial_\tau \mathbf{u}_d$  and  $\partial_\xi \mathbf{u}_d$ . We claim that  $E_+^{\text{ss}}(0)$  and  $E_-^{\text{uu}}(0)$  intersect trivially. Indeed, as a consequence of Corollary 5.1, the linear combinations  $(k_+ \partial_\tau + \partial_\xi) \mathbf{u}_d(\xi, \cdot)$  and  $(k_- \partial_\tau + \partial_\xi) \mathbf{u}_d(\xi, \cdot)$  are the unique linear combinations that result in exponentially decaying functions as  $\xi \rightarrow \infty$  and  $\xi \rightarrow -\infty$ , respectively. Since  $k_- \neq k_+$ , however, these combinations do not match, and none of the linear combinations will therefore decay at both  $\xi = \infty$  and  $\xi = -\infty$ . This shows that there are no solutions to (5.5) that decay exponentially as  $|\xi| \rightarrow \infty$ , and the sink is therefore transverse.

Conversely, assume that the dimension of the null space of  $\iota'_{\text{si}}$  is at least three, then there exists a solution  $\mathbf{u}_*$  to (5.5) which is linearly independent of  $\partial_\xi \mathbf{u}_d$  and  $\partial_\tau \mathbf{u}_d$ . Since the spatial Floquet exponent  $\nu = 0$  of the equation for the asymptotic wave trains is simple, we may write the solution  $\mathbf{u}_*$  as

$$\mathbf{u}_*(\xi, \cdot) = a_\pm \mathbf{u}'_{\text{wt}}(k_\pm \xi - \cdot; k_\pm) + O(e^{-\delta|\xi|})$$

for some  $\delta > 0$  as  $\xi \rightarrow \pm\infty$ . Exploiting the expansion for  $\mathbf{u}_d$  and the fact that  $k_- \neq k_+$ , we find constants  $c_1$  and  $c_2$  so that

$$\mathbf{u}_* + c_1 \partial_\tau \mathbf{u}_d + c_2 \partial_\xi \mathbf{u}_d$$

decays exponentially as  $|\xi| \rightarrow \infty$ . This shows that the null space of the linearized period map, considered in  $L^2_{\eta_-, \eta_+}$  with  $\eta_- > 0 > \eta_+$  close to zero, is not trivial.

**Sources:** Assume that  $\iota'_{\text{so}}$  is onto. The first components of the two bounded, linearly independent solutions  $\partial_\xi \mathbf{u}_d$  and  $\partial_\tau \mathbf{u}_d$  of (5.5) form a two-dimensional subspace in the null space of the linearized period map  $\Phi_d$  considered in  $L^2_{\eta_-, \eta_+}$  with  $\eta_- < 0 < \eta_+$ . Since the null space of  $\iota'_{\text{so}}$  contains all solutions with sufficiently mild exponential growth, the geometric multiplicity of  $\lambda = 0$  is equal to two. We need to exclude generalized eigenfunctions. Assume therefore that  $\check{u}_*$  satisfies

$$\check{u}_*(\cdot, 2\pi) = \Phi_d \check{u}_*(\cdot, 0) = \check{u}_*(\cdot, 0) + (c_1 \partial_\tau + c_2 \partial_\xi) u_d(\cdot, 2\pi).$$

If we set

$$u_*(\xi, \tau) = \check{u}_*(\xi, \tau) - \frac{\tau}{2\pi} [c_1 \partial_\tau + c_2 \partial_\xi] u_d(\xi, \tau),$$

then  $\mathbf{u}_* = (u_*, \partial_\xi u_*)$  is in  $Y$  for all  $\xi$  and satisfies

$$\begin{aligned} u_\xi &= v \\ v_\xi &= D^{-1}[\omega_d \partial_\tau u - c_d v - f'(u_d(\xi, \cdot))u - (\omega_d/2\pi)(c_1 \partial_\tau u_d(\xi, \cdot) + c_2 v_d(\xi, \cdot))], \end{aligned} \tag{5.6}$$

where  $\mathbf{u}_d = (u_d, v_d)$ . Equation (5.6) is exactly the variational equation in the extended phase space, where  $\omega$  and  $c$  are considered as additional variables. In particular, this equation in the extended phase space has a bounded solution that is linearly independent of the derivatives of the defect

with respect to  $\tau$  and  $\xi$ . As a consequence, the null space of  $\iota'_{\text{so}}$  is at least three-dimensional, and  $\iota'_{\text{so}}$  cannot be onto. This proves that the algebraic multiplicity of  $\lambda = 0$  is equal to two.

Conversely, assume that the algebraic multiplicity of the linearized period map  $\Phi_{\text{d}}$  is two, but that  $\iota'_{\text{so}}$  is not onto. By Fredholm theory, either the null space of  $\partial_{(\mathbf{u}^-, \mathbf{u}^+) \iota_{\text{so}}}$  has dimension larger than two or else the ranges of  $\partial_{(\omega, c) \iota_{\text{so}}}$  and of  $\partial_{(\mathbf{u}^-, \mathbf{u}^+) \iota_{\text{so}}}$  have a non-trivial intersection. In the first case, we can easily construct additional eigenfunctions and, in the second case, generalized eigenfunctions of the linearized period map  $\Phi_{\text{d}}$ , contradicting our starting assumption.

**Transmission defects:** We assume that  $\iota'_{\text{tr}}$  is onto. Arguing as for sources, we conclude that the geometric multiplicity of  $\lambda = 0$  is equal to one with the null space of  $\Phi_{\text{d}}$  spanned by  $(k_+ \partial_\tau + \partial_\xi) u_{\text{d}}$ . We argue by contradiction and assume there is a generalized eigenvector. As for sources, this assumption gives a solution of

$$\begin{aligned} u_\xi &= v \\ v_\xi &= D^{-1}[\omega_{\text{d}} \partial_\tau u - c_{\text{d}} v - f'(u_{\text{d}}(\xi, \tau))u - v_{\text{d}}(\xi, \tau) - k_+ \partial_\tau u_{\text{d}}(\xi, \tau)] \end{aligned} \quad (5.7)$$

which is bounded as  $\xi \rightarrow -\infty$  and decays exponentially as  $\xi \rightarrow \infty$ . The construction of  $\iota_{\text{tr}}$  in (5.3) shows that (5.7) is the variational equation associated with  $\partial_c \iota$ . Therefore,  $\iota'_{\text{tr}}$  will have a null space of dimension larger than two, contradicting our assumption. The converse follows similarly. ■

### 5.3 Contact defects

Recall that  $E_{\pm}^{\text{c}}$  is two-dimensional for contact defects. We shall need the two injection maps

$$\begin{aligned} \iota_+ : \quad & W_-^{\text{cu}} \times W_+^{\text{ss}} \longrightarrow Y, \quad (\mathbf{u}^-, \mathbf{u}^+) \longmapsto \mathbf{u}^- - \mathbf{u}^+ \\ \iota_- : \quad & W_-^{\text{uu}} \times W_+^{\text{cs}} \longrightarrow Y, \quad (\mathbf{u}^-, \mathbf{u}^+) \longmapsto \mathbf{u}^- - \mathbf{u}^+. \end{aligned} \quad (5.8)$$

Both maps depend smoothly on additional parameters if any are present. Counting dimensions, the bordering lemma 3.5 shows that  $\iota_{\pm}$  are both Fredholm maps with index zero.

**Lemma 5.5** *Contact defects occur as robust one-parameter families in the asymptotic wavenumber  $k = k_{\pm}$  provided both  $\iota'_+$  and  $\iota'_-$  are onto (and therefore invertible).*

**Proof.** First note that, since  $\iota_+$  is onto, so is the map  $\iota$  from (5.1). In particular, via Lyapunov–Schmidt reduction, the intersection of center-unstable and center-stable manifolds persists. We claim that the defect lies neither in the strong-stable nor the strong-unstable manifold. Indeed, if it were,  $\iota_+$  or  $\iota_-$  would have a non-trivial kernel and could therefore not be onto. The complement of the strong-stable manifold in the center-stable manifold of the wave train is an open subset of the center-stable manifold (initially in a neighborhood of the wave train, but then also in a neighborhood of  $\mathbf{u}_{\text{d}}(0)$  upon using continuity of the evolution on the center-stable manifold). In particular, the perturbed intersection points in  $W_+^{\text{cs}}$  still belong to the interior of the center-stable manifold. A similar description is true for the center-unstable manifold which shows persistence

for nearby wavenumbers and parameters upon varying  $c_d = \omega'_{\text{nl}}(k)$  appropriately. Smooth dependence of contact defects on parameters in a  $\xi$ -uniform topology is achieved after an appropriate reparametrization of the spatial time variable  $\xi$ . ■

**Proposition 5.6** *The injection maps  $\iota'_\pm$  are both onto if, and only if, the minimal-spectrum assumption holds, i.e., if, and only if, the contact defect is transverse.*

**Proof.** The null spaces of  $\iota'_-$  and  $\iota'_+$  consist exactly of eigenfunctions of the linearized period map  $\Phi_d$  in  $L^2_{\eta_-, \eta_+}$  with exponential weights  $\eta_- = \eta_+ < 0$  and  $\eta_- = \eta_+ > 0$ , respectively. ■

Lemma 5.5 and Proposition 5.6 implicitly show that higher-dimensional intersections of center-stable and center-unstable manifolds would contribute to the null spaces of  $\iota_+$  and  $\iota_-$ . They would, however, typically not contribute an additional root of the extension into  $\lambda = 0$  of the Evans function  $\mathcal{E}(\lambda)$  of Theorem 2. Indeed, we proved in [49] that roots of the extended Evans function are generated by solutions of the linearized equation that decay like  $1/|\xi|$ . The additional solutions  $\mathbf{u}_*$  of the linearized equation, which correspond to the additional direction in the intersection of center-stable and center-unstable manifolds, would have asymptotics of the form  $\mathbf{u}_* \approx a_\pm \mathbf{u}'_{\text{wt}}$  as  $\xi \rightarrow \pm\infty$ . We expect  $a_+ \neq a_-$ , and since  $\partial_\tau u_d$  and  $\partial_\xi u_d$  have the same asymptotics at  $\xi = \infty$  and at  $\xi = -\infty$  (recall that  $k_- = k_+$  for contact defects), we cannot make  $a_- = a_+ = 0$  by adding appropriate linear combinations of  $\partial_\tau \mathbf{u}_d$  and  $\partial_\xi \mathbf{u}_d$ .

Similarly, the orbit-flip situation where the contact defect lies in the strong-stable or the strong-unstable manifold cannot be excluded from considerations of the extended Evans function that we constructed in [49]. We refer to Section 6.4 for some puzzling consequences of these facts.

**Proof of Theorem 1.** For transverse sinks, sources, and transmission defects, Proposition 5.4 shows that we can apply Lemma 5.3 to find locally unique and robust families of defects. On the other hand, the maps  $\iota'_j$ , evaluated along this family, remain onto which, using the equivalence proved in Proposition 5.4, shows that the defects in the family are transverse, i.e., that they satisfy the minimal-spectrum assumption. For contact defects, the same conclusion is reached by combining Lemma 5.5 and Proposition 5.6. ■

## 6 Stability, bifurcations, pinning, and truncation

We collect various consequences of our results and point out a number of open problems related to the proposed classification of defects in one-dimensional media.

### 6.1 Stability

An important feature of transverse defects are the point and essential spectra of the linearized period map. The following theorem summarizes our findings, illustrated also in Figure 6.1, for the temporal Floquet exponents of  $\Phi_d$ .

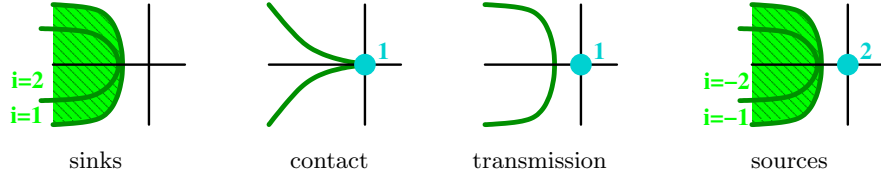


Figure 6.1: Plotted are the Floquet spectra near  $\lambda = 0$  of the maps  $\Phi_d$ , posed on  $L^2_\eta(\mathbb{R}, \mathbb{C}^n)$ , for transverse sinks, contact defects, transmission defects, and sources with weights  $\eta = (\eta_-, \eta_+)$  as in (6.1). Solid lines denote the Floquet spectra of the asymptotic wave trains, while the shaded areas correspond to regions where  $\Phi_d - \rho$  is Fredholm with non-zero index  $i$ . The bullets label eigenvalues with the attached number indicating their multiplicity (the algebraic and geometric multiplicities coincide).

**Theorem 4** *The following is true for transverse sinks, contact defects, transmission defects, and sources. Choose weights  $\eta = (\eta_-, \eta_+)$  close to zero such that*

$$\begin{aligned}
\eta_- < 0 < \eta_+ & \quad \text{for sinks} \\
\eta_- = \eta_+ = 0 & \quad \text{for contact defects} \\
\eta_-, \eta_+ > 0 & \quad \text{for transmission defects with } c_g^\pm < c_d \\
\eta_- > 0 > \eta_+ & \quad \text{for sources.}
\end{aligned} \tag{6.1}$$

The Floquet spectra, in a sufficiently small neighborhood of  $\lambda = 0$ , of the period map  $\Phi_d$  posed on  $L^2_\eta(\mathbb{R}, \mathbb{C}^n)$  are as shown in Figure 6.1.

Transverse sinks that have no additional isolated eigenvalues in the closed right half-plane are nonlinearly asymptotically stable for (1.1) in that perturbations decay in  $L^2_\eta$  for weights  $\eta$  as in (6.1). For transverse sources, the two eigenfunctions of the adjoint operator  $\Phi_d^{\text{ad}} - \mathbf{1}$  on  $L^2_{-\eta}(\mathbb{R}, \mathbb{C}^n)$  are exponentially localized.

**Proof.** We proved in Lemma 4.3 that the essential Floquet spectrum of sinks, sources, and transmission defects lies in the left half-plane for the weights chosen in (6.1). For contact defects, there is an additional subtlety: The curve that corresponds to the linear dispersion relation of the asymptotic wave train has a cusp at  $\lambda = 0$ . Indeed, the dispersion relation in the frame moving with speed  $c_d$  is given by (3.12)

$$\lambda_{\text{lin}}(\nu) = [c_d - c_g]\nu + d_{\parallel}\nu^2 + d_3\nu^3 + O(\nu^4)$$

where the coefficients  $d_{\parallel}$  and  $d_3$  are real. Since we have  $c_d = c_g$ , we obtain

$$\lambda(i\gamma) = -d_{\parallel}\gamma^2 + id_3\gamma^3 + O(\gamma^4) \tag{6.2}$$

so that  $\text{Re } \lambda = [d_3 \text{Im } \lambda / d_{\parallel}]^{2/3}$  has a cusp point at the origin as claimed provided  $d_3 \neq 0$ .

Lemma 3.6 and 4.1 together show that the Fredholm index for sinks and sources jumps by  $+1$  and  $-1$ , respectively, when  $\lambda$  crosses  $\Sigma_{\text{wt}}^-$  or  $\Sigma_{\text{wt}}^+$  from right to left, while the Fredholm index of contact and transmission defects is zero to the left of the Floquet spectra  $\Sigma_{\text{wt}}^- \cup \Sigma_{\text{wt}}^+$ . The statements about

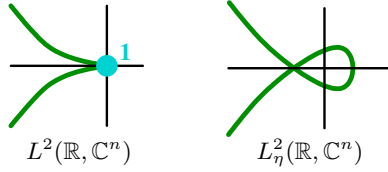


Figure 6.2: *Plotted are the Floquet spectra of contact defects near  $\lambda = 0$  of the maps  $\Phi_d$  on  $L^2(\mathbb{R}, \mathbb{C}^n)$  and  $L^2_\eta(\mathbb{R}, \mathbb{C}^n)$  for non-zero  $\eta_- = \eta_+$  close to zero. The map  $\Phi_d - \rho$  is Fredholm with index zero off the solid lines.*

the algebraic and geometric multiplicity of eigenvalues at  $\lambda = 0$  follows at once from Lemma 4.4 and the proof of Proposition 5.4. Theorem 2 shows that the Evans function of transverse contact defects has a simple root at  $\lambda = 0$ .

Nonlinear stability of spectrally stable sinks in  $L^2_\eta(\mathbb{R}, \mathbb{C}^n)$  follows easily since the period map is a contraction, while the nonlinearity  $f$  is well-defined and smooth on  $L^2_\eta(\mathbb{R}, \mathbb{C}^n)$  provided the weights are chosen as in (6.1). We refer to [10, 53] for details. Lastly, the statement about the exponential localization of the two adjoint eigenfunctions for sources is simply Corollary 4.5. ■

The spectrum of contact defects in  $L^2_\eta$  is shown in Figure 6.2. In particular, it is an immediate consequence of (6.2) that the essential spectrum is always unstable whenever the rates  $\eta_- = \eta_+$  of the exponential weights are not zero.

The above theorem implies, in particular, that spectrally stable transverse sinks are nonlinearly asymptotically stable under small exponentially localized perturbations<sup>7</sup>: these perturbations decay exponentially in time, and we recover the *same* sink with no shift in its spatial or phase position since there is no point spectrum in the closed right half-plane.

The nonlinear stability of a specific transmission defect has been proved recently in a context of small-amplitude background waves [16]. For contact defects, the only related results we know of are in the context of conservation laws where Howard [24] recently investigated degenerate shock waves. We are not aware of any nonlinear stability results for sources. We expect, however, results along the following lines:

Perturbations of transmission defects should relax to a spatio-temporal translate of the original defect that preserves the relative phase of the wave train whose group velocity is directed towards the defect. Thus, if  $c_g^+ < c_d$ , say, then an initial condition  $u(x, 0)$  close to the transmission defect  $u_d(x, 0)$  evolves towards a shifted transmission defect

$$u(x, t) \longrightarrow u_d(\check{x} - c_d \check{t}, \check{t})$$

as  $t \rightarrow \infty$  where  $k\check{x} - \omega\check{t} = kx - \omega t$ . This is immediately clear on the linearized level, using the exponential weights (6.1), and has been proved for the example considered in [16].

Sources, on the other hand, should have a unique position and a unique phase as evidenced by the fact that the adjoint eigenfunctions are exponentially localized. This implies that the spectral

<sup>7</sup>Nonlinear stability results using weaker polynomial weights have been established in specific examples [14, 28].

projection onto the two-dimensional eigenspace consisting of space and time translations of the defect is well defined in  $L^2_\eta$  with weights as in (6.1). Thus, the linear analysis predicts that the shifts in space  $\check{x} - x$  and time  $\check{t} - t$  are uncorrelated.

## 6.2 Phase matching

Phase matching at defects has recently been discussed quite extensively in the physics literature [1, 22, 35, 36]. To explain this issue, we fix a continuous function  $\vartheta(k)$  and define the phase of a wave train to be its argument

$$\phi[u_{\text{wt}}(\phi; k)] := \phi - \vartheta(k) \quad (6.3)$$

after subtracting the fixed phase shift  $\vartheta(k)$ . Note that it is natural to choose  $\vartheta(k)$  subject to  $\vartheta(k) = -\vartheta(-k)$  to account for the reflection symmetry of the reaction-diffusion system (1.1).

Elementary defects  $\check{u}_d(x, t)$  with asymptotic phase, i.e. sinks, transmission defects and sources, satisfy

$$\check{u}_d(x, t) - u_{\text{wt}}^\pm(k_\pm x - \omega_{\text{nl}}(k_\pm)t + \theta_\pm; k_\pm) \longrightarrow 0$$

as  $x \rightarrow \pm\infty$  for appropriate constant phase corrections  $\theta_\pm$ . If we wish to measure the phase mismatch  $[\phi]$  across the characteristic  $x - c_d t = \xi_{\text{pm}}$  for some fixed  $\xi_{\text{pm}} \in \mathbb{R}$ , we can do so by defining the two phases

$$\begin{aligned} \phi_\pm(t) &:= \phi[u_{\text{wt}}^\pm(k_\pm x - \omega_{\text{nl}}(k_\pm)t + \theta_\pm; k_\pm)] = \phi[u_{\text{wt}}^\pm(k_\pm \xi_{\text{pm}} - \omega_d t + \theta_\pm; k_\pm)] \\ &= k_\pm \xi_{\text{pm}} - \omega_d t + \theta_\pm - \vartheta(k_\pm) \end{aligned}$$

and then take their difference to get

$$[\phi] := \phi_+(t) - \phi_-(t) = [k]\xi_{\text{pm}} + [\theta] - [\vartheta] \quad (6.4)$$

where we use the notation  $[F] = F(k_+) - F(k_-)$  to denote jumps of functions across the defect. We call  $[\phi]$  the *phase slip* across the defect along the characteristic line  $x - c_d t = \xi_{\text{pm}}$ . Note that the position  $\xi_{\text{pm}}$  along which we measure the phase slip is somewhat arbitrary. We also emphasize that the definition of the phase slip relies on the assumption that the frequencies of the asymptotic wave trains coincide when computed in the frame that moves with the speed  $c_d$  of the defect.

The phase slip  $[\phi]$  for transmission defects with  $k_- = k_+$  is given by  $[\phi] = [\theta] = \theta_+ - \theta_-$  and therefore independent of the position  $\xi_\pm$ . Instead, it depends only on the difference between the asymptotic phase corrections  $\theta_\pm$ . For contact defects, we can also define a phase slip. Contact defects satisfy [10, 49]

$$\check{u}_d(x, t) - u_{\text{wt}}(kx - \omega_{\text{nl}}(k)t + \theta_\pm + \check{\theta} \log(x - c_d t); k) \longrightarrow 0$$

so that their phase slip is again given by  $[\phi] = [\theta]$  since the logarithmic terms cancel.

In summary, sinks and sources have a phase slip  $[\phi] = [k]\xi_{\text{pm}} + [\theta - \vartheta]$  that is periodic in  $\xi_{\text{pm}}$  with period  $2\pi/[k]$ . In particular, we can always arrange to obtain zero phase-slip  $[\phi] = 0$  by measuring

at the “correct” characteristic line. For contact defects and for transmission defects with  $[k] = 0$ , the phase slip  $[\phi] = [\theta]$  is an intrinsic property of the defect that, in particular, does not depend on where we measure it.

We may use the phase slip to track the *position*  $x = \xi_{\text{pm}} + c_{\text{d}}t$  of sinks and sources (even though the phase slip defines the position only in  $S^1$  which is a minor complication when we consider small perturbations of a given defect). A given phase slip  $[\phi]$  therefore gives a certain well defined position  $x = \xi_{\text{pm}} + c_{\text{d}}t$  of the defect. We may then compare the position of an unperturbed defect with the position of the defect after adding a small perturbation. For sinks, the asymptotic relaxation of perturbations to exactly the same sink guarantees that the position of the perturbed defect is the same as the position of the unperturbed defect, whereas we expect shifts of the position for sources.

### 6.3 Reflection symmetries

The reaction-diffusion system (1.1) respects the reflection symmetry  $x \mapsto -x$  in addition to the spatio-temporal translation symmetries. Thus, defects with speed zero are somewhat distinguished. We therefore set  $c = 0$  in this section, so that  $x$  is the spatial variable in the modulated-wave equation (4.2)

$$\begin{aligned} u_x &= v \\ v_x &= D^{-1}[\omega_{\text{d}}\partial_{\tau}u - f(u)]. \end{aligned} \tag{6.5}$$

The reflection symmetry  $x \mapsto -x$  for (1.1) manifests itself as a reversibility for (6.5). In fact, exploiting also the time-shift symmetry of (6.5), both

$$\mathcal{R}_0 : (u, v)(\tau) \mapsto (u, -v)(\tau) \quad \text{and} \quad \mathcal{R}_{\pi} : (u, v)(\tau) \mapsto (u, -v)(\tau + \pi) \tag{6.6}$$

are reversibility operators that anti-commute with the right-hand side of (6.5).

We may now seek symmetric defects to (1.1) which correspond to reversible homoclinic and heteroclinic orbits of (6.5). Reversible connecting orbits can be found as intersections of the center-unstable manifold of the asymptotic wave train at  $x = -\infty$  with the fixed-point spaces  $\text{Fix}(\mathcal{R}_0) = \{(u, v); v = 0\}$  or  $\text{Fix}(\mathcal{R}_{\pi}) = \{(u, v); v(\tau) = -v(\tau + \pi)\}$  of the reversibility operators  $\mathcal{R}_0$  or  $\mathcal{R}_{\pi}$ , respectively. Note that the resulting defects have  $k_+ = -k_-$ , and therefore  $c_{\text{g}}^+ = -c_{\text{g}}^-$  since  $\omega_{\text{nl}}(-k) = -\omega_{\text{nl}}(k)$ . In particular, transmission defects cannot be symmetric, since the group velocities to the left and right can have the same sign only if they both vanish.

Using the map

$$\iota_j : W_-^{\text{cu}} \times \text{Fix}(\mathcal{R}_j) \longrightarrow Y, \quad (\mathbf{u}^-, \mathbf{u}^0) \longmapsto \mathbf{u}^- - \mathbf{u}^0$$

for  $j = 0, \pi$ , we can again compute its Fredholm index and compare it with robustness properties of symmetric defects. We obtain that symmetric sinks (with respect to either  $\mathcal{R}_0$  or  $\mathcal{R}_{\pi}$ ) arise as robust one-parameter families, while symmetric sources and contact defects are robust and occur for isolated values of the parameter  $k_-$  (note that  $c = 0$  is required for symmetric defects). We remark that both  $\mathcal{R}_{\pi}$ -symmetric sources [37] and  $\mathcal{R}_{\pi}$ -symmetric contact defects [57] have been observed in experiments.

## 6.4 Bifurcations

We address instabilities of defects and transitions between different defect types. From the spatial-dynamics perspective, this amounts to investigating homoclinic and heteroclinic bifurcations.

### Saddle-node bifurcations of wave trains

As outlined in Example II of Section 1.3, stable sinks with “small” amplitude are created at saddle-node bifurcations of wave trains [10, 25]. Indeed, if we consider the modulated-wave equation near a wave train in the frame that moves with its group velocity  $c_d = c_g$ , then the wave train has an algebraically double spatial Floquet exponent  $\nu = 0$  (see Section 3.4 and Figure 3.1). If we keep the defect speed fixed at  $c_d = c_g(k_*)$ , then the saddle node can be unfolded by varying the frequency  $\omega_d$  near  $\omega_{nl}(k_*)$ , where  $k_*$  is the wavenumber of the wave train we started with. The vector field on the resulting two-dimensional center manifold is invariant under the temporal time-shift symmetry and is given by

$$\phi_\xi = q + O(q^2), \quad \lambda''_{\text{lin}}(0)q_\xi = \tilde{\omega} - \omega''_{nl}(k)q^2 + O(|\tilde{\omega}^2| + |\tilde{\omega}q| + |q|^3) \quad (6.7)$$

where  $(\phi, q)$  correspond roughly to phase and wavenumber, and where  $\omega = \tilde{\omega} + \omega_{nl}(k_*)$ . To leading order, we therefore recover the steady-state equation of Burgers equation (1.19) which, as discussed in Section 1.3, admits stable sinks. We refer to Figure 6.3 for an illustration.

Large-amplitude sinks arise close to contact defects. If we vary frequency or speed so that the saddle-node wave trains splits into two wave trains, then the saddle-node homoclinic orbit that corresponds to the contact defect becomes a heteroclinic orbit—in fact, a sink—that connects the two wave trains (as illustrated in the lower-left half of Figure 6.4). It is an interesting problem to determine whether the resulting sink is stable or not. On account of Theorem 2, the Evans function of the contact defect will have a simple zero at the origin, while the sink does not have an eigenvalue at  $\lambda = 0$ . Thus, we expect that the sink will have either a weakly stable or a weakly unstable eigenvalue near zero.

We remark that the bottom of Figure 6.4 also illustrates that the same wave trains can accommodate several distinct defects. Indeed, the two wave trains in the bottom plot of Figure 6.4 are connected by a “small-amplitude” and a “large-amplitude” sink.

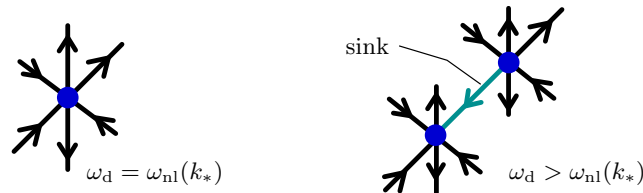


Figure 6.3: *The unfolding of a saddle-node wave train generates a “small-amplitude” sink that connects two wave trains (the sketch assumes that  $\omega''_{nl}(k_*) > 0$ ).*

## Folds

Next, we discuss what happens when the minimal-spectrum assumption, which is equivalent to the transversality condition for center-stable and center-unstable manifolds in the proof of Theorem 1, is violated. In this case, sinks acquire a simple eigenvalue at  $\lambda = 0$  in the space  $L^2_\eta$  with sign  $\eta_\pm = \pm 1$ . This degeneracy corresponds to a tangency of the center-unstable and center-stable manifolds of the wave trains in the modulated-wave equation (4.2). Thus, if the tangency is quadratic as expected, it will persist along a curve in  $(k_-, k_+)$ -parameter space. On one side of this curve, there exists a pair of sinks, while there are no sinks on its other side. It is not hard to prove that the additional critical eigenvalue near  $\lambda = 0$  will stabilize one of the two sinks and destabilize the other one. The scenario for transmission defects and sources is similar since the linearization acquires a Jordan block of length two. For transmission defects, we then see two defects for  $k < k_*$ , say, and none for  $k > k_*$ , while folds for sources occur only when an additional external parameter is present.

Contact defects behave differently. If the center-stable and center-unstable manifolds intersect tangentially, we expect again a standard saddle-node bifurcation of contact defects in the modulated-wave equation that is unfolded by the wavenumber  $k$ . Since the asymptotic wavenumbers are identical, the tangency will, however, *not* generate a localized eigenfunction of the linearization. In particular, the Evans function near  $\lambda = 0$  does not change at all. Thus, none of the two contact defects will acquire any additional eigenvalues, and both of them will be spectrally stable! Instead, an unstable root arises for the Evans functions associated with the maps  $\iota_\pm$  from (5.8) which have the wrong Morse index. Of course, the two stable contact defects are not close to each other in the supremum norm which precludes viewing one of them as a small perturbation of the other one.

## Locking and unlocking via flip bifurcations

Contact defects are also destroyed at values of  $k$  at which the center-unstable manifold intersects the center-stable manifold along the strong-stable manifold of the asymptotic wave train. The

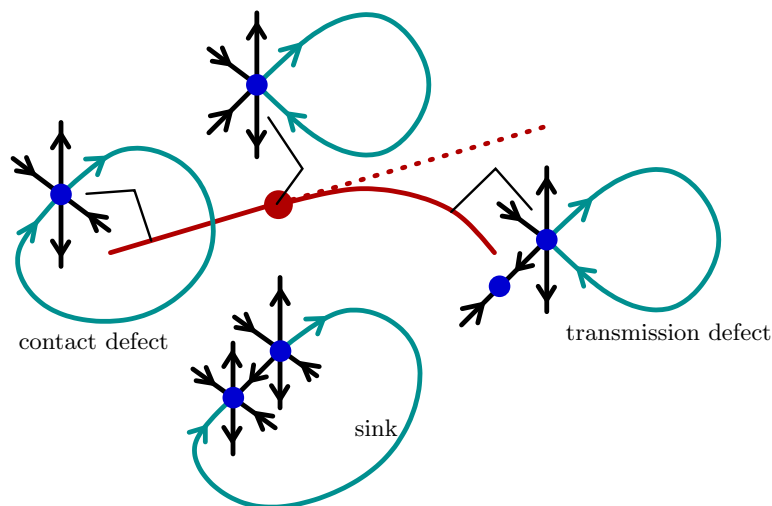


Figure 6.4: *The saddle-node homoclinic bifurcation in the two-dimensional parameter space.*

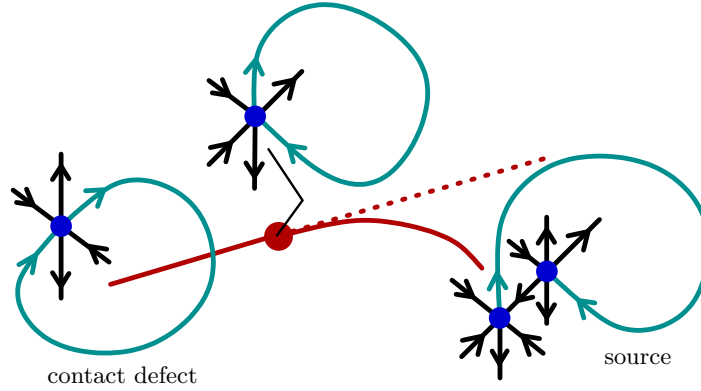


Figure 6.5: *The double-flip homoclinic bifurcation in the three-dimensional parameter space.*

associated homoclinic flip bifurcation has been analysed in [5] for ODEs, and the resulting bifurcation diagram is shown in Figure 6.4. We remark that it is straightforward to obtain the same for (4.2) by using exponential dichotomies and foliations of center-stable and center-unstable manifolds. Note that the contact defect exists for wavenumbers below a critical wavenumber, say, and its speed is therefore determined solely by the group velocity. Above the critical wavenumber, the defect changes into a transmission defect whose speed is now determined by a Melnikov integral that depends on the profile of the defect. Thus, we may refer to this bifurcation as an unlocking bifurcation at which the speed of the defect unlocks from the group velocity of the underlying wave trains. We remark that neither the transmission defect nor the contact defect acquires any additional eigenvalues during this transition. Phenomenologically, the unlocking transition is preceded by an increasing localization of the defect structure. At the bifurcation point, the convergence towards the wave trains changes from algebraic to exponential. The unlocked transmission defect approaches the wave train ahead<sup>8</sup> of it with a uniform exponential rate, whereas the relaxation towards the wave train behind the defect occurs with a weak exponential rate. A similar phenomenon occurs when transmission defects bifurcate from pulses at parameter values where the homogeneous background undergoes a Turing instability [43].

A more dramatic unlocking bifurcation occurs if we allow an additional external parameter  $\mu$  to vary. It can then happen that both the strong-stable and strong-unstable manifolds of a saddle-node periodic orbit intersect, which can be interpreted as the simultaneous unlocking of the contact defect at both end points. The analysis of this bifurcation is very similar to the one for localized inhomogeneities of wave trains with zero group velocity that we will discuss in Section 6.5. According to the bifurcation diagram shown in Figure 6.5, we find contact defects before the bifurcation and sources afterwards. Note that the source coexists with the small-amplitude sink that is created in the saddle-node bifurcation. Source and sink together can now form a bound state that corresponds to a transmission defect.

<sup>8</sup>If  $c_g(k_{\pm}) < c_d$ , then we say, *by definition*, that the wave train at  $\xi = -\infty$  is behind the defect, while the wave train at  $\xi = \infty$  is ahead of the defect. If  $c_g(k_{\pm}) > c_d$ , then we reverse these definitions.

## Other bifurcations

Defects may also arise when additional harmonic frequencies are introduced. Motivated by experiments [57] and numerical simulations [17], we have analysed which defects can be created near period-doubling bifurcations of wave trains. We showed in [51] that phase-slip defects can arise as interfaces between spatially homogeneous oscillations with a relative phase shift of  $\pi$ .

Of course, there are many more bifurcations that we expect to encounter. Sinks, for instance, persist even if we vary the two wavenumbers of the asymptotic wave trains independently, and we should therefore expect to observe any heteroclinic bifurcation of codimension two. In fact, even non-transverse homoclinic orbits may occur for large sets in parameter space.

The examples above notwithstanding, homoclinic and heteroclinic bifurcations can result in very complicated solution structures, and a complete classification appears to be impossible. To give a few examples, homoclinic orbits with complex spatial Floquet exponents are accompanied by a plethora of multi-loop solutions. Sources and sinks that travel with the same speed form a heteroclinic loop, and the resulting heteroclinic bifurcation may lead to various different source-sink bound states (each being a transmission defect).

## 6.5 Pinning at inhomogeneities

Most of the counting arguments in Sections 4 and 5 rely on the fact that  $\partial_\tau u_d$  and  $\partial_\xi u_d$  provide bounded solutions of the linearization of (4.2) about a defect, while  $\omega_d$  and  $c_d$  provided the corresponding Lagrange multipliers. Spatial inhomogeneities break the translation symmetry, which prevents us from using moving frames. In particular, we will only be able to study defects with vanishing speed  $c_d = 0$ . Thus, consider the equation

$$u_t = Du_{xx} + f(u) + \varepsilon g(x, u) \quad (6.8)$$

where we assume that the inhomogeneity  $g$  is localized so that  $g(x, u) \rightarrow 0$  exponentially as  $x \rightarrow \pm\infty$ . The following result shows that standing sources persist at isolated positions for  $\varepsilon \neq 0$  and are therefore pinned to the inhomogeneity. Similar results are true for contact defects with zero speed.

**Theorem 5** *Suppose that  $u_d(x, \tau)$  is a transverse source of (1.1) with  $c_d = 0$ . If we define<sup>9</sup>*

$$M(p) := \int_{-\infty}^{\infty} \int_0^{2\pi} \langle \psi_d^c(x, \tau), g(x - p, u_d(x, \tau)) \rangle_{\mathbb{R}^n} d\tau dx,$$

*then the source  $u_d(x + p, \tau)$  persists as a solution to (6.8) for  $\varepsilon$  close to zero provided  $p$  is a simple root of the Melnikov function  $M(p)$ . Furthermore, the temporal frequency  $\omega_d^*(\varepsilon)$  of the perturbed source is given by*

$$\omega_d^*(\varepsilon) = \omega_d + \varepsilon \int_{-\infty}^{\infty} \int_0^{2\pi} \langle \psi_d^\omega(x, \tau), g(x - p, u_d(x, \tau)) \rangle_{\mathbb{R}^n} d\tau dx + O(\varepsilon^2).$$

---

<sup>9</sup>The functions  $\psi_d^c(x, \tau)$  and  $\psi_d^\omega(x, \tau)$  have been defined in Corollary 4.5.

**Proof.** The result follows from Lyapunov–Schmidt reduction applied to the spatial dynamical system (4.2). We omit the details and refer instead to [38, Section 5] and [48, Section 8], where analogous analyses have been carried out. ■

**Corollary 6.1** *If the hypotheses of the preceding theorem are met, and both the source and the inhomogeneity are symmetric (i.e. invariant under  $x \mapsto -x$ ), then the Melnikov function  $M(p)$  is odd. The symmetric source located at  $x = 0$  persists for  $\varepsilon \neq 0$  provided*

$$\int_{-\infty}^{\infty} \int_0^{2\pi} \langle \psi_d^c(x, \tau), g_x(x, u_d(x, \tau)) \rangle d\tau dx \neq 0.$$

**Proof.** The bounded solution of (2.17) that corresponds to  $\psi_d^c$  is of the form

$$\psi(\xi, \tau) = \begin{pmatrix} c_d \psi(\xi, \tau) - \partial_\xi \psi(\xi, \tau) \\ D\psi(\xi, \tau) \end{pmatrix}.$$

It is a consequence of [56] and the discussion in Section 6.3 that  $\psi(0, \cdot)$  lies in the fixed-point space  $\text{Fix}(\mathcal{R}_0)$  of the reversibility operator  $\mathcal{R}_0$ . In particular,  $\psi_d^c(x, \tau)$  is odd in  $x$ , and the corollary follows then from Theorem 5. ■

In summary, large-amplitude sources with zero speed will be pinned to inhomogeneities, and their temporal frequency will change according to Theorem 5. In general, we therefore expect to see several pinned sources that have different temporal frequencies which depend on the location of the defects. Thus, our analysis seems to corroborate the statements made in [22, §6.2.1] where inhomogeneities are mentioned as a possible explanation for the occurrence of what appears to be a one-parameter family of sources in the experiments [1]. The experimental observations reported in [35] seem to indicate, however, that these sources drift and are therefore not pinned. This issue therefore warrants further investigation.

For sinks with  $c_d = 0$ , we do not expect pinning. Indeed, the intersection of center-unstable and center-stable manifolds is transverse for sinks at  $\varepsilon = 0$  and therefore persists as a family of transverse intersections for all small  $\varepsilon$  independently of where we place the sink.

An alternative heuristic way of investigating the interaction of small-amplitude sinks with even smaller localized slowly-varying inhomogeneities is via the approximation by Burgers equation that we discussed in Section 1.3. For  $\varepsilon = 0$ , the sinks or shocks in Burgers equation have an eigenvalue at zero which is induced by translation symmetry. The resulting normally-hyperbolic invariant manifold that consists of all translates of the sink persists for all  $\varepsilon$  close to zero. The leading-order terms of the perturbed flow on the invariant manifold are obtained by projecting the term in Burgers equation that represents the inhomogeneous term  $g(x, u)$  in (6.8) onto the manifold using the adjoint eigenfunction associated with the translation eigenvalue. In conservation laws, the null space of the adjoint is spanned by the constant function, so that the perturbed flow is given by the mass of the term that represents the inhomogeneity  $g(x, u)$ . Since Burgers equation (1.19) is written in terms of the wavenumber, it turns out that the derivative  $g_x(x, u)$  of the inhomogeneity

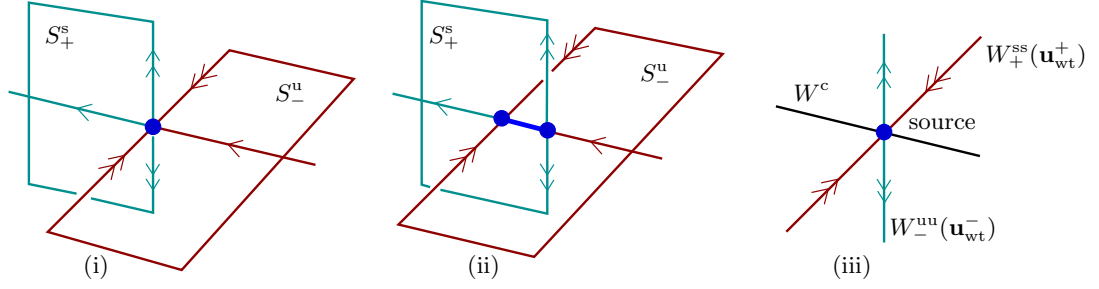


Figure 6.6: *Inhomogeneities may create contact defects (ii) or sources (iii).*

arises in Burgers equation. Therefore, since the mass of  $g_x(x, u)$  is zero, the reduced flow on the perturbed manifold vanishes to leading order, and the family of sinks persists with positions that are independent of the inhomogeneity. The spatial-dynamics argument presented above shows that the higher-order terms do not make a difference and that the situation remains unchanged for large-amplitude sinks and, typically, for large inhomogeneities.

This analysis of Burgers equation suggests also that sinks with  $c_d \neq 0$  will simply outrun the inhomogeneity without experiencing a noticeable change of velocity, so that the inhomogeneity will merely affect the asymptotic wave train. Thus, we shall now briefly discuss the influence of inhomogeneities on wave trains. Note that wave trains with non-zero group velocity are not affected by an inhomogeneity as they arise as transverse intersections of their center-stable and center-unstable manifolds of (6.8) with  $\varepsilon = 0$  which persist for all  $\varepsilon$  close to zero. In this setting, we may interpret inhomogeneities as pinned transmission defects.

Wave trains with zero group velocity behave differently since small localized inhomogeneities create either contact defects or sources within such wave trains. To prove this, we again interpret wave trains as transverse intersections of center-unstable and center-stable manifolds. For wave trains with zero group velocity, this intersection, which consists precisely of the center manifold, is two-dimensional, and the vector field on it is given by (6.7) [10]. Factoring out the  $S^1$ -symmetry that is generated by the temporal time-shift, we are left with a small line segment parametrized by the wavenumber  $q$ . As illustrated in Figure 6.6(i), this line segment, considered as a subset of  $W_-^{cu}$ , is separated at  $\mathbf{u}^{uu}$  into two half-lines by the strong-unstable manifold of the periodic orbit that corresponds to the wave train. Similarly, the strong-stable manifold cuts the line segment, considered as a subset of  $W_+^{cs}$ , into two half-lines at  $\mathbf{u}_+^{ss}$ . Without an inhomogeneity, we have  $\mathbf{u}_+^{ss} = \mathbf{u}^{uu} = \mathbf{u}_{wt}$  as shown in Figure 6.6(i). The set of those initial data in  $W_-^{cu}$  whose solutions converge towards the wave train as  $\xi \rightarrow -\infty$  (which we will refer to as the unstable set  $S_-^u$ ) consists of points with line-segment coordinate  $\mathbf{u} < \mathbf{u}^{uu}$ , i.e. of “half” of  $W_-^{cu}$ . Analogously, the stable set  $S_+^s$  of those data whose solutions converge to the wave train as  $\xi \rightarrow \infty$  consists of points whose line-segment coordinate satisfies  $\mathbf{u} > \mathbf{u}_+^{ss}$ .

Upon introducing the inhomogeneity, the transverse intersection will persist, but the stable and unstable sets may split. If  $\mathbf{u}^{uu} > \mathbf{u}_+^{ss}$  as illustrated in Figure 6.6(ii), then an intersection

$$S_+^s \cap S_-^u = \{\mathbf{u} \in W_-^{cu} \cap W_+^{cs}; \mathbf{u}^{uu} > \mathbf{u} > \mathbf{u}_+^{ss}\}$$

occurs which corresponds to a one-parameter family of contact defects with *varying* phase-slip. If the stable and unstable sets split in the opposite direction, so that  $\mathbf{u}_{-}^{\text{uu}} < \mathbf{u}_{+}^{\text{ss}}$ , then contact defects cannot appear. In this case, we may, however, use the parameter  $\omega = \omega_{\text{nl}}(k_*) + \tilde{\omega}$  to unfold the saddle-node wave trains at  $x = \pm\infty$ . While the intersection points on the fibers move linearly with  $\tilde{\omega}$ , the dynamics on the base points of the fibers changes with the square root of  $\tilde{\omega}$ . Thus, we denote the strong-stable manifold of the wave train  $\mathbf{u}_{\text{wt}}^{+}$  at  $x = \infty$  with positive group velocity by  $W_{+}^{\text{ss}}(\mathbf{u}_{\text{wt}}^{+})$  and, analogously, the strong-unstable manifold of the wave train  $\mathbf{u}_{\text{wt}}^{-}$  at  $x = -\infty$  with negative group velocity by  $W_{-}^{\text{uu}}(\mathbf{u}_{\text{wt}}^{-})$ . Furthermore, we denote their intersections with the one-dimensional manifold  $W^c$  at  $x = 0$  by  $\mathbf{v}_{+}^{\text{ss}}$  and  $\mathbf{v}_{-}^{\text{uu}}$ , respectively. We then have  $\mathbf{v}_{+}^{\text{ss}}(\tilde{\omega}) = \mathbf{u}^{\text{ss}}(\varepsilon) - a_{+}\sqrt{\tilde{\omega}}$  and  $\mathbf{v}_{-}^{\text{uu}}(\tilde{\omega}) = \mathbf{u}^{\text{uu}}(\varepsilon) + a_{-}\sqrt{\tilde{\omega}}$  for certain positive coefficients  $a_{\pm} > 0$ . In particular, we find a unique  $\tilde{\omega}$  such that  $\mathbf{u}_{+}^{\text{ss}}(\tilde{\omega}) = \mathbf{u}_{-}^{\text{uu}}(\tilde{\omega})$  which corresponds to a source as claimed.

## 6.6 Frequency locking through periodic forcing

Time-periodic forcing of the reaction-diffusion system breaks the temporal translation invariance and therefore tends to lock the frequency of defects to integer multiples of the forcing frequency  $\omega_f$ . As a consequence, the frequency is effectively removed as a parameter, and the time-derivative  $\partial_{\tau}u_{\text{d}}$  of defects does no longer contribute to the null space of  $\Phi_{\text{d}}$ . Wave trains are still parametrized by their wavenumber  $k$  and arise as time-periodic solutions in a frame that moves with speed  $c$  where

$$\omega_{\text{nl}}(k) - kc = \omega_f. \quad (6.9)$$

Note that the forcing frequency  $\omega_f$  and the nonlinear dispersion relation  $\omega_{\text{nl}}$  in the above equation can be replaced by rational multiples which leads to further complications. For simplicity, we therefore focus on the simplest possible scenario. Thus, assume that the autonomous system (4.2) admits a transverse defect so that (6.9) is met for both  $k = k_{-}$  and  $k = k_{+}$  with  $c = c_{\text{d}}$ . We then add a forcing term  $\varepsilon g(t, u)$  with temporal frequency  $\omega_f$  to (1.1). A sink will persist regardless of its phase relative to the periodic forcing since the map  $\iota_{\text{si}}$  defined in (5.2) is onto (here, we add  $\varepsilon$  as a parameter and keep  $k_{\pm}$  fixed). For sources, we cannot vary the variable  $\omega_{\text{d}}$  that appears in the map  $\iota_{\text{so}}$  from (5.4). Instead, we use the relative phase difference  $\theta$  defined via  $u_{\text{d}}(\xi, \tau + \theta)$ . As in Section 6.5, we can then prove that sources persist for phase differences that correspond to simple roots of an appropriate Melnikov function  $M(\theta)$ . There should be an even number of such roots, which correspond to persisting sources that are alternately spectrally stable and unstable.

Alternatively, we may seek small-amplitude defects by studying the effect of temporal forcing on wave trains. As outlined above, wave trains will simply adjust their speed to ensure that (6.9) is met, and small-amplitude defects will therefore not occur. This works except when the forcing is in resonance with the group velocity so that

$$\omega_{\text{nl}}(k_*) - k_*c_g(k_*) = \omega_f.$$

The spatial dynamics near the forced wave train is then described by an autonomous saddle-node bifurcation

$$\theta_{\xi} = k_* + \check{k} + \text{O}(\varepsilon), \quad \check{k}_{\xi} = \check{c}(k_* + \check{k}) - \check{k}^2 + \text{O}(\varepsilon)$$

of a periodic orbit whose temporal frequency is locked to  $\omega_f$ . The variables  $\check{k}$  and  $\check{c}$  denote the deviations from the wavenumber  $k_*$  and the group velocity  $c_g(k_*)$ , respectively. Thus, we find small heteroclinic orbits that correspond to small-amplitude sinks. If we wish to find more complicated defects, we need to consider forcing frequencies that are in resonance with spatially homogeneous oscillations for which  $k_* = 0$ .

## 6.7 Locking of defect speed and phase velocity

Frequency locking can also occur when  $\omega_d$  vanishes at a given defect. In this case, the defect does not depend on time when considered in its co-moving frame, and therefore satisfies the travelling-wave ODE (2.4). We briefly discuss for each defect type with what codimension this situation arises. Note that  $\omega_d = 0$  if, and only if, the phase velocities  $c_p(k_-) = c_p(k_+)$  are equal. Since we are mainly interested in waves with a non-zero group velocity, we assume that the nonlinear dispersion relation  $\omega_{\text{nl}}(k)$  is not constant on any open non-empty interval.

Transmission defects with  $k_- = k_+$  occur as transverse homoclinic connections of a hyperbolic periodic orbit of (2.4). The periodic orbits as well as the homoclinic connection therefore persist if we vary  $k_- = k_+$ , provided we choose  $c = c_p = \omega_{\text{nl}}(k)/k$ . Thus, transmission defects arise with the same codimension as travelling waves and as proper modulated waves. In particular, defect speed and phase velocities can lock.

In contrast, phase velocity and defect speed of sinks, sources, and contact defects do not lock, since these defects arise as travelling waves only with a larger codimension than as defects with  $\omega_d \neq 0$ . Indeed, sinks and sources have  $k_- \neq k_+$ , so that the condition  $c_p(k_-) = c_p(k_+)$  is a genuine additional equation that raises the codimension by one. For contact defects, we need  $c_p(k) = c_g(k)$  along the branch which holds only if  $\omega_{\text{nl}}''(k) = 0$  as an explicit computation shows.

## 6.8 Large bounded domains

So far, we focused on defects on the unbounded real line. Experiments, however, take place on bounded domains in a fixed laboratory frame. Thus, defects with non-zero speed are transient phenomena that disappear by colliding either with other defects or with the domain boundaries. Defects with speed close to zero, however, should exist over much longer time intervals. In this section, we shall therefore discuss the persistence of defects on large but bounded domains.

An additional motivation is provided by the need for computational tools that allow us to compute defects in an efficient way. Stable defects can, of course, be computed using direct simulations. If we are, however, interested in computing defects for many different parameter values, in finding their bifurcation points, or in computing unstable defects, then a formulation as a boundary-value problem that allows for a systematic continuation—using, for instance, AUTO97 [8]—would be desirable. To obtain such a formulation, we consider (4.2) in the frame of the defect, truncate the real line to a finite bounded interval, and impose appropriate phase and boundary conditions. We currently implement this procedure in AUTO97.

## Boundary layers

We begin by investigating how wave trains interact with boundaries. Thus, consider the half line  $\mathbb{R}^+$  with a boundary at  $x = 0$ . We focus on  $c = 0$  and seek defects that are caused by the boundary conditions at  $x = 0$ . In the context of the modulated-wave equation (4.2), the boundary conditions at  $x = 0$  are represented by the infinite-dimensional subspace  $B_-$  of  $Y$  that consists of all elements of  $Y$  which satisfy the boundary conditions. We are interested in finding defects as orbits of (4.2) that lie in the intersection of  $B_-$  and the center-stable manifold  $W_+^{\text{cs}}(\mathbf{u}_{\text{wt}})$  of a wave train  $\mathbf{u}_{\text{wt}}$ . Thus, in analogy to Section 6.3, we consider the map

$$\iota_{\text{bc}} : B_- \times W_+^{\text{cs}} \longrightarrow Y, \quad (\mathbf{u}^0, \mathbf{u}^+) \longmapsto \mathbf{u}^0 - \mathbf{u}^+.$$

For boundary conditions such as Dirichlet, Neumann and various mixed conditions, for which the reaction-diffusion system (1.1) is well-posed, the injection map  $\iota_{\text{bc}}$  is Fredholm, and its index is zero if  $c_g > 0$ , and one if  $c_g \leq 0$ .

Therefore, we expect one-parameter families of sinks for wave trains, with group velocity  $c_g < 0$  towards the boundary, that connect to the boundary at  $x = 0$ . This family of sinks is parametrized by the wavenumber  $k$  of the wave train at  $x = \infty$ . On the other hand, boundary-layer sources, which connect to wave trains with group velocity  $c_g > 0$  away from the boundary, occur only for isolated wavenumbers  $k$ . Similarly, there is typically only a finite number of boundary-layer contact defects since  $c_g = 0$  is fixed, even though the Fredholm index is one.

Examples of boundary-layer contact defects are homogeneous oscillations under Neumann boundary conditions. For small wavenumbers, and group velocities directed towards the boundary, we then find boundary-layer sinks which, for Neumann boundary conditions, can be thought of as symmetric sinks since we can extend the equation to the entire real line by reflecting across the boundary. Our discussion of inhomogeneities in Section 6.5 can also be used to show that, for any homogeneous oscillation, there exists an open set, in fact a half space, of Robin boundary conditions that emit wave trains. The resulting defects are therefore boundary-layer sources. The boundary conditions in the complementary half space produce solutions that are asymptotically homogeneous oscillations, that is, boundary-layer contact defects. We also refer to the discussion in [54, Section 5.3] on the existence of two-dimensional radially symmetric target patterns that are generated by boundary conditions imposed at a small hole in the domain.

## Truncation

We are now prepared to discuss whether defects on  $\mathbb{R}$  can be approximated by defects on large but bounded intervals  $(-L, L)$ . The discussion in the preceding section shows that the boundary conditions should be compatible in the sense that boundary-layer defects exist which absorb or generate the wave trains in the far field of the sources, contact defects or sinks whose persistence we would like to prove.

Suppose, for instance, that there exists a source between wave trains with asymptotic wavenumbers  $k_{\pm}$  and boundary-layer sinks that absorb these wave trains at the boundaries  $x = \pm L$ . As in [32],

it then follows that the source persists as a solution to the truncated problem in a frame moving with speed  $c(L)$  provided the frequency is adjusted to  $\omega(L)$ . Here, the corrections to speed and frequency satisfy  $(c(L), \omega(L)) = (c_d, \omega_d) + O(e^{-\delta L})$  for some  $\delta > 0$ . Furthermore, the solution is  $O(e^{-\delta L})$  close to the profile of the defect on  $\mathbb{R}$  for  $|\xi| < L/2$  and to the boundary-layer sinks for  $|\xi| > L/2$ . For symmetric sources and symmetric boundary conditions<sup>10</sup> at  $\xi = \pm L$ , we have  $c(L) \equiv 0$ .

Similar results are true for sinks, although there is the severe restriction that both asymptotic wave trains need to be created by boundary-layer sources. For contact defects, we need to assume the existence of boundary-layer contact defects that connect to the boundary. To obtain persistence, we need to unfold the saddle-node wave trains in a fashion similar to the discussion in Section 6.5. We omit the details.

## Stability

Stability properties of defects on bounded intervals  $(-L, L)$  with fixed boundary conditions are remarkably different from their counterparts on  $\mathbb{R}$ . First, the period map  $\Phi_d^L$  of a defect on  $(-L, L)$  will have only point spectrum. We denote the union of all Floquet exponents of  $\Phi_d^L$  by  $\Sigma_L$ . If we take the limit as  $L \rightarrow \infty$ , then the set  $\Sigma_L$  converges to a limiting set in the symmetric Hausdorff distance where the convergence is uniform on bounded subsets of  $\mathbb{C}$  [46]. The limiting set is the disjoint union of three sets, namely the boundary spectrum  $\Sigma_{\text{bdy}}$ , the extended point spectrum  $\Sigma_{\text{ext}}$ , and the absolute spectrum  $\Sigma_{\text{abs}}$ . Before defining them in detail, we remark that  $\Sigma_{\text{bdy}}$  and  $\Sigma_{\text{ext}}$  are discrete, while  $\Sigma_{\text{abs}}$  is continuous in a sense that will be made precise below. The convergence of  $\Sigma_L$  towards both the boundary spectrum and the extended spectrum is exponential in  $L$  and includes convergence of the algebraic multiplicity. The convergence towards the absolute spectrum, however, is algebraic of order  $O(1/L)$ , and the number of elements in  $\Sigma_L$  in any fixed neighborhood of an element of  $\Sigma_{\text{abs}}$  tends to infinity as  $L \rightarrow \infty$ .

We now define the three sets whose union is the limiting spectral set, and begin with the absolute spectrum. We say that  $\lambda$  belongs to the complement of the absolute spectrum in  $\mathbb{C}$  if there exist exponential weights  $\eta_{\pm}$  such that  $\Phi_d - \rho$  is Fredholm with index zero on  $L^2_{\eta_-, \eta_+}(\mathbb{R}, \mathbb{C}^n)$  and the relative Morse index of both asymptotic wave trains is zero relative to the exponential weights<sup>11</sup>. The absolute spectrum consists of a countable union of semi-algebraic curves which end precisely in spatial double roots  $\nu$  with  $\text{Re } \nu = \eta_{\pm}$  of the dispersion relation of one of the asymptotic wave trains. We refer to [45, 46] for more details.

The extended point spectrum consists of all  $\lambda \in \mathbb{C}$  for which there are exponential weights  $\eta_{\pm}$  with the same properties as above so that the null space of  $\Phi_d - \rho$  on  $L^2_{\eta_-, \eta_+}(\mathbb{R}, \mathbb{C}^n)$  is not trivial. Lastly, the boundary spectrum is defined as the extended point spectrum of the boundary-layer defects that are involved in the construction of the defect on  $(-L, L)$ .

<sup>10</sup>We say that the boundary conditions  $\mathcal{B}_-$  and  $\mathcal{B}_+$  at  $\xi = -L$  and  $\xi = L$  are symmetric if  $\mathcal{R}_0(\mathcal{B}_-) = \mathcal{B}_+$  with  $\mathcal{R}_0$  as in (6.6).

<sup>11</sup>Which means that the relative Morse indices are computed for (4.6) with  $\eta = \eta_{\pm}$  and  $\mathbf{u}_d$  replaced by the asymptotic wave train.

Since we assumed that the wave trains are spectrally stable, we see that the absolute spectrum of sinks, transmission defects, and sources lies in the open left half-plane since the group velocities of the asymptotic wave trains are not zero. The absolute spectrum of contact defects always touches the imaginary axis at  $\lambda = 0$  and consists, in fact, of a line segment  $\lambda < 0$  inside a sufficiently small neighborhood of the origin. Indeed, the two roots  $\nu_{\pm}$  near zero of the dispersion relation (6.2)  $\lambda = d_{\parallel}\nu^2 + d_3\nu^3 + O(\nu^4)$  are complex conjugates for  $\lambda < 0$ .

The extended point spectrum of sinks, transmission defects, and sources contains  $\lambda = 0$  with multiplicity

$$\begin{array}{ll} 0 & \text{for sinks} \\ 1 & \text{for transmission defects} \\ 2 & \text{for sources.} \end{array} \tag{6.10}$$

Lastly, the boundary spectrum near the origin is given as follows:

$$\begin{array}{ll} 0 & \text{for each boundary-layer sink} \\ 1 & \text{for each boundary-layer source} \end{array} \tag{6.11}$$

where the time-derivative of the boundary-layer source provides the eigenfunction.

Thus, in summary, if we consider the union of boundary and extended point spectrum near the origin for truncated sinks and sources, then both of them have two eigenvalues near the origin. For truncated sinks, these two eigenvalues arise due to the two boundary-layer sources near the boundaries  $x = \pm L$ , whereas the eigenvalues for truncated sources occur from the source itself with the two boundary-layer sinks not contributing any eigenvalues. While one of the two eigenvalues for truncated sinks or sources accounts for the time-derivative, i.e. for the temporal translation symmetry that is still present, the other eigenvalue, which is associated with the position of the defect relative to the boundary, is free to move and may stabilize or destabilize the truncated defect.

## 6.9 Interactions of defects

Heuristically, the interaction of defects with each other or with boundaries can be explained to a large extent by deriving formal solvability conditions. These conditions arise when we try to match defects, and they can be calculated by projecting certain matching terms onto the null space of  $\Phi_d - \mathbb{1}$ , i.e. onto the eigenfunctions associated with  $\lambda = 0$ , using the adjoint eigenfunctions [12, 13, 42].

First, we need to clarify what we mean when we refer to the eigenfunctions of  $\Phi_d$  associated with the Floquet exponent  $\lambda = 0$ , since the essential spectrum of  $\Phi_d$  touches  $\lambda = 0$ . We believe that the eigenfunctions and eigenvalues that we need to take into account are those that arise in the weighted spaces given in Theorem 4. Indeed, the essential spectrum of defects is generated by the asymptotic wave trains, and its effect is accounted for by Burgers equation (1.19). Given our spatial-dynamics interpretation of the group velocities, we believe that the interaction of defects manifests itself in their spectra in the spaces  $L^2_{\eta}(\mathbb{R}, \mathbb{R}^n)$  with  $\eta$  chosen as in Theorem 4.

Transverse sinks do not have any eigenvalues at  $\lambda = 0$  (see Theorem 4). They do therefore not interact with the tails of adjacent sources but instead react passively by adjusting their speed via

(1.8) according to changes of the wavenumbers in the far field. Changing the phase (6.3) of one of the asymptotic wave trains will cause the sink to correct its position and temporal phase according to the algebraic phase jump condition (6.4).

Transverse sources have a double eigenvalue at  $\lambda = 0$  that is induced by the derivatives of the source with respect to time and space. Therefore, for each source, we obtain two differential equations that define the time derivatives of its position and its phase as functions of perturbations in the far field. Since the associated adjoint eigenfunctions at  $\lambda = 0$  are exponentially localized by Theorem 4, sources interact with adjacent defects or boundaries only very weakly, namely exponentially small in the distance.

Transmission defects have a simple eigenvalue at  $\lambda = 0$ , and the associated adjoint eigenfunction is localized behind the defect, where the group velocity points away from the interface, and constant ahead of the defect. We therefore believe that transmission defects will adjust their phase instantaneously whenever the phase of the wave train ahead of them is changed. Position and temporal phase of transmission defects are also affected by the presence of boundaries or perturbations in their wake. These interactions are described by a single differential equation. Note that position and temporal phase are implicitly related through phase matching with the wave trains ahead of the transmission defect (see Sections 6.1 and 6.2).

Interactions that involve contact defects have, to our knowledge, not been studied previously (not even on a formal level). We believe that Theorem 2, which asserts that the Evans function has a simple root at  $\lambda = 0$ , may play an important role, since this root may change the temporal algebraic decay rate of localized perturbations [34].

## 6.10 Genericity

Our goal in this paper has been to present a list of transverse defects. It is a challenging task to prove whether, and in what sense, this list is complete.

From a formal point of view, we included all possible combinations of group velocities  $c_g^\pm$  relative to the defect velocity  $c_d$  with the exception of *one-sided contact defects* for which one of the group velocities is equal to the defect speed but the other one is not, i.e. for which either  $c_g^- = c_d \neq c_g^+$  or  $c_g^- \neq c_d = c_g^+$ . The reason for omitting one-sided contact defects is that they form part of the boundary of the region in  $(k_-, k_+)$  space where transverse sinks exist. Put differently, in any given system, we expect that only a finite number of wavenumbers occur that are generated by boundaries or by sources. In general, there is no reason why one-sided defects should be selected as they occur only in one-parameter families. For the same reasons, we do not take degenerate sinks, transmission defects, or contact defects into account even though degeneracies, such as eigenvalues at the origin with higher multiplicity, can typically be found by varying only the asymptotic wavenumbers. If we therefore wish to exclude degenerate defects as well as one-sided contact defects, we may consider introducing a notion of genericity that requires the persistence of generic defects when we truncate the real line to a large but finite interval with *generic* boundary layers in the sense of Section 6.8. The reason for including sources as generic defects is that they actively select wavenumbers. Sim-

ilarly, we wish to regard contact and transmission defects as generic since they occur within a background of wave trains with identical wavenumber. In other words, the reason for their generic existence is that they accommodate phase slips within an oscillatory medium (see Section 6.2). Interpreted in a different way, contact and transmission defect occur in open sets of wavenumbers once we impose the constraint that  $k_- = k_+$ .

From a purely mathematical viewpoint, and thinking solely in terms of the codimension with which a certain heteroclinic orbit exists, there is no difference between, say, transmission defects and one-sided contact defects. However, the goal would be to find a notion of genericity that accurately reflects the physical intuition that we described above, i.e., that allows sources, for instance, but rejects one-sided contact defects.

### 6.11 Higher space dimensions

The classification we have presented is valid for *essentially* one-dimensional media. In particular, our approach, and therefore our results, apply equally well to problems on cylindrical domains with a bounded higher-dimensional cross section. Indeed, the key feature that we exploited are exponential dichotomies which exist provided the operators encountered enjoy certain compactness properties that are satisfied for the cross-sectional variables whenever the cross section is bounded [38, 48].

In fact, our results can also be adapted immediately to cover line defects in the plane that are spatially periodic in the direction parallel to the line defect [51]. If we, for the sake of clarity, choose coordinates so that the line defect corresponds to  $x = 0$ , so that  $y$  denotes the variable parallel to the line defect, then the modulated-wave equation (4.2) would contain the Laplace operator in the  $y$  variable, while the spatial evolution variable would be the  $x$ -variable transverse to the defect. We would then pose (4.2) on the space of functions that are periodic in time and in  $y$ . For instance, line defects between planar wave trains that propagate in a direction parallel to the defect can be easily analysed in this framework.

Certain two-dimensional point defects, such as spiral waves and target patterns in the Belousov–Zhabotinsky reaction or stationary focus patterns in convection experiments, are amenable to a similar description since we can measure group velocities in the radial variable [52, 54]. A classification analogous to the one presented here has not yet been attempted in higher space dimensions.

## 7 Example: The cubic–quintic Ginzburg–Landau equation

In this section, we illustrate that all four elementary transverse defects arise in the complex cubic–quintic Ginzburg–Landau equation (CQGL) for appropriate values of the coefficients. In fact, the existence of sources, sinks, and transmission defects in the CQGL has been established in [9], and we therefore focus here on the existence of contact defects. Thus, consider the CQGL

$$\check{A}_t = (1 + i\check{\alpha})\check{A}_{xx} + \check{A} - (1 + i\check{\gamma})\check{A}|\check{A}|^2 - (\check{\delta}_0 + i\check{\delta})\check{A}|\check{A}|^4 \quad (7.1)$$

where  $x \in \mathbb{R}$ ,  $\check{A}(x, t) \in \mathbb{C}$ , and all coefficients are real. The CQGL arises as a special case of the modulation equation that describes degenerate Hopf bifurcations in reaction-diffusion systems [11] and, for  $\check{\alpha} = 0$ , coincides with the  $\lambda$ - $\omega$  system that has been investigated, for instance, in [31]. The CQGL respects the gauge symmetry  $\check{A} \mapsto e^{i\phi}\check{A}$  so that we should seek relative equilibria of the form

$$\check{A}(x, t) = A(x - \check{c}t)e^{-i\check{\omega}t}.$$

Substituting this ansatz into (7.1) yields the ODE

$$A'' = -\frac{1}{1 + i\check{\alpha}} [(1 + i\check{\omega})A + \check{c}A' - (1 + i\check{\gamma})A|A|^2 - (\check{\delta}_0 + i\check{\delta})A|A|^4]. \quad (7.2)$$

We choose  $1 + \check{\alpha}\check{\gamma} > 0$ , which allows us to rescale  $A$  and the parameters so that (7.2) becomes

$$A'' = -(1 + i\omega)A - cA' + (1 + i\gamma)A|A|^2 + (\delta_0 + i\delta)A|A|^4. \quad (7.3)$$

For the sake of clarity, we set  $\delta_0 = 0$  from now on, but remark that most of the subsequent analysis remains valid, with appropriate modifications, when  $\delta_0 > 0$ . An essential assumption is that we take the remaining parameters  $(\gamma, \delta, \omega, c)$  to be close to zero, so that we perturb from the real cubic Ginzburg–Landau equation.

In summary, we consider the complex two-dimensional ODE

$$\begin{aligned} A' &= B \\ B' &= -(1 + i\omega)A - cB + (1 + i\gamma)A|A|^2 + i\delta A|A|^4 \end{aligned} \quad (7.4)$$

with small external parameters  $(\gamma, \delta)$  and small internal parameters  $(\omega, c)$ . In passing, we remark that (7.4) has the same structure as the modulated-wave equation (4.2). In fact, regardless of whether (7.4) is derived near a degenerate Hopf bifurcation or represents a  $\lambda$ - $\omega$  system, (7.4) is the modulated-wave equation, restricted to either a center manifold or a finite-dimensional Fourier subspace. In each case, the gauge invariance is induced by the time-shift symmetry and is therefore a genuine symmetry rather than a normal-form symmetry. For  $c = 0$ , (7.4) has two reversibility symmetries given by

$$\mathcal{R}_0 : (A, B) \mapsto (A, -B), \quad \mathcal{R}_\pi : (A, B) \mapsto (-A, B).$$

As already alluded to, we study (7.4) as a perturbation from the real Ginzburg–Landau equation

$$\begin{aligned} A' &= B \\ B' &= -A + A|A|^2. \end{aligned} \quad (7.5)$$

Note that (7.5) is a Hamiltonian system where the Hamiltonian  $H$  and the symplectic matrix  $J$  are given by

$$H = |A|^2 + |B|^2 - \frac{1}{2}|A|^4, \quad J(A, B, \bar{A}, \bar{B}) = (\bar{B}, -\bar{A}, B, -A).$$

The real Ginzburg–Landau equation (7.5) has a family

$$A(x; k) = \sqrt{1 - k^2}e^{ikx} \quad (7.6)$$

of wave trains for  $|k| < 1$ . In particular, the dispersion relation  $\omega = \omega_{\text{nl}}(k)$  is degenerate as all these wave trains have  $\omega = 0$ . There also is an explicit defect given by

$$A(x) = \tanh\left(\frac{x}{\sqrt{2}}\right) \quad (7.7)$$

which connects the wave trains with zero wavenumber with a phase slip of  $\pi$  (see Section 6.2).

Once  $\gamma$  or  $\delta$  are non-zero, the wave trains (7.6) are solutions to (7.4) if, and only if,

$$\omega = \omega_{\text{nl}}(k; \gamma, \delta, c) = (1 - k^2)\gamma + (1 - k^2)^2\delta - kc \quad (7.8)$$

which is the dispersion relation in the frame moving with speed  $c$ . The wave trains disappear in saddle-node bifurcations precisely when

$$c = c_g(k; \gamma, \delta) = -2k\gamma + 4k(k^2 - 1)\delta. \quad (7.9)$$

We are interested in the fate of the defect (7.7) for  $(\gamma, \delta)$  small but non-zero.

It will be convenient to eliminate the gauge symmetry of (7.5). Often, this is achieved by introducing the blow-up coordinates  $B/A$  (or  $A/B$ ) and  $|A|^2$ . In our example, however, this would force us to use two blow-up charts since both  $A$  and  $B$  vanish somewhere along the defect. Instead, we use the generators of the ring of invariant polynomials with respect to the  $S^1$ -gauge symmetry as new coordinates and define

$$R = A\bar{A}, \quad S = B\bar{B}, \quad N = A\bar{B}, \quad (7.10)$$

with  $N = N_r + iN_i$ . A result by Hilbert (see, for instance, [4]) shows that the invariants smoothly parametrize the group orbits of the  $S^1$ -symmetry. For later use, we remark that, if we evaluate  $N$  on the wave trains (7.6), we obtain  $N = A\bar{A}' = -ik(1 - k^2)$  so that

$$N_i = -k(1 - k^2). \quad (7.11)$$

In the new variables (7.10), equation (7.5) becomes

$$\begin{aligned} R' &= 2N_r \\ S' &= 2(R - 1)N_r - 2cS + 2(\omega - \gamma R - \delta R^2)N_i \\ N_r' &= S - cN_r - R + R^2 \\ N_i' &= -cN_i + \omega R - \gamma R^2 - \delta R^3. \end{aligned} \quad (7.12)$$

Note that we eliminated the phase invariance without reducing the dimension, at the expense of introducing an algebraic relation

$$\mathcal{C}(R, S, N) := RS - N\bar{N} = 0 \quad (7.13)$$

which must be satisfied for solutions of (7.12) to correspond to solutions of (7.5). For  $c = 0$ , (7.12) is reversible under  $N \mapsto -N$  (which represents both  $\mathcal{R}_0$  and  $\mathcal{R}_\pi$ ).

For  $(\gamma, \delta) = (\omega, c) = 0$ , we find

$$\begin{aligned}
R' &= 2N_r \\
S' &= 2(R-1)N_r \\
N_r' &= S - R + R^2 \\
N_i' &= 0.
\end{aligned} \tag{7.14}$$

We note that both  $\mathcal{C}$  and  $H$  are conserved along trajectories of (7.14). Exploiting that the Hamiltonian is now given by

$$H = S + R - \frac{R^2}{2} \tag{7.15}$$

equation (7.14) can therefore be written as

$$R'' = 2H - 4R + 3R^2, \quad S = H - R + R^2/2, \quad N = R'/2. \tag{7.16}$$

The equilibria of (7.14) are given by  $S = R - R^2$  and  $N_r = 0$  for arbitrary  $R$  and  $N_i$ . Using (7.11) and the algebraic relation (7.13), we obtain the parametrization

$$(R^\infty, S^\infty, N_r^\infty, N_i^\infty) = (1 - k^2)(1, k^2, 0, -k), \quad H^\infty = \frac{(1 - k^2)(1 + 3k^2)}{2} \tag{7.17}$$

for those equilibria of (7.12) that correspond to solutions of (7.5). The eigenvalues of the linearization of (7.14) about the equilibria (7.17) are given by two zero eigenvalues,  $\lambda_1 = \lambda_2 = 0$ , which arise due to translation symmetry and the conserved quantity  $\mathcal{C}$ , and two eigenvalues  $\lambda_{3/4} = \pm \sqrt{2(1 - 3k^2)}$ , which are hyperbolic if  $k^2 < 1/3$ . Since the waves with  $k^2 > 1/3$  are known to be unstable with respect to long-wavelength perturbations, the well-known Eckhaus instability, we focus exclusively on the case

$$|k| < \frac{1}{\sqrt{3}} \tag{7.18}$$

so that we are away from the Eckhaus instability.

On the other hand, solving (7.16), we find the one-parameter family

$$\begin{aligned}
R_d(x) &= (1 - k^2) - (1 - 3k^2) \operatorname{sech}^2 \left( \sqrt{1 - 3k^2} x / \sqrt{2} \right) \\
S_d(x) &= H^\infty - R_d(x) + \frac{1}{2} R_d^2(x) \\
N_{d,r}(x) &= R_d'(x) / 2 \\
N_{d,i}(x) &= -k(1 - k^2)
\end{aligned} \tag{7.19}$$

of homoclinic orbits that are parametrized by the asymptotic wavenumber  $k$ . Linearizing (7.14) about these orbits gives the variational equation

$$\begin{aligned}
R' &= 2N_r \\
S' &= 2(R_d(x) - 1)N_r + R_d'(x)R \\
N_r' &= S - R + 2R_d(x)R \\
N_i' &= 0
\end{aligned} \tag{7.20}$$

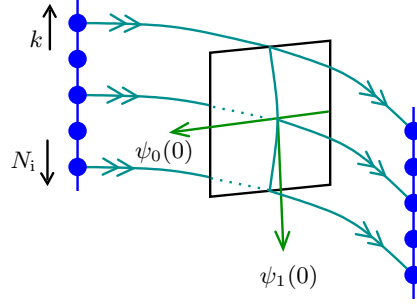


Figure 7.1: The dynamics of (7.14) within the level set  $\mathcal{C} = 0$  is illustrated. The two lines of equilibria are drawn separately even though they both correspond to the same family given in (7.22).

and the corresponding adjoint variational equation

$$\begin{aligned}
 r' &= -R'_d(x)s - (2R_d(x) - 1)n_r \\
 s' &= -n_r \\
 n'_r &= -2r - 2(R_d(x) - 1)s \\
 n'_i &= 0.
 \end{aligned} \tag{7.21}$$

Solutions to the adjoint variational equation (7.21) can be computed explicitly in various different ways. One approach is to observe, and exploit, that

$$[s']''' = (6R_d(x) - 4)[s'].$$

Alternatively, the gradients  $\nabla\mathcal{C}$  and  $\nabla H$  of the conserved quantity (7.13) and the energy (7.15) are automatically solutions to (7.21). Either way, we see that three bounded solutions to (7.15) are given by

$$\begin{aligned}
 \psi_0(x) &= \left( \frac{1}{2}R_d^2(x) + (R^\infty - 1)R_d(x) + R^\infty - \frac{3}{2}(R^\infty)^2, R_d(x) - R^\infty, -R'_d(x), 0 \right) \\
 \psi_1(x) &= (0, 0, 0, 1) \\
 \psi_2(x) &= \nabla H(x) = (1 - R_d(x), 1, 0, 0),
 \end{aligned}$$

while the fourth, linearly independent solution  $\psi_3(x)$  is unbounded. Note that  $\psi_0(x)$  decays exponentially and points into the direction perpendicular to the sum of the center-stable and center-unstable manifolds along the homoclinic orbit (7.19). The two vectors  $\psi_0(x)$  and  $\psi_1(x)$  together are part of the orthogonal complement of the strong-unstable manifold, which coincides with the strong-stable manifold. We refer to Figure 7.1 for an illustration.

Our goal is to understand the intersections of various stable and unstable manifolds as well as their dependence on the wavenumber  $k$  of the wave trains. Their intersections will be studied using the Melnikov integrals in the directions of  $\psi_0$  and  $\psi_1$  for the derivatives of the right-hand side of (7.12) with respect to  $(\gamma, \delta, \omega, c)$ . The resulting bifurcation scenario is, in fact, similar to the double-flip bifurcation that we discussed in Sections 6.4 and 6.5 in the context of transitions from contact defects to sources and of inhomogeneities embedded in media of wave trains with zero group velocity.

We begin with a local analysis of the slow manifold

$$(R^\infty, S^\infty, N_r^\infty, N_i^\infty) = (1 - k^2, k^2(1 - k^2), 0, -k(1 - k^2)) \quad (7.22)$$

that consists of all equilibria of (7.14) that satisfy (7.13). The tangent space to this family of equilibria is spanned by

$$\frac{d}{dk}(R^\infty, S^\infty, N_r^\infty, N_i^\infty) = (-2k, 2k(1 - 2k^2), 0, 3k^2 - 1), \quad (7.23)$$

while the associated adjoint eigenvector is

$$\psi_1^\infty = (0, 0, 0, 1).$$

The flow along the family of equilibria for  $(\gamma, \delta, \omega, c) \neq 0$  is obtained [15] by evaluating the derivatives of the right-hand side of (7.12) with respect to  $(\gamma, \delta, \omega, c)$  at the equilibria and projecting them with  $\psi_1^\infty$ . If we parametrize the center manifold by the wavenumber  $k$ , the reduced equation is

$$(3k^2 - 1)\dot{k} = ck(1 - k^2) + \omega(1 - k^2) - \gamma(1 - k^2)^2 - \delta(1 - k^2)^3 + O(2), \quad (7.24)$$

where  $O(2)$  denotes quadratic terms in  $(\gamma, \delta, \omega, c)$ . A point  $k_*$  is an equilibrium if, and only if,  $\omega$  is given by the nonlinear dispersion relation (7.8)

$$\omega = \omega_{\text{nl}}(k_*; \gamma, \delta, c) = \gamma(1 - k_*^2) + \delta(1 - k_*^2)^2 - ck_* \quad (7.25)$$

in which case (7.24) becomes

$$\dot{k} = -\frac{1 - k^2}{1 - 3k^2} [\omega_{\text{nl}}(k_*; \gamma, \delta, c) - \omega_{\text{nl}}(k; \gamma, \delta, c)] + O(2).$$

The linearization of (7.24) about an equilibrium  $k_*$  is therefore not hyperbolic precisely when  $c$  is given by the group velocity (7.9)

$$\begin{aligned} c &= c_g(k_*; \gamma, \delta) = -2k_*\gamma - 4k_*(1 - k_*^2)\delta \\ \omega &= \omega_{\text{nl}}(k_*; \gamma, \delta, c_g(k_*)) = (1 + k_*^2)\gamma + (1 - k_*^2)(1 + 3k_*^2)\delta. \end{aligned} \quad (7.26)$$

With these choices of  $\omega$  and  $c$ , the slow reduced equation near  $k = k_*$  is given by

$$\dot{\kappa} = -\frac{1 - k_*^2}{1 - 3k_*^2} [\gamma + 2\delta(1 - 3k_*^2)] \kappa^2 + O(\kappa^3) \quad (7.27)$$

in the variable  $\kappa = k - k_*$ . In particular, to leading order in  $\kappa$ , the unstable manifold  $W^u$  of the equilibrium  $k = k_*$  is contained in  $k < k_*$  if  $\gamma + 2\delta > 0$ , and in  $k > k_*$  if  $\gamma + 2\delta < 0$ .

We now compute the Melnikov integrals in the direction of  $\psi_0(x)$  which are defined by

$$M_0^j = \int_{\mathbb{R}} \langle \psi_0(x), \partial_j F(R_d, S_d, N_{d,r}, N_{d,i})(x) \rangle dx$$

where  $F$  denotes the right-hand side of (7.12) and  $j = \gamma, \delta, \omega, c$ . These integrals show how the center-stable and center-unstable manifolds split along the homoclinic orbit given in (7.19) upon varying  $(\gamma, \delta, \omega, c)$  near zero. A tedious calculation gives

$$\begin{aligned} M_0^\gamma(k) &= -\frac{4}{3}k(1-k^2)(1+3k^2)\sqrt{2(1-3k^2)} \\ M_0^\delta(k) &= -\frac{4}{15}k(1-k^2)(3+2k^2+27k^4)\sqrt{2(1-3k^2)} \\ M_0^\omega(k) &= 4k(1-k^2)\sqrt{2(1-3k^2)} \\ M_0^c(k) &= \frac{4}{3}(1-k^2)\sqrt{2(1-3k^2)}. \end{aligned} \quad (7.28)$$

The distance of the center-unstable and center-stable manifolds is given by the expression

$$\Delta_0(k; \gamma, \delta, \omega, c) = \omega M_0^\omega(k) + c M_0^c(k) + \gamma M_0^\gamma(k) + \delta M_0^\delta(k) + \mathcal{O}(2).$$

If we seek contact defects, we should find intersections related to a saddle-node equilibrium  $k_*$  of (7.26). Thus, we shall choose  $(\omega, c)$  according to (7.26), and investigate roots of the splitting distance

$$\begin{aligned} \Delta_0^{\text{cd}}(k, k_*; \gamma, \delta) &= \omega_{\text{nl}}(k_*) M_0^\omega(k) + c_{\text{g}}(k_*) M_0^c(k) + \gamma M_0^\gamma(k) + \delta M_0^\delta(k) + \mathcal{O}(2) \\ &= \frac{4}{3}(1-k^2)(2-3kk_*-3k^2)(k-k_*)\sqrt{2(1-3k^2)}\gamma \\ &\quad + \frac{4}{15}(1-k^2)(k[12-2k^2-27k^4]-k_*[20(1-k_*^2)+15kk_*(3k_*^2-2)]) \\ &\quad \times \sqrt{2(1-3k^2)}\delta + \mathcal{O}(2) \end{aligned} \quad (7.29)$$

of the center-unstable and center-stable manifolds of the equilibrium  $k_*$  along the homoclinic orbit at level  $k$ .

Next, we investigate the splitting of the strong-stable and strong-unstable manifolds in the center direction which is given by Melnikov integrals in the direction of  $\psi_1(x)$ . We therefore choose  $\omega$  and  $c$  as in (7.26) so that a given point  $k = k_*$  on the manifold of equilibria persists as a saddle-node equilibrium for  $(\gamma, \delta) \neq 0$ . We define the Melnikov integrals

$$\begin{aligned} M_1^\gamma(k_*) &= \int_{\mathbb{R}} \langle \psi_1(x), [\partial_\gamma + (1+k_*^2)\partial_\omega - 2k_*\partial_c]F(R_d, S_d, N_{d,r}, N_{d,i})(x) \rangle dx \\ M_1^\delta(k_*) &= \int_{\mathbb{R}} \langle \psi_1(x), [\partial_\delta + (1-k_*^2)(1+3k_*^2)\partial_\omega - 4k_*(1-k_*^2)\partial_c]F(R_d, S_d, N_{d,r}, N_{d,i})(x) \rangle dx \end{aligned}$$

where  $F$  denotes again the right-hand side of (7.12). A tedious but straightforward computation gives

$$M_1^\gamma(k_*) = \frac{2}{3}(1-3k_*^2)\sqrt{2(1-3k_*^2)} > 0, \quad M_1^\delta(k_*) = \frac{16}{15}(1-3k_*^2)^2\sqrt{2(1-3k_*^2)} > 0. \quad (7.30)$$

We are now ready to describe the bifurcation picture for small  $(\gamma, \delta)$ . Consider a two-dimensional section transverse to the flow that lies in a small neighborhood of  $(R_d, S_d, N_{d,r}, N_{d,i})(0)$  in the three-dimensional manifold described by the algebraic relation (7.13). In this two-dimensional section,

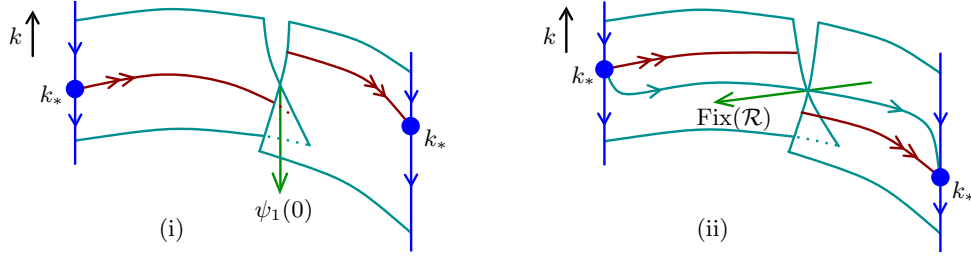


Figure 7.2: The splitting of the strong-unstable and strong-stable manifolds of the equilibrium  $k_* = 0$  of (7.12) is illustrated for  $\gamma + \frac{8}{5}\delta > 0$  in (i) and for  $\gamma + \frac{8}{5}\delta < 0$  in (ii). The sketch of the flow on the slow manifold assumes  $\gamma + 2\delta > 0$ .

the center-stable and center-unstable manifolds coincide when  $(\gamma, \delta, \omega, c) = 0$ . Their intersection forms a line which is parametrized by the coordinate  $k$  of the base point of the corresponding strong-stable fiber on the center manifold (which is, in fact, the manifold of equilibria). Since the general bifurcation diagram is rather complicated, we focus separately on the two cases  $\delta = 0$  (the cubic Ginzburg–Landau equation) and  $k_* = 0$ .

First, we set  $\delta = 0$ . Since we are interested in contact defects, we choose  $(\omega, c)$  according to (7.26) so that the fixed base point  $k_*$  persists as a saddle-node equilibrium. To find contact defects, we need to solve  $\Delta_0^{\text{cd}}(k, k_*; \gamma, 0) = 0$ . Using its definition (7.29), we see that the non-trivial roots of this equation are given by  $k = \pm 1/\sqrt{3}$  and by  $k = k_*$ . The first case is close to the Eckhaus instability, and we will not consider it here. Instead, we show that the second case cannot lead to contact defects: We focus first on the region  $\gamma > 0$ , so that the unstable manifold of the saddle-node equilibrium  $k_*$  for (7.27) is the set  $k < k_*$ . Since  $M_1^\gamma(k_*) > 0$ , however, the strong-unstable manifold of the equilibrium  $k_*$  will miss the stable set of the equilibrium  $k_*$  as illustrated in Figure 7.2(i). For  $\gamma < 0$ , both the sign of the splitting distance and the flow on the slow manifold change sign, and we again conclude that there is no homoclinic orbit to  $k_* = 0$ . In particular, there are no contact defects for  $\delta = 0$ . Varying  $\omega$  and  $c$  to unfold the saddle node at  $k = k_*$ , we see that sources are created. Indeed, we can parametrize the equilibria in the unfolding of the saddle node using  $\mu_1 := \sqrt{|\omega - \omega_{\text{nl}}(k_*)|}$  or  $\mu_2 := \sqrt{|c - c_g(k_*)|}$ . The Melnikov integrals with respect to  $\mu_j$  vanish since the parameters  $\mu_j$  enter only at second order. The base points, however, change to leading order in  $\mu_j$  which allows us to find an intersection of the strong-stable and strong-unstable fibers. These intersections, which correspond to sources, are known as the Nozaki–Bekki holes and can be given explicitly in terms of elementary functions [2, 40].

Next, we set  $k_* = 0$ . In particular,  $c = c_g = 0$  by (7.26) which makes (7.12) reversible under  $\mathcal{R} : N \mapsto -N$  with fixed-point space  $\{N = 0\}$ . The unstable manifold of the equilibrium  $k_* = 0$  of equation (7.27) is the set  $k < 0$  when  $\gamma + 2\delta > 0$  and the set  $k > 0$  for  $\gamma + 2\delta < 0$ . The splitting distance of the strong-unstable and the strong-stable manifold, on the other hand, is given by

$$\Delta_1^{\text{cd}}(\gamma, \delta) = \langle \psi_1(0), W^{\text{uu}}(0) - W^{\text{ss}}(0) \rangle = M_1^\gamma(0)\gamma + M_1^\delta(0)\delta + O(2) \stackrel{(7.30)}{=} \frac{2\sqrt{2}}{3} \left[ \gamma + \frac{8}{5}\delta \right] + O(2).$$

As shown in (7.23) and indicated in Figure 7.1, the vector  $\psi_1(0)$  points to the positive  $N_i$  and the negative  $k$  direction. Thus, the strong-unstable and stable manifolds of  $k_* = 0$  split as shown in

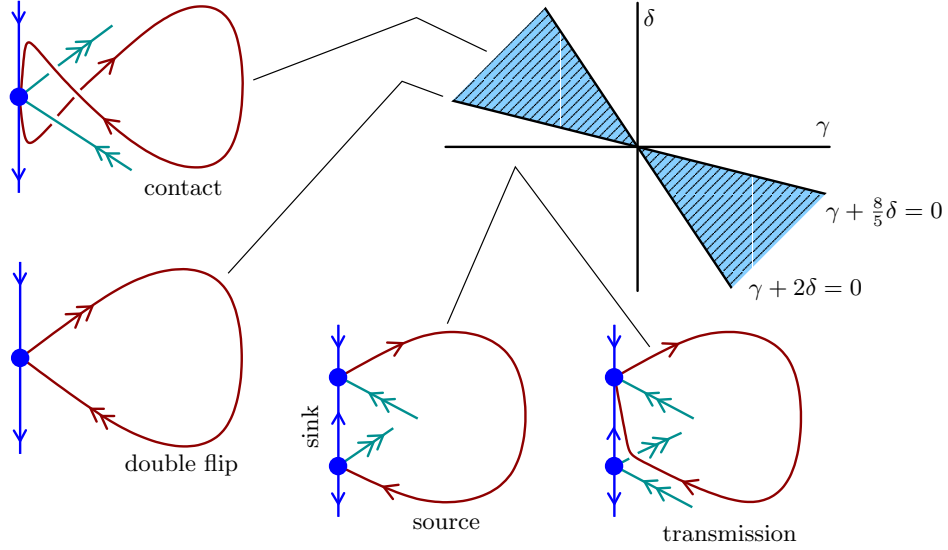


Figure 7.3: The plot in upper right corner shows the parameter space  $(\gamma, \delta)$ . Contact defects exist in the shaded region, while sources and transmission defects exist outside. Along the line  $\gamma + \frac{8}{5}\delta = 0$ , contact defects and sources collide in a double-flip configuration as outlined in Section 6.4.

Figure 7.2. We therefore need

$$(\gamma + 2\delta) \left( \gamma + \frac{8}{5}\delta \right) + O(3) < 0 \quad (7.31)$$

to get a reversible homoclinic connection of the saddle-node equilibrium  $k_* = 0$  as in Figure 7.2(ii). The inequality (7.31) defines, to leading order, a small non-empty cone in the  $(\gamma, \delta)$ -plane (see Figure 7.3). The reversible connection indeed exists as both the center-unstable and the center-stable manifold intersect the fixed-point space  $\{N = 0\}$  of the reversibility operator transversely, which follows from the expression for  $\psi_1(0)$  and since  $N'_d(0) = R''_d(0)/2 \neq 0$ . Lastly, we show that the reversible contact defects persist if we vary the wavenumber  $k_*$  near  $k_* = 0$ . To accomplish this, it suffices to prove that the center-unstable and center-stable manifolds of the equilibrium  $k_* = 0$  intersect transversely along the contact defect. Thus, we evaluate their splitting distance (7.29) at  $k_* = 0$  which yields

$$\begin{aligned} \Delta_0^{\text{cd}}(k, 0; \gamma, \delta) &= \frac{4}{3}k(1 - k^2)(2 - 3k^2)\sqrt{2(1 - 3k^2)}\gamma \\ &\quad + \frac{4}{15}k(1 - k^2)(12 - 2k^2 - 27k^4)\sqrt{2(1 - 3k^2)}\delta + O(2) \\ &= \frac{8\sqrt{2}}{3}k \left[ (1 + O(k))\gamma + \left( \frac{6}{5} + O(k) \right) \delta + O(2) \right], \end{aligned}$$

where we exploited the fact that the splitting distance vanishes at  $k = 0$  due to reversibility of (7.12). We infer from the above expression that the center-unstable and center-stable manifolds intersect transversely at  $k = 0$  provided  $\gamma + \frac{6}{5}\delta + O(2) \neq 0$ . This curve, along which transversality fails, lies outside the existence cone (7.31) for contact defects, which proves that the reversible contact defects are robust and persist under variations of  $k_*$ .

**Theorem 6** Equation (7.31) defines a non-empty open cone in  $(\gamma, \delta)$ -space with the property that the complex cubic-quintic Ginzburg–Landau equation (7.4) has, for each fixed  $(\gamma, \delta)$  in that cone, a one-parameter family of elementary transverse contact defects parametrized by the wavenumber  $k$  with  $k$  close to zero.

We remark that, at the boundary  $\gamma + \frac{8}{5}\delta = 0$  of (7.31), a double-flip transition between sources and contact defects occurs, while at the other boundary  $\gamma + 2\delta = 0$ , the nonlinear dispersion relation of the asymptotic wave trains of the contact defects changes from convex to concave.

Transmission defects can be found as bound states of the Nozaki–Bekki holes and the small sinks that arise in the unfolding of the saddle-node on the center manifold. We refer to Figure 7.3 for an illustration.

## 8 Conclusion

We have presented a framework that allows us to systematically study interfaces between nonlinear wave trains with possibly different wavenumber. We used this approach to analyse sinks, contact defects, transmission defects and sources which are specific defects with distinguished characteristics that occur robustly in reaction-diffusion systems. In addition, we discussed the stability and interaction properties of these defects and investigated some of their bifurcations.

The major open problem is the completeness of the above classification. Other open issues are the nonlinear stability of contact defects, transmission defects and sources. We also emphasize that the list of bifurcations that we discussed is not exhaustive. Lastly, it would be interesting to see how individual defects can be accounted for in a macroscopic description of oscillatory media by coupling mean-field equations of Burgers type to ordinary differential equations for the position and phases of defects.

## A Invariant manifolds

We prove the invariant-manifold Theorem 3 and establish the existence of exponential dichotomies for the linearization of the spatial dynamical system about the defect.

### A.1 Existence of center-stable manifolds

Our first goal is to prove the existence of a center-stable manifold for the modulated-wave equation

$$\begin{aligned} u_\xi &= v \\ v_\xi &= D^{-1}[\omega_d \partial_\tau u - c_d v - f(u)] \end{aligned} \tag{A.1}$$

near a given defect. We use the notation  $\mathbf{u} = (u, v)$  and recall the spaces

$$Y = H^{1/2}(S^1) \times L^2(S^1), \quad Y^1 = H^1(S^1) \times H^{1/2}(S^1).$$

Throughout the appendix, we assume that  $\mathbf{u}_d(\xi, \tau)$  is a defect solution of (A.1) so that  $\mathbf{u}_d(\xi, \cdot) - \mathbf{u}_{\text{wt}}(k_d \xi + \theta_d(\xi) - \cdot)$  converges to zero as  $\xi \rightarrow \infty$  for an appropriate differentiable phase-correction function  $\theta_d(\xi)$  with  $\theta'_d(\xi) \rightarrow 0$  as  $\xi \rightarrow \infty$ . We will show later how changes of  $(\omega, c)$  can be accounted for.

We write (A.1) as the abstract differential equation

$$\mathbf{u}_\xi = \mathcal{A}_0 \mathbf{u} + \mathcal{F}(\mathbf{u}) \quad (\text{A.2})$$

where

$$\mathcal{A}_0 = \begin{pmatrix} 0 & \mathbb{1} \\ \omega_d D^{-1} \partial_\tau & -c_d D^{-1} \end{pmatrix}, \quad \mathcal{F}(\mathbf{u}) = \begin{pmatrix} 0 \\ -D^{-1} f(u) \end{pmatrix}. \quad (\text{A.3})$$

We use the ansatz

$$\mathbf{u}(\xi, \tau) = \mathbf{u}_d(\xi, \theta(\xi) + \tau) + \mathbf{w}(\xi, \tau) \quad (\text{A.4})$$

together with the pointwise normalization

$$\langle \mathbf{w}(\xi, \cdot), \partial_\tau \mathbf{u}_d(\xi, \theta(\xi) + \cdot) \rangle_Y = 0. \quad (\text{A.5})$$

We emphasize that we do not shift  $\mathbf{w}$  relative to the group since this would change the type of the equation we are considering. Equation (A.2) becomes

$$\theta' \partial_\tau \mathbf{u}_d(\xi, \theta(\xi) + \cdot) + \mathbf{w}_\xi = \mathcal{A}_0 \mathbf{w} + \mathcal{F}(\mathbf{u}_d(\xi, \theta(\xi) + \cdot) + \mathbf{w}) - \mathcal{F}(\mathbf{u}_d(\xi, \theta(\xi) + \cdot)). \quad (\text{A.6})$$

For later use, we differentiate (A.5) and obtain the relation

$$\langle \partial_\xi \mathbf{w}(\xi, \cdot), \partial_\tau \mathbf{u}_d(\xi, \theta(\xi) + \cdot) \rangle = -\langle \mathbf{w}(\xi, \cdot), [\partial_\xi + \theta'(\xi) \partial_\tau] \partial_\tau \mathbf{u}_d(\xi, \theta(\xi) + \cdot) \rangle. \quad (\text{A.7})$$

From now on, we shall use the notation  $\mathbf{u}^\theta(\xi) := \mathbf{u}_d(\xi, \theta(\xi) + \cdot)$ . To derive differential equations for  $\theta$  and  $\mathbf{w}$ , we take the scalar product of (A.6) with  $\partial_\tau \mathbf{u}_d(\xi, \theta(\xi) + \cdot)$  and substitute (A.7), which gives the equation

$$\begin{aligned} \theta_\xi &= \frac{1}{|\partial_\tau \mathbf{u}_d|^2 - \langle \mathbf{w}, \partial_{\tau\tau} \mathbf{u}_d^\theta \rangle} \left( \langle \partial_{\tau\xi} \mathbf{u}_d^\theta, \mathbf{w} \rangle + \langle \partial_\tau \mathbf{u}_d^\theta, \mathcal{A}_0 \mathbf{w} + \mathcal{F}(\mathbf{u}_d^\theta + \mathbf{w}) - \mathcal{F}(\mathbf{u}_d^\theta) \rangle \right) \\ &= \mathcal{B}_0(\theta) \mathbf{w} + \mathcal{G}_0(\theta, \mathbf{w}) \end{aligned} \quad (\text{A.8})$$

for  $\theta$ . The scalar products and norms that appear in (A.8) are in  $Y$ , and we introduced the linear operator

$$\mathcal{B}_0(\theta) := \frac{\langle \partial_{\tau\xi} \mathbf{u}_d^\theta + [\mathcal{A}_0 + \mathcal{F}_{\mathbf{u}}(\mathbf{u}_d^\theta)]^* \partial_\tau \mathbf{u}_d^\theta, \cdot \rangle}{|\partial_\tau \mathbf{u}_d|^2}, \quad (\text{A.9})$$

where  $*$  denotes the adjoint, with the nonlinear term  $\mathcal{G}_0(\theta, \mathbf{w})$  making up the difference. For  $\mathbf{w}$ , we obtain

$$\mathbf{w}_\xi = \mathcal{A}_0 \mathbf{w} + \mathcal{F}_{\mathbf{u}}(\mathbf{u}_d^\theta) \mathbf{w} + \left[ \mathcal{F}(\mathbf{u}_d^\theta + \mathbf{w}) - \mathcal{F}(\mathbf{u}_d^\theta) - \mathcal{F}_{\mathbf{u}}(\mathbf{u}_d^\theta) \mathbf{w} \right] - [\mathcal{B}_0(\theta) \mathbf{w} + \mathcal{G}_0(\theta, \mathbf{w})] \partial_\tau \mathbf{u}_d^\theta. \quad (\text{A.10})$$

To prepare for the later use of the contraction-mapping principle, we modify the nonlinear terms. We choose two cut-off functions  $\chi_0(r)$  and  $\chi_1(r)$  such that  $\chi'_0(r) \geq 0$ ,  $\chi'_1(r) \leq 0$  and

$$\chi_0(r) = \begin{cases} r & \text{for } 0 \leq r \leq 1 \\ 2 & \text{for } r \geq 2 \end{cases} \quad \chi_1(r) = \begin{cases} 1 & \text{for } 0 \leq r \leq 1 \\ 0 & \text{for } r \geq 2. \end{cases}$$

Instead of (A.8) and (A.10), we then consider the equations

$$\theta_\xi = \delta\chi_0 \left( \frac{\mathcal{B}_0(\theta)\mathbf{w} + \mathcal{G}_0(\theta, \mathbf{w})}{\delta} \right) \quad (\text{A.11})$$

$$\mathbf{w}_\xi = \mathcal{A}(\theta)\mathbf{w} + \mathcal{G}_1(\theta, \mathbf{w}) \quad (\text{A.12})$$

where

$$\mathcal{A}(\theta) = \mathcal{A}_0 + \mathcal{F}_u(\mathbf{u}_d^\theta) - \left[ \partial_\tau \mathbf{u}_d^\theta \right] \mathcal{B}_0(\theta) \quad (\text{A.13})$$

$$\mathcal{G}_1(\theta, \mathbf{w}) = \chi_1 \left( \frac{|\mathbf{w}|_Y}{\delta} \right) \left[ \mathcal{F}(\mathbf{u}_d^\theta + \mathbf{w}) - \mathcal{F}(\mathbf{u}_d^\theta) - \mathcal{F}_u(\mathbf{u}_d^\theta)\mathbf{w} - \mathcal{G}_0(\theta, \mathbf{w})\partial_\tau \mathbf{u}_d^\theta \right].$$

We emphasize that our cut-off preserves the  $S^1$ -equivariance with respect to the symmetry  $\theta \mapsto \theta + \check{\theta}$  for  $\check{\theta} \in \mathbb{R}$ . In addition, the cut-off is chosen so that solutions to the modified equations (A.11)–(A.12) give solutions to the original equations (A.8)–(A.10) provided  $|\mathbf{w}|_Y$  is less than  $\delta$  for all  $\xi$ . In other words, there is no restriction on the norm of  $\theta$ .

We remark that

$$\begin{aligned} |\mathcal{G}_0(\theta, \mathbf{w})| &= O(|\mathbf{w}|_Y^2), & |\partial_{(\theta, \mathbf{w})} \mathcal{G}_0(\theta, \mathbf{w})|_{L(\mathbb{R} \times Y^1, \mathbb{R})} &= O(|\mathbf{w}|_Y) \\ |\mathcal{G}_1(\theta, \mathbf{w})|_Y &= O(|\mathbf{w}|_{Y^1}^2), & |\partial_{(\theta, \mathbf{w})} \mathcal{G}_1(\theta, \mathbf{w})|_{L(\mathbb{R} \times Y^1, Y)} &= O(|\mathbf{w}|_{Y^1}) \end{aligned}$$

uniformly in  $\theta$ , which allows us to replace  $\mathbf{w} \rightarrow \delta\mathbf{w}$  for any small  $\delta > 0$ . We obtain the new equation

$$\theta_\xi = \delta\chi_0(|\mathbf{w}|_Y) \left[ \mathcal{B}_0(\theta)\mathbf{w} + \frac{1}{\delta}\mathcal{G}_0(\theta, \delta\mathbf{w}) \right] = \delta\check{\mathcal{G}}_0(\theta, \mathbf{w}) \quad (\text{A.14})$$

$$\mathbf{w}_\xi = \mathcal{A}(\theta)\mathbf{w} + \frac{1}{\delta}\mathcal{G}_1(\theta, \delta\mathbf{w}) = \mathcal{A}(\theta)\mathbf{w} + \check{\mathcal{G}}_1(\theta, \mathbf{w}). \quad (\text{A.15})$$

There is a constant  $C_0 > 0$  so that  $\check{\mathcal{G}}_0$  and  $\check{\mathcal{G}}_1$  are bounded by  $C_0$  with Lipschitz constants less than  $C_0\delta$  uniformly in  $(\theta, \mathbf{w})$ .

**Lemma A.1** *There are positive numbers  $\kappa$  and  $C_1$  such that the equation*

$$\mathbf{w}_\xi = \mathcal{A}(\theta_0)\mathbf{w} \quad (\text{A.16})$$

*has exponential dichotomies  $\Phi_{\theta_0}^{\text{cs}}(\xi, \zeta)$  and  $\Phi_{\theta_0}^{\text{uu}}(\xi, \zeta)$  with rate  $\kappa$  and constant  $C_1$  for each  $\theta_0 \in \mathbb{R}$ .*

**Proof.** We will prove the lemma by beginning with an equation for which we know that exponential dichotomies exist and then successively changing the equation until we arrive at (A.16). We will make sure that the equations will have exponential dichotomies at each stage by appealing to the roughness theorem for dichotomies [38] and to Theorem 7 in Section A.2. To save notation, we consider the linear equation

$$\mathbf{w}_\xi = \mathcal{A}\mathbf{w}$$

and simply give the different operators  $\mathcal{A}$  in our chain of equations.

We begin by recalling that the linearization  $\mathcal{A} = \mathcal{A}_0 + \mathcal{F}_u(\mathbf{u}_{\text{wt}}(k\xi + \theta_0))$  about the asymptotic wave train has center-stable and strong-unstable exponential dichotomies uniformly in  $\theta_0$  by [33,

Chapter 2]. Since  $\theta'_d(\xi) \rightarrow 0$  as  $\xi \rightarrow \infty$ , Theorem 7 in Section A.2 implies that there is a  $\xi_0 > 0$  so that  $\mathcal{A}_0 + \mathcal{F}_{\mathbf{u}}(\mathbf{u}_{\text{wt}}(k\xi + \theta_d(\xi)))$  has center-stable and strong-unstable exponential dichotomies for  $\xi \geq \xi_0$ . Invoking the roughness theorem [38, Theorem 1] finally shows that  $\mathcal{A}_0 + \mathcal{F}_{\mathbf{u}}(\mathbf{u}_d(\xi))$  has center-stable and strong-unstable dichotomies for  $\xi \geq 0$  with rate  $\kappa$  and constant  $C_1$ .

In summary, we showed that

$$\mathbf{w}_\xi = [\mathcal{A}_0 + \mathcal{F}_{\mathbf{u}}(\mathbf{u}_d(\xi))] \mathbf{w} \quad (\text{A.17})$$

has center-stable and strong-unstable dichotomies for  $\xi \geq 0$ . It therefore remains to establish the same result for

$$\mathbf{w}_\xi = [\mathcal{A}_0 + \mathcal{F}_{\mathbf{u}}(\mathbf{u}_d(\xi)) - [\partial_\tau \mathbf{u}_d] \mathcal{B}_0(0)] \mathbf{w} \quad (\text{A.18})$$

where  $\theta \equiv 0$ . Note that, by construction, any solution  $\mathbf{w}(\xi)$  of (A.18) for which  $\langle \mathbf{w}(0), \partial_\tau \mathbf{u}_d(0) \rangle = 0$  satisfies

$$\langle \mathbf{w}(\xi), \partial_\tau \mathbf{u}_d(\xi) \rangle = 0 \quad (\text{A.19})$$

for all  $\xi$ . It is then not difficult to see that (A.18) restricted to solutions that satisfy (A.19) has center-stable and strong-unstable dichotomies since (A.18) is merely part of the decomposition of solutions to (A.17) into  $\mathbf{w}(\xi)$  and  $\alpha(\xi) \partial_\tau \mathbf{u}_d(\xi)$  for real-valued functions  $\alpha$ . Since we wish to consider (A.18) for all  $\mathbf{w}$ , we have to calculate the solution to (A.18) with initial data  $\mathbf{w}(0) = \partial_\tau \mathbf{u}_d(0)$ . Fortunately, it is easy to see that  $\alpha(\xi) \partial_\tau \mathbf{u}_d(\xi)$  is the desired solution to (A.18) where  $\alpha(\xi)$  satisfies

$$\alpha_\xi = -\alpha \frac{d}{d\xi} [\log |\partial_\tau \mathbf{u}_d(\xi)|_Y^2], \quad \alpha(0) = 1$$

so that  $\alpha(\xi) = |\partial_\tau \mathbf{u}_d(0)|_Y^2 / |\partial_\tau \mathbf{u}_d(\xi)|_Y^2$  for all  $\xi$ . This shows that (A.18) with  $\mathbf{w} \in Y$  has center-stable and strong-unstable dichotomies for  $\xi \geq 0$ . The remaining statements are once more a consequence of Theorem 7.  $\blacksquare$

The following corollary summarizes the first part of the proof of the preceding lemma.

**Corollary A.2** *The linearization*

$$\mathbf{w}_\xi = [\mathcal{A}_0 + \mathcal{F}_{\mathbf{u}}(\mathbf{u}_d(\xi))] \mathbf{w}$$

*about the defect has exponential dichotomies in appropriate weighted spaces if, and only if, the linearization about the asymptotic wave trains has dichotomies in these spaces.*

For each  $\eta \in \mathbb{R}$ , we define the spaces

$$\mathcal{Y}_\eta = L_\eta^2(\mathbb{R}^+, Y), \quad \mathcal{Y}_\eta^1 = L_\eta^2(\mathbb{R}^+, Y^1) \cap H_\eta^1(\mathbb{R}^+, Y) \quad (\text{A.20})$$

where  $L_\eta^2$  refers to the exponentially weighted  $L^2$ -space with norm

$$|\mathbf{u}|_{L_\eta^2(\mathbb{R}^+)} = |e^{-\eta\xi} \mathbf{u}(\xi)|_{L^2(\mathbb{R}^+)}.$$

We are interested in proving the existence of a center-stable manifold of class  $\mathcal{C}^\ell$ , say, for some integer  $\ell > 0$  that we fix from now on. We will then choose  $\eta_0$  and  $\delta$  with  $0 < \delta < \eta_0 < \kappa/\ell$ , where  $\kappa$  appeared in Lemma A.1.

For every  $\eta > \delta$ , and each  $\mathbf{w} \in \mathcal{Y}_\eta^1$ , equation (A.14)

$$\theta_\xi = \delta \check{\mathcal{G}}_0(\theta, \mathbf{w}(\xi)), \quad \theta(0) = 0$$

can be solved uniquely for  $\theta(\xi)$ , and we have  $\sup_{\xi \geq 0} |\theta'(\xi)| \leq C_0 \delta$ . Furthermore, the function  $\mathbf{w} \mapsto \theta$  is Lipschitz as a map from  $\mathcal{Y}_\eta^1$  into itself with Lipschitz constant bounded by  $C_0 \delta / (\eta - \delta)$  (see [41, Lemma 2.4(ii)]). We denote this map by  $\theta = \theta[\mathbf{w}]$ .

Thus, it remains to solve the equation (A.15) for  $\mathbf{w}$  which reads

$$\mathbf{w}_\xi = \mathcal{A}(\theta[\mathbf{w}])\mathbf{w} + \check{\mathcal{G}}_1(\theta[\mathbf{w}], \mathbf{w}) \quad (\text{A.21})$$

after substituting  $\theta = \theta[\mathbf{w}]$ . After decreasing  $\delta > 0$  if necessary, Lemma A.1 together with the properties of the map  $\mathbf{w} \mapsto \theta[\mathbf{w}]$  imply that the linear part of (A.21) has center-stable and strong-unstable dichotomies  $\Phi_{\theta[\mathbf{w}]}^{\text{cs}}(\xi, \zeta)$  and  $\Phi_{\theta[\mathbf{w}]}^{\text{uu}}(\xi, \zeta)$ , respectively, which allows us to write (A.21) as the integral equation

$$\begin{aligned} \mathbf{w}(\xi) &= \Phi_{\theta[\mathbf{w}]}^{\text{cs}}(\xi, 0)\mathbf{w}_0^{\text{cs}} + \int_0^\xi \Phi_{\theta[\mathbf{w}]}^{\text{cs}}(\xi, \zeta) \check{\mathcal{G}}_1(\theta[\mathbf{w}](\zeta), \mathbf{w}(\zeta)) \, d\zeta \\ &\quad + \int_\infty^\xi \Phi_{\theta[\mathbf{w}]}^{\text{uu}}(\xi, \zeta) \check{\mathcal{G}}_1(\theta[\mathbf{w}](\zeta), \mathbf{w}(\zeta)) \, d\zeta. \end{aligned} \quad (\text{A.22})$$

From this point on, we can proceed, with very minor modifications, as in the proof of Fenichel's theorem given in [41, Section 2 and Appendix A] by setting up a contraction-mapping argument on the space  $\mathcal{Y}_{\eta_0}^1$ . Since the proof in [41] is very detailed, we decided not to repeat it here. We should, however, comment on an additional result that we need to make the proof in [41] work. In order to apply the arguments on [41, Page 73], we need the following optimal-regularity result.

**Lemma A.3** *If we fix any function  $\theta(\xi)$  with  $\sup_{\xi \geq 0} |\theta'(\xi)| \leq C_0 \delta$  and denote by  $\Phi_\theta^{\text{cs}}(\xi, \zeta)$  and  $\Phi_\theta^{\text{uu}}(\xi, \zeta)$  the dichotomies of*

$$\mathbf{w}_\xi = \mathcal{A}(\theta(\xi))\mathbf{w},$$

*then the operator  $\mathcal{S} : \mathcal{Y}_\eta \rightarrow \mathcal{Y}_\eta^1$  defined by*

$$[\mathcal{S}\mathbf{g}](\xi) = \int_0^\xi \Phi_\theta^{\text{cs}}(\xi, \zeta)\mathbf{g}(\zeta) \, d\zeta + \int_\infty^\xi \Phi_\theta^{\text{uu}}(\xi, \zeta)\mathbf{g}(\zeta) \, d\zeta$$

*is well defined and bounded as long as  $0 < \eta < \kappa$ .*

**Proof.** Define  $E_0^{\text{u}} = \text{Rg}(\Phi_\theta^{\text{uu}}(0, 0))$ , and consider the operator

$$\mathcal{T} : \quad \text{D}(\mathcal{T}) \longrightarrow \mathcal{Y}_\eta, \quad \mathbf{u} \longmapsto \frac{d\mathbf{w}}{d\xi} - \mathcal{A}(\theta(\cdot))\mathbf{w} \quad (\text{A.23})$$

with domain

$$\text{D}(\mathcal{T}) = \mathcal{Y}_\eta^1 \cap \{\mathbf{w} \in \mathcal{Y}_\eta^1; \mathbf{w}(0) \in E_0^{\text{u}}\}. \quad (\text{A.24})$$

It follows as in [48, §5.2] that  $\mathcal{T}$  is a closed unbounded operator on  $\mathcal{Y}_\eta$  with inverse given by  $\mathcal{S}$ , which proves the lemma.  $\blacksquare$

The optimal-regularity result allows us also to prove smooth dependence of the fixed point on the parameters  $(\omega, c)$ . Indeed, if we define

$$\check{\mathcal{F}}(\check{\mathbf{u}}) = \begin{pmatrix} v \\ -\check{\omega}D^{-1}\partial_\tau u - \check{c}D^{-1}v - D^{-1}f(u) \end{pmatrix}, \quad \check{\mathbf{u}} = (u, v, \check{\omega}, \check{c}),$$

we can replace  $\mathbf{u}$  and  $\mathcal{F}$  by  $\check{\mathbf{u}}$  and  $\check{\mathcal{F}}$  and proceed exactly as above.

Finally, we mention that the resulting center-stable manifold is constructed in the artificially augmented phase space  $\mathbf{w} \in Y^1$ . The intersection of this manifold with the smooth bundle defined by (A.5) is transverse, since the normal direction to the bundle is contained in the center subspace. Therefore, the ‘‘true’’ center-stable manifold, defined as the intersection of the center-stable manifold that we constructed above and the bundle given by (A.5), is the desired smooth and flow-invariant center-stable manifold. The statements about fibers can be proved as in [41].

## A.2 Slowly varying coefficients

We consider the equation

$$\mathbf{w}_\xi = \mathcal{A}(\theta)\mathbf{w} \tag{A.25}$$

for a given function  $\theta = \theta(\xi)$  where  $\mathcal{A}(\theta)$  has been defined in (A.13). We assume that (A.25) has an exponential dichotomy on  $\mathbb{R}^+$  for each constant function  $\theta(\xi) \equiv \theta_0 \in \mathbb{R}$  and that the rate  $\kappa$  and the constant  $C$  of the dichotomies can be chosen independently of  $\theta_0 \in \mathbb{R}$ .

The following theorem, proved in [6, 23] for ODEs and PDEs, respectively, shows that (A.25) has then dichotomies for any slowly varying function  $\theta(\xi)$ .

**Theorem 7** *There are positive constants  $\varepsilon_0$ ,  $\check{\kappa}$  and  $\check{C}$  such that (A.25) has an exponential dichotomy on  $\mathbb{R}^+$  with rate  $\check{\kappa}$  and constant  $\check{C}$  for each differentiable function  $\theta(\xi)$  with  $\theta(0) = 0$  and  $\sup_{\xi \geq 0} |\theta'(\xi)| \leq \varepsilon_0$ .*

**Proof.** We denote by  $\Phi_{\theta_0}^s(\xi, \zeta)$  and  $\Phi_{\theta_0}^u(\xi, \zeta)$  the exponential dichotomies of the equation

$$\mathbf{w}_\xi = \mathcal{A}(\theta_0)\mathbf{w}$$

for constant functions  $\theta(\xi) \equiv \theta_0 \in \mathbb{R}$ . Since the  $\theta_0$ -dependent terms of the operator  $\mathcal{A}(\theta_0)$  are bounded and depend smoothly on  $\theta_0$ , see (A.13) and (A.9), the robustness theorem for exponential dichotomies [6, 23, 38] implies that these dichotomies can be chosen to depend smoothly on  $\theta_0 \in \mathbb{R}$ .

In fact, there are positive constants  $C$  and  $\kappa$  such that

$$\left\| \frac{d\Phi_{\theta_0}^s}{d\theta}(\xi, \zeta) \right\| + \left\| \frac{d\Phi_{\theta_0}^u}{d\theta}(\zeta, \xi) \right\| \leq C e^{-\kappa|\xi-\zeta|} \tag{A.26}$$

uniformly in  $\xi \geq \zeta \geq 0$ . We denote by  $E_0^u$  the range of the unstable projection  $\Phi_0^u(0, 0)$  for  $\theta_0 = 0$ .

Next, pick a function  $\theta(\xi)$  so that  $\theta(0) = 0$  and  $\sup_{\xi \geq 0} |\theta'(\xi)| \leq \varepsilon_0$ . Consider the operator

$$\mathcal{T}(\theta) : \quad D(\mathcal{T}(\theta)) \longrightarrow L^2(\mathbb{R}^+, Y), \quad \mathbf{u} \longmapsto \frac{d\mathbf{u}}{d\xi} - \mathcal{A}(\theta(\cdot))\mathbf{u} \tag{A.27}$$

with domain

$$D(\mathcal{T}(\theta)) = L^2(\mathbb{R}^+, Y^1) \cap \{\mathbf{u} \in H^1(\mathbb{R}^+, Y); \mathbf{u}(0) \in E_0^u\}, \quad (\text{A.28})$$

which is independent of  $\theta$ . We may consider  $\mathcal{T}$  as a closed unbounded operator on  $L^2(\mathbb{R}^+, Y)$ . If we can prove that  $\mathcal{T}(\theta)$  has a bounded inverse with bounds that are independent of  $\theta$ , then the theorem is proved as we may then proceed as in [48, §5.3.1] to construct exponential dichotomies of (A.25) with constants and rates that do not depend on  $\theta$ .

Thus, we have to solve the equation

$$\frac{d\mathbf{u}}{d\xi} = A(\theta(\xi))\mathbf{u} + \mathbf{g}(\xi) \quad (\text{A.29})$$

for a given  $\mathbf{g} \in L^2(\mathbb{R}^+, Y)$ . We define

$$\mathbf{u}(\xi) = [\check{\mathcal{L}}(\theta)\mathbf{g}](\xi) = \int_0^\xi \Phi_{\theta(\xi)}^s(\xi, \zeta)\mathbf{g}(\zeta) d\zeta + \int_\infty^\xi \Phi_{\theta(\xi)}^u(\xi, \zeta)\mathbf{g}(\zeta) d\zeta. \quad (\text{A.30})$$

and set  $\check{\mathcal{L}}(\theta)\mathbf{g} := \mathbf{u}$ . It follows from [48] that  $\mathbf{u}(\xi)$  lies in  $D(\mathcal{T}(\theta))$  and that

$$\frac{d\mathbf{u}}{d\xi} = A(\theta(\xi))\mathbf{u} + \mathbf{g}(\xi) + [\mathcal{S}(\theta)\mathbf{g}](\xi) \quad (\text{A.31})$$

where

$$[\mathcal{S}(\theta)\mathbf{g}](\xi) = \left[ \int_0^\xi \frac{d\Phi_{\theta(\xi)}^s}{d\theta}(\xi, \zeta)\mathbf{g}(\zeta) d\zeta + \int_\infty^\xi \frac{d\Phi_{\theta(\xi)}^u}{d\theta}(\xi, \zeta)\mathbf{g}(\zeta) d\zeta \right] \theta'(\xi). \quad (\text{A.32})$$

Using (A.26), we see that

$$\mathcal{S}(\theta) : L^2(\mathbb{R}^+, Y) \longrightarrow L^2(\mathbb{R}^+, Y)$$

with  $\|\mathcal{S}(\theta)\| \leq \varepsilon_0 C_1$  for some  $C_1 > 0$  that does not depend on  $\theta$ . Therefore,  $\mathbf{1} + \mathcal{S}(\theta)$  is invertible on  $L^2(\mathbb{R}^+, Y)$  uniformly in  $\theta$  provided  $\varepsilon_0 > 0$  is smaller than  $2/C_1$ . The desired solution to (A.29) is then given by

$$\mathbf{u} := \mathcal{L}(\theta)\mathbf{g} = \check{\mathcal{L}}(\theta)[\mathbf{1} + \mathcal{S}(\theta)]^{-1}\mathbf{g}$$

where  $\check{\mathcal{L}}(\theta)$  has been defined in (A.30). This proves that  $\mathcal{T}(\theta)$  has a bounded inverse on  $L^2(\mathbb{R}^+, Y)$  and, together with the fact that  $\mathcal{T}(\theta)$  is closed, shows that the inverse is bounded as an operator into the domain of  $\mathcal{T}(\theta)$ . Since the bounds are clearly independent of  $\theta$ , we have proved our claim and therefore the theorem.  $\blacksquare$

## B Parameter values for the numerical simulations

The numerical simulations in Figure 1.2(i) and (ii) show the  $v$ -component of solutions to the Brusselator

$$\begin{aligned} u_t &= d_1 u_{xx} + a + (b+1)u + u^2 v \\ v_t &= d_2 v_{xx} + bu - u^2 v \end{aligned} \quad (\text{B.1})$$

on the interval  $[0, L]$  with Neumann boundary conditions. The parameters are as in [37] so that

$$d_1 = 4.11, \quad d_2 = 9.73, \quad a = 2.5, \quad b = 10.0.$$

The length  $L$  of the spatial interval is chosen between 250 and 650. Sources and sinks are created from the initial condition

$$(u_0, v_0)(x) = \left( a + \frac{1}{2} \tanh \left( x - \frac{L}{2} \right), \frac{b}{a} + \frac{1}{10} \cos x \right)$$

which excites both Turing and Hopf modes. We solved the system (B.1) using a forward Euler scheme in time and centered finite differences in space.

**Acknowledgments** B. Sandstede was partially supported by the Alfred P Sloan Foundation and by the NSF through grant DMS-0203854. A. Scheel was partially supported by the NSF through grant DMS-0203301. A. Scheel is grateful to the Sonderforschungsbereich 555 and the Fachbereich Mathematik at the FU Berlin for their kind support during a one-month research visit.

## References

- [1] R. Alvarez, M. van Hecke and W. van Saarloos. Sources and sinks separating domains of left- and right-travelling waves: Experiment versus amplitude equations. *Phys. Rev. E* **56** (1997) R1306–1309.
- [2] I.S. Aranson and L. Kramer. The world of the complex Ginzburg–Landau equation. *Rev. Mod. Phys.* **74** (2002) 99–143.
- [3] J. Burguete, H. Chaté, F. Daviaud and N. Mukolobwicz. Bekki–Nozaki amplitude holes in hydrothermal nonlinear waves. *Phys. Rev. Lett.* **82** (1999) 3252–3255.
- [4] P. Chossat and R. Lauterbach. *Methods in equivariant bifurcations and dynamical systems*. World Scientific, Singapore, 2000.
- [5] S.-N. Chow and X.-B. Lin. Bifurcation of a homoclinic orbit with a saddle-node equilibrium. *Diff. Int. Eqns.* **3** (1990) 435–466.
- [6] W.A. Coppel. *Dichotomies in stability theory*. Lecture Notes in Mathematics **629**. Springer, Berlin, 1978.
- [7] B. Dionne, M. Golubitsky, M. Silber and I. Stewart. Time-periodic spatially periodic planforms in Euclidean equivariant partial differential equations. *Philos. Trans. Roy. Soc. London A* **352** (1995) 125–168.
- [8] E. Doedel, A.R. Champneys, T.F. Fairgrieve, Yu.A. Kuznetsov, B. Sandstede and X. Wang. *AUTO97: Continuation and bifurcation software for ordinary differential equations (with HOMCONT)*. Technical Report, Concordia University, 1997.
- [9] A. Doelman. Breaking the hidden symmetry in the Ginzburg–Landau equation. *Physica D* **97** (1996) 398–428.

- [10] A. Doelman, B. Sandstede, A. Scheel and G. Schneider. The dynamics of modulated wave trains. In preparation.
- [11] W. Eckhaus and G. Iooss. Strong selection or rejection of spatially periodic patterns in degenerate bifurcations. *Physica D* **39** (1989) 124–146.
- [12] S.-I. Ei. The motion of weakly interacting pulses in reaction-diffusion systems. *J. Dynam. Diff. Eqns.* **14** (2002) 85–137.
- [13] C. Elphick, E. Meron and E.A. Spiegel. Patterns of propagating pulses. *SIAM J. Appl. Math.* **50** (1990) 490–503.
- [14] H. Engler. Asymptotic stability of travelling wave solutions for perturbations with algebraic decay. *J. Diff. Eqns.* **185** (2002) 348–369.
- [15] N. Fenichel. Geometric singular perturbation theory for ordinary differential equations. *J. Diff. Eqns.* **31** (1979) 53–98.
- [16] T. Gallay, G. Schneider and H. Uecker. Stable transport of information near essentially unstable localized structures. *Discrete Cont. Dyn. Syst. B* (to appear).
- [17] A. Goryachev, H. Chaté and R. Kapral. Synchronization defects and broken symmetry in spiral waves. *Phys. Rev. Lett.* **80** (1998) 873–876.
- [18] P. Habdas, M.J. Case and J.R. de Bruyn. Behavior of sinks and source defects in a one-dimensional traveling finger pattern. *Phys. Rev. E* **63** (2001) 066305.
- [19] C.T. Hamik and O. Steinbock. Shock structures and bunching fronts in excitable reaction-diffusion systems. *Phys. Rev. E* **65** (2002) 046224.
- [20] M. van Hecke. Building blocks of spatiotemporal intermittency. *Phys. Rev. Lett.* **80** (1998) 1896–1899.
- [21] M. van Hecke. Coherent and incoherent structures in systems described by the 1D CGLE: Experiments and identification. *Physica D* **174** (2003) 134–151.
- [22] M. van Hecke, C. Storm and W. van Saarloos. Sources, sinks and wavenumber selection in coupled CGL equations and experimental implications for counter-propagating wave systems. *Physica D* **134** (1999) 1–47.
- [23] D. Henry. *Geometric theory of semilinear parabolic equations*. Lecture Notes in Mathematics **804**. Springer, New York, 1981.
- [24] P. Howard. Pointwise estimates and stability for degenerate viscous shock waves. *J. Reine Angew. Math.* **545** (2002) 19–65.
- [25] L.N. Howard and N. Kopell. Slowly varying waves and shock structures in reaction-diffusion equations. *Studies Appl. Math.* **56** (1976/77) 95–145.
- [26] G. Iooss, A. Mielke and Y. Demay. Theory of steady Ginzburg–Landau equation, in hydrodynamic stability problems. *Europ. J. Mech. B/Fluids* **8** (1989) 229–268.
- [27] T. Kapitula. Stability of weak shocks in  $\lambda$ - $\omega$  systems. *Indiana Univ. Math. J.* **40** (1991) 1193–1219.

- [28] T. Kapitula. Existence and stability of singular heteroclinic orbits for the Ginzburg–Landau equation. *Nonlinearity* **9** (1996) 669–685.
- [29] K. Kirchgässner. Wave-solutions of reversible systems and applications. *J. Diff. Eqns.* **45** (1982) 113–127.
- [30] P. Kolodner. Extended states of nonlinear traveling-wave convection II: Fronts and spatiotemporal defects. *Phys. Rev. A* **45** (1992) 6452–6468.
- [31] N. Kopell and L.N. Howard. Plane wave solutions to reaction-diffusion equations. *Stud. Appl. Math.* **52** (1973) 291–328.
- [32] G.J. Lord, D. Peterhof, B. Sandstede and A. Scheel. Numerical computation of solitary waves on infinite cylinders. *SIAM J. Numer. Anal.* **37** (2000) 1420–1454.
- [33] A. Mielke. A spatial center manifold approach to steady bifurcations from spatially periodic patterns. In: *Dynamics in dissipative systems: reductions, bifurcations and stability*, G. Dangelmayr, B. Fiedler, K. Kirchgässner and A. Mielke. Pitman Research Notes **352**. Longman, Harlow, 1996.
- [34] M. Murata. Large time asymptotics for fundamental solutions of diffusion equations. *Tohoku Math. J.* **37** (1985) 151–195.
- [35] L. Pastur, M.-T. Westra and W. van de Water. Sources and sinks in 1D traveling waves. *Physica D* **174** (2003) 71–83.
- [36] L. Pastur, M.-T. Westra, D. Snouck, W. van de Water, M. van Hecke, C. Storm and W. van Saarloos. Sources and holes in a one-dimensional traveling-wave convection experiment. *Phys. Rev. E* **67** (2003) 036305.
- [37] J.-J. Perraud, A. De Wit, E. Dulos, P. De Kepper, G. Dewel and P. Borckmans. One-dimensional “spirals”: Novel asynchronous chemical wave sources. *Phys. Rev. Lett.* **71** (1993) 1272–1275.
- [38] D. Peterhof, B. Sandstede and A. Scheel. Exponential dichotomies for solitary-wave solutions of semi-linear elliptic equations on infinite cylinders. *J. Diff. Eqns.* **140** (1997) 266–308.
- [39] J. Rademacher. Tracefiring of pulses. In preparation.
- [40] W. van Saarloos and P.C. Hohenberg. Fronts, pulses, sources and sinks in generalized complex Ginzburg–Landau equations. *Physica D* **56** (1992) 303–367.
- [41] K. Sakamoto. Invariant manifolds in singular perturbation problems for ordinary differential equations. *Proc. Roy. Soc. Edinburgh A* **116** (1990) 45–78.
- [42] B. Sandstede. Stability of travelling waves. In: *Handbook of Dynamical Systems II* (B. Fiedler, ed.). Elsevier, Amsterdam, (2002) 983–1055.
- [43] B. Sandstede and A. Scheel. Essential instability of pulses, and bifurcations to modulated travelling waves. *Proc. Roy. Soc. Edinburgh A* **129** (1999) 1263–1290.
- [44] B. Sandstede and A. Scheel. Spectral stability of modulated travelling waves bifurcating near essential instabilities. *Proc. Roy. Soc. Edinburgh A* **130** (2000) 419–448.

- [45] B. Sandstede and A. Scheel. Absolute versus convective instability of spiral waves. *Phys. Rev. E* **62** (2000) 7708–7714.
- [46] B. Sandstede and A. Scheel. Absolute and convective instabilities of waves on unbounded and large bounded domains. *Physica D* **145** (2000) 233–277.
- [47] B. Sandstede and A. Scheel. Essential instabilities of fronts: bifurcation, and bifurcation failure. *Dynam. Syst.* **16** (2001) 1–28.
- [48] B. Sandstede and A. Scheel. On the structure of spectra of modulated travelling waves. *Math. Nachr.* **232** (2001) 39–93.
- [49] B. Sandstede and A. Scheel. Evans function and blow-up methods in critical eigenvalue problems. *Discrete Cont. Dyn. Syst. B* (to appear).
- [50] B. Sandstede and A. Scheel. Absolute instabilities of pulses. Preprint (2003).
- [51] B. Sandstede and A. Scheel. Period-doubling bifurcations of spiral waves. In preparation.
- [52] B. Sandstede and A. Scheel. Stability and instability of spiral waves. In preparation.
- [53] D.H. Sattinger. On the stability of waves of nonlinear parabolic systems. *Adv. Math.* **22** (1976) 312–355.
- [54] A. Scheel. Radially symmetric patterns of reaction-diffusion systems. *Mem. Amer. Math. Soc.* **165** (2003).
- [55] G. Schneider. Hopf bifurcation in spatially extended reaction-diffusion systems. *J. Nonlinear Sci.* **8** (1998) 17–41.
- [56] A. Vanderbauwhede and B. Fiedler. Homoclinic period blow-up in reversible and conservative systems. *Z. Angew. Math. Phys.* **43** (1992) 292–318.
- [57] M. Yoneyama, A. Fujii and S. Maeda. Wavelength-doubled spiral fragments in photosensitive monolayers. *J. Amer. Chem. Soc.* **117** (1995) 8188–9191.